BOEING
ENGINEERING
&CONSTRUCTION
THE BOEING COMPANY

Solar Energy Systems

Central Receiver Solar Thermal Power System

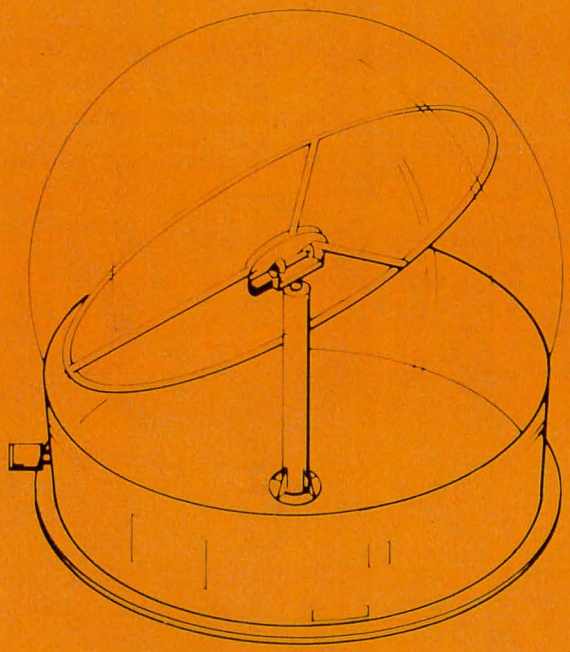

Collector Subsystem Detail Design Report

DISCLAIMER

D277-10022-1

CENTRAL-RECEIVER SOLAR-THERMAL POWER SYSTEM

Collector Subsystem
Research Experiments
Detail Design Report

February 24, 1976

Prepared for
United States
Energy Research and Development Administration

under

Contract E-(04-3)-1111

by

Boeing Engineering and Construction
a Division of The Boeing Company
Seattle, Washington

MGW

THIS PAGE

WAS INTENTIONALLY

LEFT BLANK

FOREWORD

This document contains the Detail Design of research experiment hardware for the collector subsystem of a 10 MW_e solar thermal pilot plant. It was prepared by Boeing Engineering and Construction, a division of The Boeing Company, in fulfillment of Data Requirement No. 6 under ERDA Contract E(04-3)-1111. Detailed drawings of components were provided at the Detail Design Review, and are available upon request. Simplified versions of these drawings and schematics are included in this report.

THIS PAGE

WAS INTENTIONALLY

LEFT BLANK

TABLE OF CONTENTS

Table of Contents - continued

Table of Contents - continued

Table of Contents - continued

1.0 EXECUTIVE OVERVIEW

This document contains the detail design (DD) of research experiment hardware to support the 10 MW_e Pilot Plant preliminary design (PD). Additionally, test plans for assembly, integration, and array tests are presented, along with results of completed component/material tests.

Research experiment DD and tests described herein were planned to provide design verification and supporting data, with hardware which either duplicates, or closely simulates the Pilot Plant PD baseline.

1.1 RESEARCH EXPERIMENT HARDWARE DESIGN

Significant features of the research experiment heliostat design are summarized in Figure 1.1-1. The Tedlar dome will be supported from a 1.09m -high (43 in.) steel ring, which is in turn attached to a concrete foundation. The ring is designed to allow the lower portion of the reflector to extend below the base plane of the dome, when oriented near vertical. This feature allows a larger reflector size within a fixed dome size, which ultimately reduces collector subsystem costs. It also elevates the dome material above adjacent soil and vegetation. The Tedlar dome will be tethered and sealed to the steel ring by use of a segmented clamping ring.

A blower assembly, mounted on the inside wall of the dome support ring, provides filtered air at a pressure of 0.038 N/sq. cm (0.056 psi) to support the dome. The need for humidity control will be established during preliminary tests on domes prior to installation of reflectors. Access to the dome interior will be provided through a hinged door in the support ring. Calculations have shown that entry can be made without the use of an airlock during periods of off-peak wind velocity.

The reflective assembly utilizes a commercially-available 0.05 mm (2 mils) thick Mylar film which is coated with vacuum-deposited aluminum on one surface. The aluminum coating functions as a front-surface reflector, hence providing maximum reflectance, and protecting the Mylar from direct sunlight. The research experiment membrane reflector employs an aluminum coating on only one side of the Mylar film. Long term desert exposure tests

are underway on similar Mylar films protected by Tedlar. If these tests indicate that sufficient ultraviolet radiation passes through the Tedlar dome to damage the Mylar during the Pilot Plant lifetime, an aluminum coating will be applied to both surfaces of the Mylar in the final PD.

A toroidal aluminum ring, 4.57 m (15 ft.) diameter, supports the membrane reflector in the required planar configuration. The membrane is pre-tensioned and bonded to a flat reference surface on the toroidal ring. A three-point support is used to interface the toroidal ring with the orientation gimbal and base. Membrane tension will be nominally fixed at 6189 MN/sq.m (1000 psi), which will be adequate to eliminate wrinkles and compensate for thermal expansion/contraction and creep effects. Subsequent studies on focusing effects, long-term creep, and dome buffeting may indicate the desirability of selecting other tension values for the final PD.

A functional diagram of the research experiment drive and control assembly is shown in Figure 1.1-2. The heliostat control command configuration shown, incorporates a central control simulator, a mini-computer, drive actuators, and a gimbal assembly on each heliostat. The central control simulator commands operational modes, provides the system clock for synchronization, and provides heliostat failure information. The mini-computer (field controller) directly controls 3 individual heliostats. The basic control concept is an open-loop system utilizing incremental positional feedback from optical-encoders on each heliostat drive. Open-loop control is performed commanding the reflective assembly to a predicted angle based upon the known geometric relationship between the sun, the heliostat, and the central receiver. Microprocessors in the field controller accept operational mode signals from central control, and generate position control signals for each heliostat.

Initial and subsequent alignment checking of heliostats is accomplished using a laser/geodolite mounted on the tower near the image display area. Deviations of the DD from the PD baseline include: hard-wired simulation of central control interface and heliostat interface eliminating the use of coded serial-bit data transmission required when a full array of 64 heliostats is involved; and manual assistance in the automated laser alignment technique planned for the PD baseline.

HELIOSTAT FEATURES

- TEDLAR DOME
  - 5.18 METER DIAMETER
  - 0.10 MM THICK
- ALUMINIZED MYLAR REFLECTOR
  - 4.57 METER DIAMETER
  - 0.05 MM THICK
- OPEN-LOOP AUTOMATED CONTROL
  - MINICOMPUTER CONTROL
  - MANUAL LASER ALIGNMENT

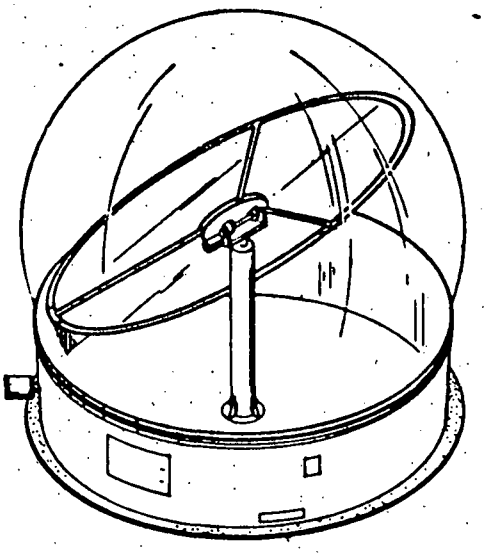

Figure: 1.1-1 Heliostat Assembly for Research Experiments

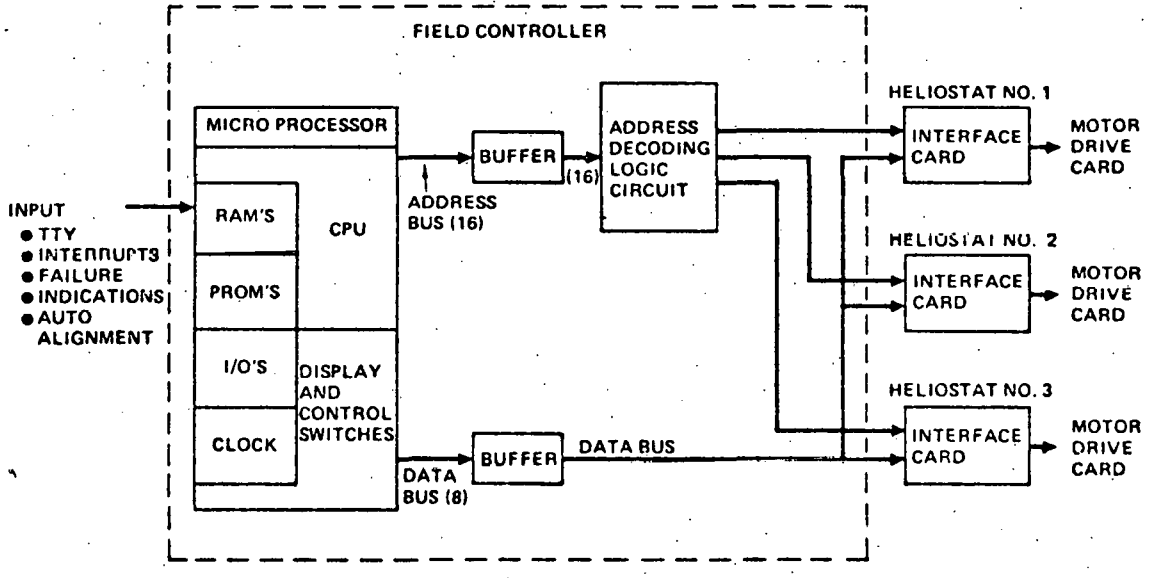

Figure: 1.1-2 Field Controller Interface Heliostats Block Diagram

1.2 TEST PLANS

Experimental work on the collector subsystem will include assembly, integration, and array tests as shown in Figure 1.2-1. Assembly tests will be aimed at qualification of the transparent enclosure assembly, reflective assembly, and drive and control assembly before integration into a complete heliostat. Integration tests will be aimed at verifying compatibility and fit of all assemblies within the heliostat prior to field testing. Array tests will demonstrate satisfactory operation of the overall collector subsystem (3 heliostats) and provide design data including: pointing accuracy, image intensity distribution; dome transmittance; and heliostat reflectance.

In assembly tests, two Tedlar domes will be exposed to ambient weather at Boardman, Oregon, over an approximately 7-month period (September, 1976 through March, 1977). Array tests will also be conducted at Boardman, but only the time period from January, 1977 through March, 1977. All other assembly and integration tests will be performed in laboratories at the Boeing facility in Kent, Washington.

1.3 RESULTS OF RESEARCH EXPERIMENTS

The first phase of Research experiments (component/materials testing) is now complete, with the exception of long-term weathering tests on selected materials which are underway at Albuquerque, New Mexico and Inyokern, California.

Testing has included: accelerated simulated sunlight exposure; creep and tensile strength of both basic materials and fabricated joints in materials; optical property measurements (reflectance and transmittance); cleanability/chemical exposure; weatherometer; and humidity tests. Component/materials testing has been aimed at developing supporting data for key design considerations: specular reflectance and transmittance of reflector and dome materials, respectively; size limitations on the dome dictated by wind loads and available thickness and tensile strength of Tedlar; and lifetime. Results of tests have generally shown that mechanical and optical properties assumed in conceptual design and PD baseline studies will be achieved with materials selected for research experiment hardware.

Accelerated simulated sunlight tests showed that of three Tedlar compositions tested, the "no-additive" variety is preferred, showing no change in transmittance and the least change in percent elongation at ultimate strength. Long-term creep tests showed that the Tedlar dome will not undergo significant dimensional changes; and tension in the Mylar reflector will remain sufficiently high to retain optical flatness after pre-tensioning and bonding. Cleaning and chemical exposure tests showed that baseline materials are cleanable using conventional methods and resistant to the chemical contaminants anticipated at the Pilot Plant.

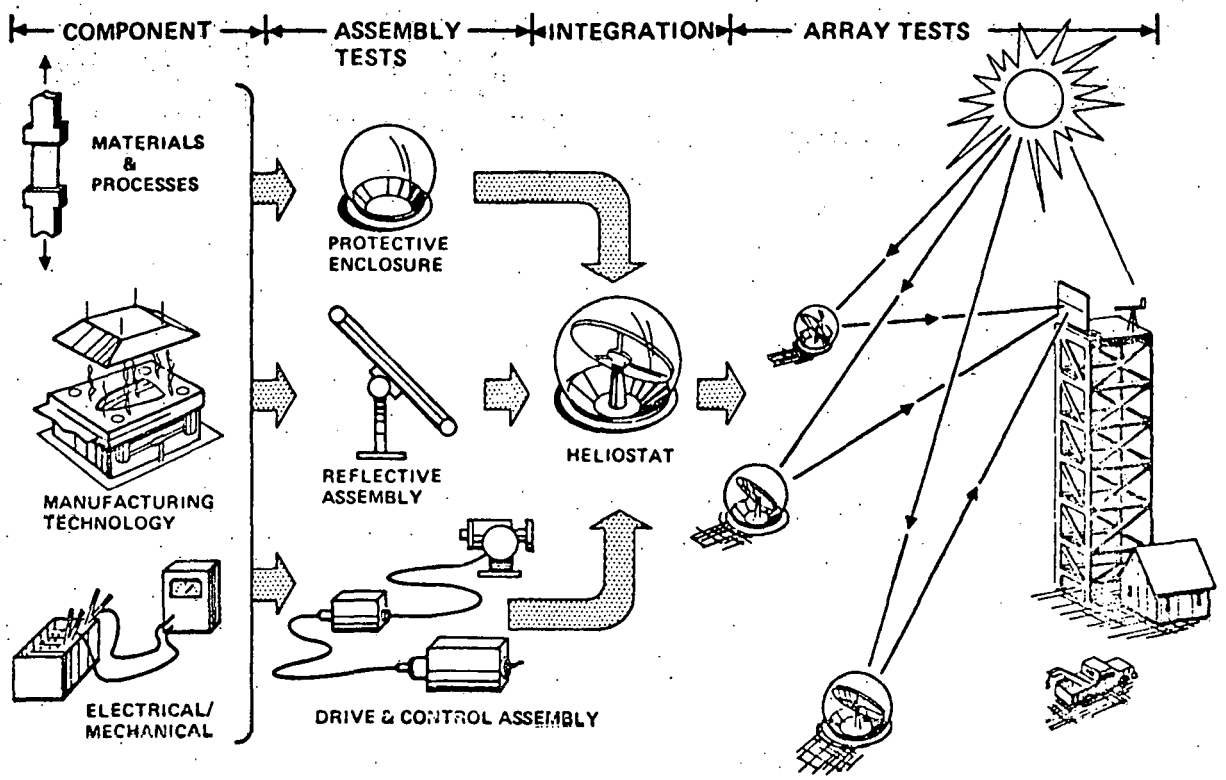

Figure: 1.2-1 Test Flow Logic

THIS PAGE

WAS INTENTIONALLY

LEFT BLANK

2.0 REQUIREMENTS/SPECIFICATIONS

Performance requirements and specifications for the research experiment hardware are summarized in Table 2.0-1. Requirements which are generally applicable are listed under the item, "Overall Heliostat Array." All other requirements are listed under the respective subassembly items "Reflective Assembly," "Transparent Enclosure Assembly," and "Drive and Control Assembly." A more detailed discussion of performance requirements and specifications is given in Reference 2-1. It must be recognized that although quantitative values have been assigned to some specifications in the table, changes to some values are likely to occur as the studies progress. Also, specifications will be quantized wherever possible throughout the research experiments.

In accordance with ERDA/Sandia program planning, the order of precedence in establishing requirements and specifications is as follows:

1) Performance
2) Capability to withstand natural environmental conditions
3) Owning cost ($/sq. meter/yr.) of collector subsystem

Generally, the detail design was chosen to meet the same requirements and specifications as the PD baseline for the 10 MW_e Pilot Plant.

TABLE 2.0-1

SUMMARY OF PERFORMANCE REQUIREMENTS

AND SPECIFICATIONS (RESEARCH EXPERIMENT HARDWARE)

Item	Performance Requirement	Specification
Overall Heliostat Array	Temperature Environment	-30 to 49°C Survival -20 + 49°C Operating
	Earthquake Environment	Seismic Zone 3
	Maintenance	Use of normal skills and minimum specialized equipment and tools.
	Transportability	Subject to all pertinent federal and state regulations.
	Electrical Transients	Protected against external and internal transients.
	Interchangeability	Major components to be interchangeable.
	Safety	Comply with pertinent OSHA rules and regulations.
Reflective Assembly	Specular Solar Reflectance	Greater than 85% within 0.3° scattering angle.
	Stowage Position	Horizontal position for maintenance and high wind conditions.
	Maintainability	Ease of replacement of reflector.
Transparent Enclosure Assembly	Specular Solar Transmittance	Greater than 86% within 0.3° scattering angle.
	Power Input	To Be Determined.

Table 2.0-1 - continued

Item	Performance Requirement	Specification
	Wind Environment	Height (meters) / Velocity (M/sec): 3 / 29; 6 / 33; 10 / 37
	Air Quality	1) Prevent condensation on internal surfaces. 2) Minimize particulate deposition on reflector, less than 10% reflectance decrease in 10 years.
	Rigidity	Provide adequate clearance from reflective assembly under all environmental conditions.
	Maintainability	1) Ease of cleaning. 2) Ease of repair of leaks. 3) Ease of replacement of parts in air supply apparatus.
	Humidity, Rain, Snow, Ice, Hail, and Sandstorm Environment	Withstand conditions at test sites.
Drive and Control Assembly	Orientation Accuracy	D&C Assembly $\pm 0.057^{o}$
		Reflective Assembly $\pm 0.057^{o}$
		Transparent Enclosure $\pm 0.057^{o}$
		Worst Case $\pm 0.171^{o}$
		RSS $\pm 0.1^{o}$

Table 2.0-1 - continued

Item	Performance Requirement	Specification
	Safety	Fail safe operation during power outage and electrical transients.
Drive and Control Assembly	Power Input	To Be Determined.
	Emergency Shutdown	Reduce incident radiation on receiver to less than 3% of initial value within 40 secs.
	Acquisition (Beam - on Command)	Orient heliostats to reflect sunlight to receiver, upon command from central control simulator.
	Normal Shutdown	Orient heliostats to safe stowage position upon command from central control simulator.
	Synthetic Tracking	Provide continuous tracking during intermittent cloudy periods.
	Manual Control	Provide manual control station outside transparent enclosure.
	Limit Controls	Provide limit control switches on drive mechanism.
	Alignment	Provide alignment check upon command from central control simulator.
	Maintainability	Ease of replacement and maintenance of components.

3.0 RESEARCH EXPERIMENT DETAIL DESIGN

This section of the report discusses the design concept and rationale for each of the major subassemblies of the collector subsystem. Additionally, thermal design and safety studies are discussed.

3.1 TRANSPARENT ENCLOSURE ASSEMBLY

Design of the transparent enclosure assembly involved configuration studies, structural analyses and materials studies. Results of these studies are discussed below.

3.1.1 Configuration

The transparent enclosure assembly for research experiments includes a transparent dome, base and an air supply system.

3.1.1.1 Dome

The dome design selected for research experiments is an air-supported transparent sphere as shown in Figure 3.1-1. The diameter is 5.18m (17 ft.) and the base is truncated at an angle of 60^{o} from the spherical center to provide a mount ring 4.48m (14.72 ft.) in diameter. The dome is fabricated from 18 gores of 0.10mm (4-mil) thick Tedlar film which is overlapped and seam welded. A circular polar cap forms the top of the dome. The bottom edges of gores are doubled back over a plastic rope and seam welded. This roped edge is attached to a steel ring base as shown in Figure 3.1-1. This attachment method was selected on the basis of cost-effectiveness and favorable experience of manufacturers of air supported buildings.

Selection of dome material involved preliminary screening of various candidate materials based on their transmittance, strength, weatherability and cost. A summary of information on the various materials is given in Figure 3.1-2. Tedlar was selected as the preferred material. Subsequent experiments were then conducted to select the optimum composition of Tedlar from three varieties: "standard"; "UV screen"; and "no additive." Results of research experiments on these specimens (detailed in Section 6.0) showed that the "no-additive" composition exhibited superior UV resistance and specular solar transmittance, and has comparable strength characteristics. Accordingly, it was selected as the baseline material for research experiment domes.

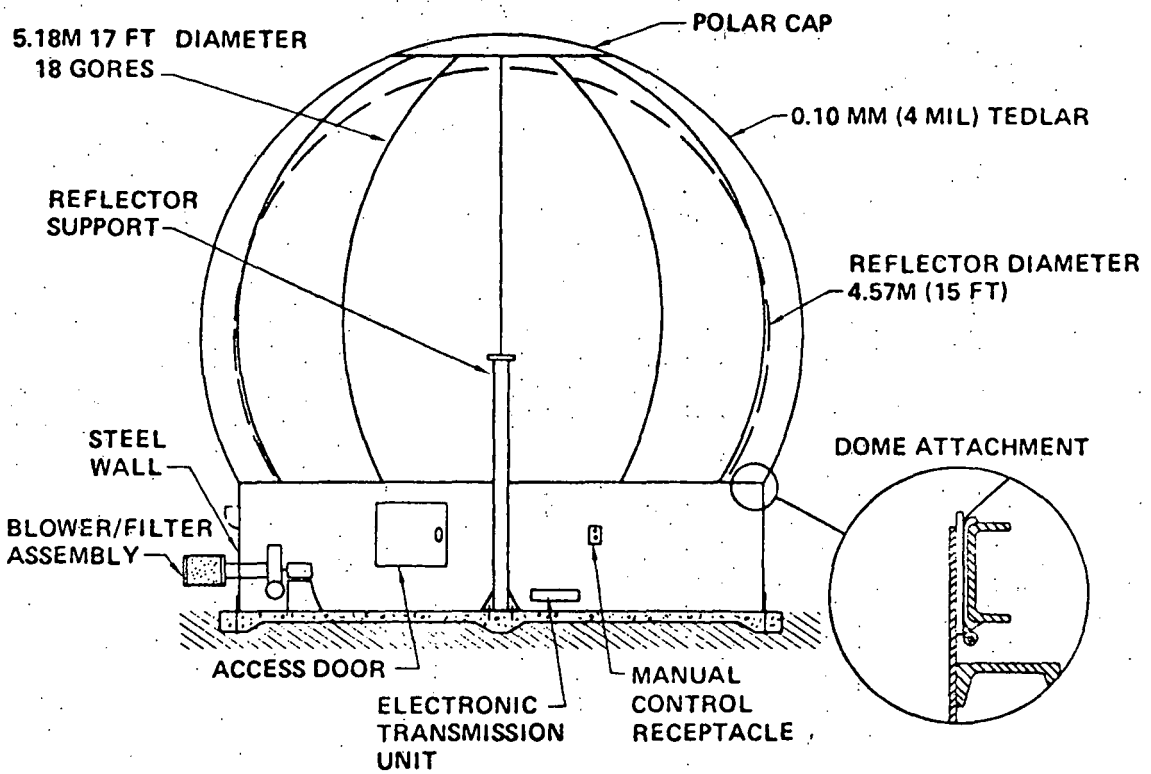

Figure: 3.1-1 Enclosure and Base Design for Research Experiments

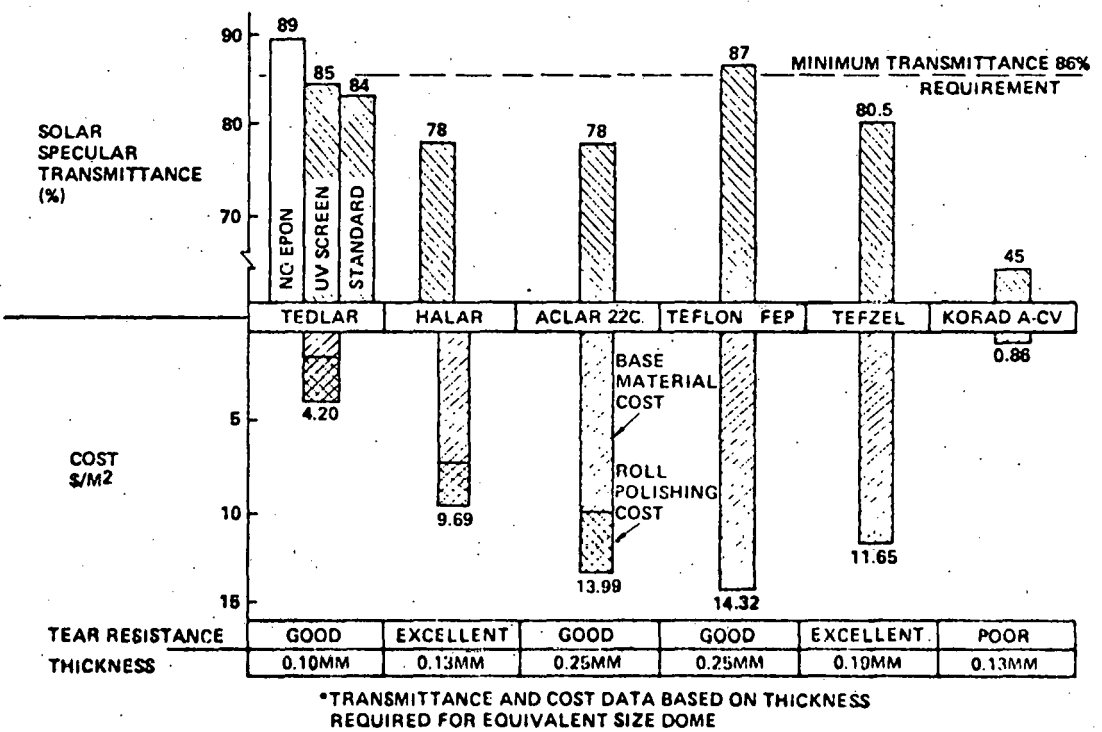

*TRANSMITTANCE AND COST DATA BASED ON THICKNESS REQUIRED FOR EQUIVALENT SIZE DOME

*Figure: 3.1-2 Summary of Dome Material Properties**

Research experiments on the baseline material showed specular solar transmittances in the range of 88 to 90% at normal incidence. Since sunlight passes through the dome at angles of incidence as large as about 68^{o} from normal, the average dome transmittance will, however, be somewhat lower. Transmittance data on typical baseline Tedlar material at various angles of incidence is shown in Figure 3.1-3. This data was integrated over a reflector/dome geometry utilizing a 7m diameter dome and 6.48m diameter reflector. Results indicate a reduction in transmittance from about 90% at normal incidence, to 86.6% averaged over the reflector area.

3.1.1.2 Base

The base design selected for research experiment hardware consists of a locally-reinforced concrete slab, a reflector support post, and a cylindrical steel ring as shown in Figure 3.1-1. Tie-downs for the reflector support post and steel ring will be imbedded in the concrete. The 1.09m (43 in.)-high x 0.25 cm (0.1 in.)-thick steel ring will be fabricated in 90^{o} segments and then assembled on the concrete slab at the test site. Mechanical fasteners will be used to facilitate assembly and dis-assembly of the ring segments.

The 183 cm (72 in.)-high reflector support post will be formed from 10.16 cm (4 in.) diameter steel pipe, and will have interface plates welded to each end. The upper plate, equipped with threaded connectors, will both interface and level the gimbal apparatus.

The base design includes a 61 cm (24 in.) square door for ingress and egress to the dome. The door will be hinged to swing inward, and will be equipped with appropriate sealing gasket material. Calculations have shown that an air-lock or auxiliary blower will not be required when entering the dome during off-peak wind velocities.

3.1.1.3 Air Supply

The air supply selected for research experiment domes is a single-stage centrifugal blower (Cincinnati Fan Model No. PB-10) which will be direct-driven with a nominal 1/3 hp DC motor. Characteristics of this blower, compared to the predicted dome leakage rate, are shown in Figure 3.1-4. Dome leak rate was estimated using the following empirical relationship from Reference 3.1-1.

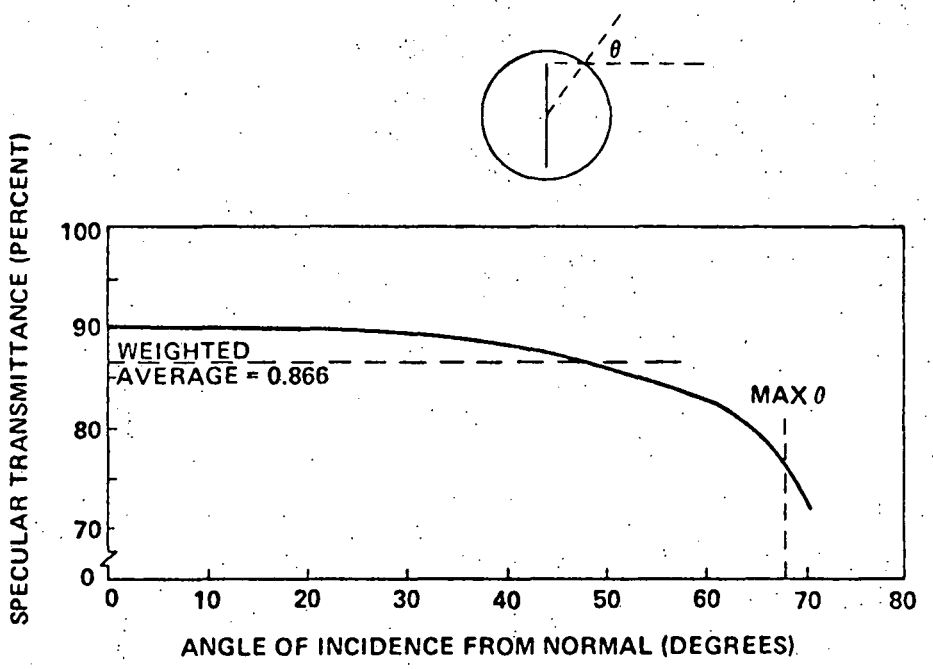

Figure: 3.1-3 Effect of Incidence Angle on Tedlar Transmittance

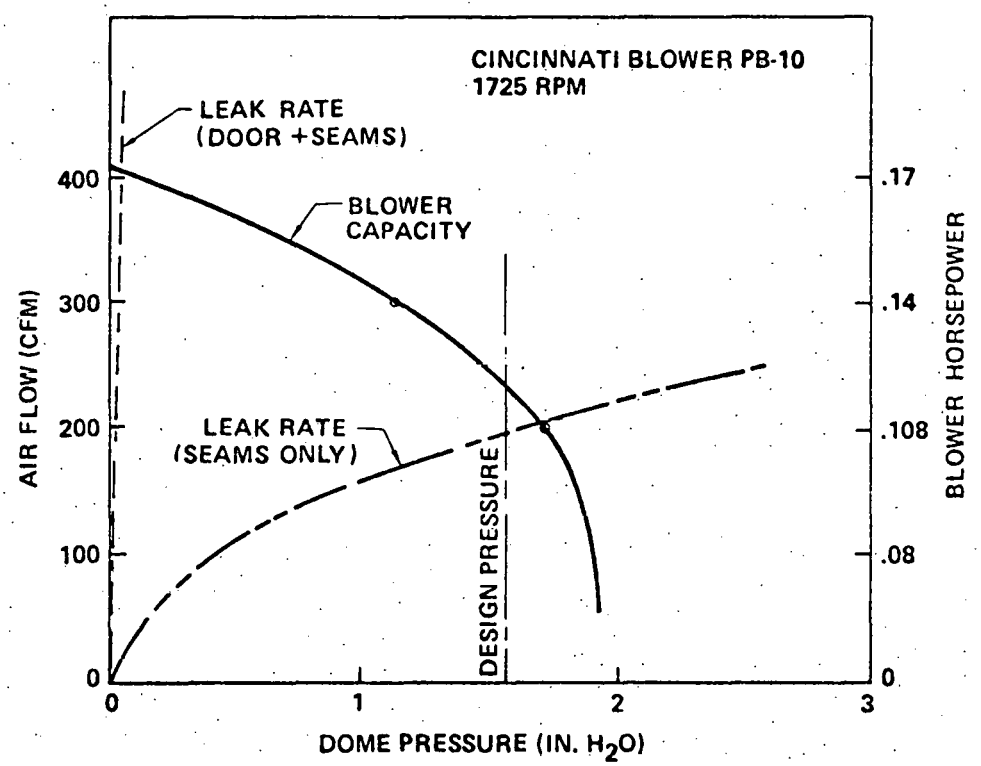

Figure 3.1-4 Transparent Enclosure Air Supply Design Data

$$Q = KL$$

Q = rate of leakage, cfm

where K = empirical constant, cfm/ft. length at 1.0 in. water pressure differential, K = 3 for curb attachment design

L = length of seal

Values of leakage rate at 1.0 in. water pressure differential were extrapolated to other pressures using a square root pressure relationship and plotted in Figure 3.1-4. As shown in the figure, a leak rate of about 195 cfm is expected at the design pressure of 3.9 cm (1.55 in.) of water. Approximately 0.1 hp will be consumed at this pressure/flow condition. The small difference between blower capacity and leak rate curves at the design pressure, will be eliminated by throttling with a variable damper at the blower inlet.

Inlet air to the blower will be filtered through a commercial cartridge filter (Model No. LM-6, manufactured by Cincinnati Fan Co.) which will be located outside the dome support ring as shown in Figure 3.1-1.

Dehumidification apparatus has not been included in the detail design. Analyses have indicated that condensation could occur on critical components inside the dome during certain winter temperature/humidity conditions. Accordingly, humidity and temperature data will be recorded and typical material/component specimens will be placed in the first domes erected at the Boardman test site. If condensation is predicted or occurs in these tests, de-humidifiers will be installed in domes for array tests.

Electrical power will be supplied to the 32 volt DC blower motor from an array of batteries. Batteries will be retained at near full-charge by an automatic charger operating with AC line power. This arrangement, although not necessarily optimized for PD hardware, was chosen for research experiment hardware based on reliability and availability considerations.

3.1.2 Structural Design

The transparent dome consists of a spherical Tedlar membrane supported by internal air pressure. The spherical shape is truncated at the base, where the Tedlar is attached to a steel ring. The principal

design parameters for the dome are:

Diameter	5.18 m (17.0 ft.)
Base Angle	60^{o}
Material	Tedlar
Thickness	0.10 mm (4 mil)
Internal Pressure (Max.)	0.038 N/cm^2 (0.056 psi)

The rationale for selecting the above design is developed in the following subsections:

3.1.2.1 Design Loads

The principal loads acting on the transparent dome are produced by the environment (wind, snow, ice and earthquake) and by the internal static air pressure.

The design wind loads are based upon annual extreme fastest-mile winds with a 50-year mean recurrence interval (Reference 3.1-2). These winds, for a height of 9.14 m (30 ft.), are reproduced from Reference 3.1-3. in Figure 3.1-5. Shown in the figure are two locations that have been discussed as possible pilot plant locations--Inyokern, California and Albuquerque, New Mexico--and the site to be used for the research experiments--Boardman, Oregon. The wind velocities are more severe at Albuquerque and are, hence, the ones used as the basis for the design loads. The wind velocity as a function of height above ground is shown in Figure 3.1-6 for all three locations. These profiles are based upon the following equation from Reference 3.1-4.

$$V_z = V_{30}\left(\frac{Z}{30}\right)^{\frac{1}{\alpha}}$$

where:

V_z = wind velocity at height z above ground

V_{30} = wind velocity at 9.14 m (30 ft.) above ground

α = a factor which is a function of ground roughness and

where the value of α is defined as:

α = 7; level or lightly rolling land with some obstructions; e.g., farm land with scattered trees and buildings and airports.

α = 5; rolling or level country broken by numerous obstruc-

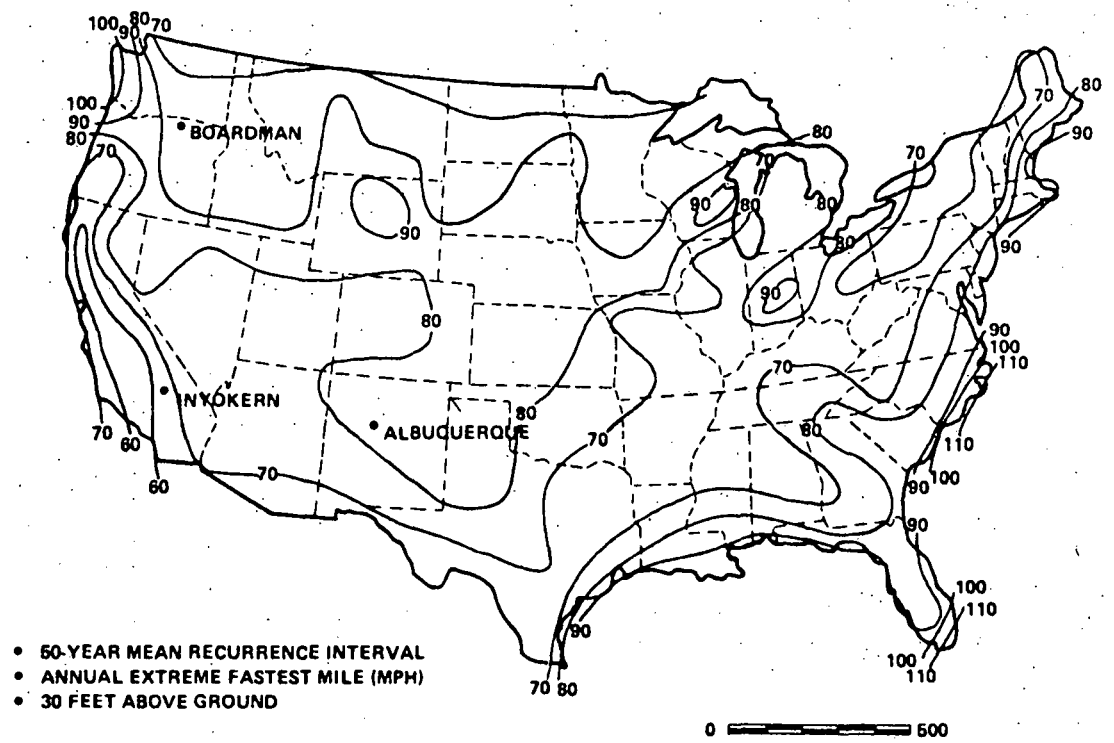

Figure: 3.1-5 Wind Speed - 50 Yr. Mean Recurrance Internal

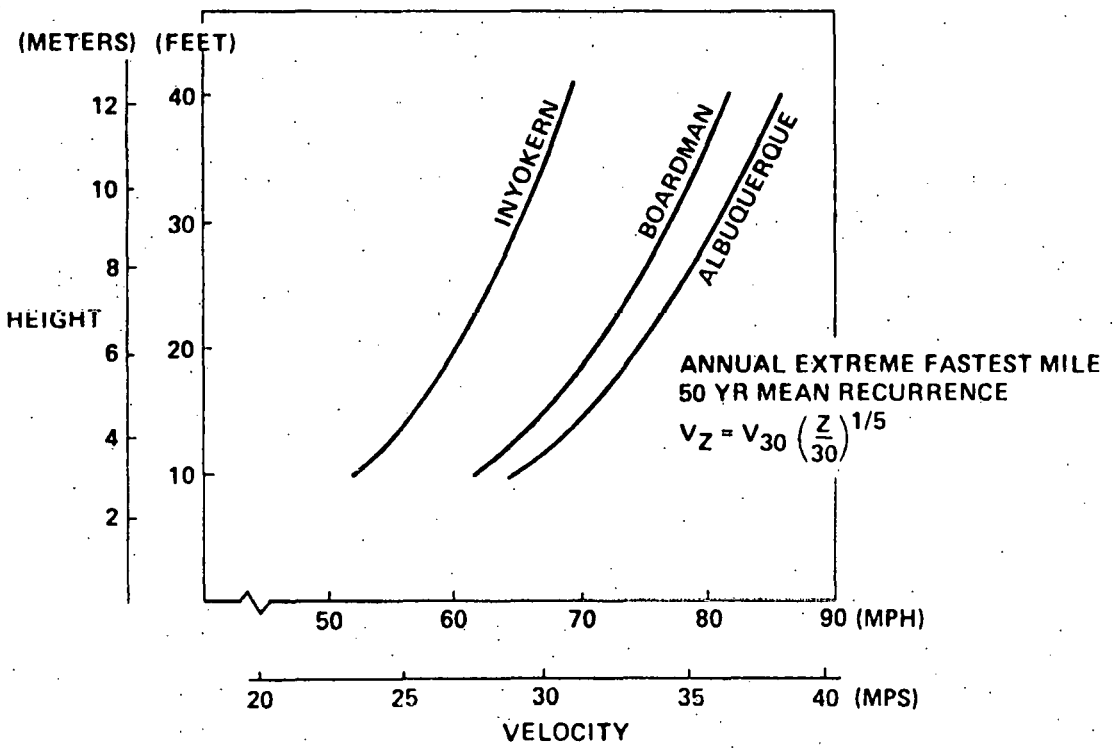

Figure: 3.1-6 Wind Velocity Variation with Height Above Grade

tions of various sizes; e.g.; suburbs where lots are 1/2 acre or more.

α = 3; broken surface with large obstructions; e.g., near suburbs with 1/4 acre or less lots and outskirts of large cities.

α = 2; large obstructions; e.g., center of large city.

A value of $\alpha = 5$ was used for determining the wind distribution on research experiment domes. The design parameter required to size the dome is the aerodynamic pressure, q .

$$q = 1/2 \rho V^2$$

where:

q = aerodynamic pressure

ρ = density of air

v = velocity of wind

The resulting pressure, P_i, on a point i of the dome is:

$$P_i = C_{P_i} \; q_i$$

where C_{P_i} is the pressure coefficient at point i on the dome. But, since the design equation used in sizing the dome has incorporated the pressure distribution, Cp, around the dome, only the value of the dynamic pressure is required. Also, since the design equation is based upon a sphere subjected to a uniform wind velocity, and the actual velocity on the dome is a function of height, an effective uniform dynamic pressure is used. The effective pressure obtained by integrating the pressure distribution over the frontal area of the dome is:

$$q \text{ effective} = 0.69 \; q \text{ max.} \qquad \text{for } \beta = 60^0$$

where $q \text{ max} = 1/2 \rho V_h^2$

V_h = wind velocity at the top of the dome

β = angle at which the dome is truncated

The corresponding wind velocity is:

$$V_{\text{effective}} = 0.83 \; V_h$$

The resulting design parameters for a base angle $\beta = 60^{o}$ are:

$V_{effective}$ 25m/sec. (56 mph)

$q_{effective}$ 0.038 N/cm^2 (0.056 psi)

The dome base connections must resist the combined aerodynamic lift and drag forces and the force produced by the internal pressurization. These loads are conservatively based upon the q at the top of the dome. The lift and drag forces are obtained from Figure 3.1-7. The upward lift due to internal pressurization, P_i, must be added to the aerodynamic lift to obtain the total upward force. The internal lift is given by:

$$F = P_i (R \sin\beta)^2$$

These loads are summarized below:

Aerodynamic Lift	9657 newtons (2171 lb.)
Aerodynamic Drag	2598 newtons (584 lb.)
Internal Lift	8158 newtons (1834 lb.)
Total Upward Force	17811 newtons (4004 lb.)

The transparent dome can withstand the weight caused by the following accumulation of precipitation without exceeding the dynamic pressure that would be caused by the design wind:

Snow	31.2 cm (12.3 in.)
Ice	4.6 cm (1.8 in.)

These capabilities exceed the accumulations expected.

The dome must also withstand a 0.85 "g" lateral load due to Zone 3 earthquake criteria (Section 3.2.2.2.3).

3.1.2.2 Configuration, Material, Size

The transparent dome is supported entirely by internal air pressure. Internal static pressure must be high enough to keep the dome in tension and thus in shape. This is accomplished by maintaining the internal pressure equal to or greater than the wind dynamic pressure. Wind deflection magnitude is a function of the wind velocity relative to the maximum design wind and the base angle at which the spherical dome is truncated. Figure 3.1-8 shows maximum relative radial deflections versus relative

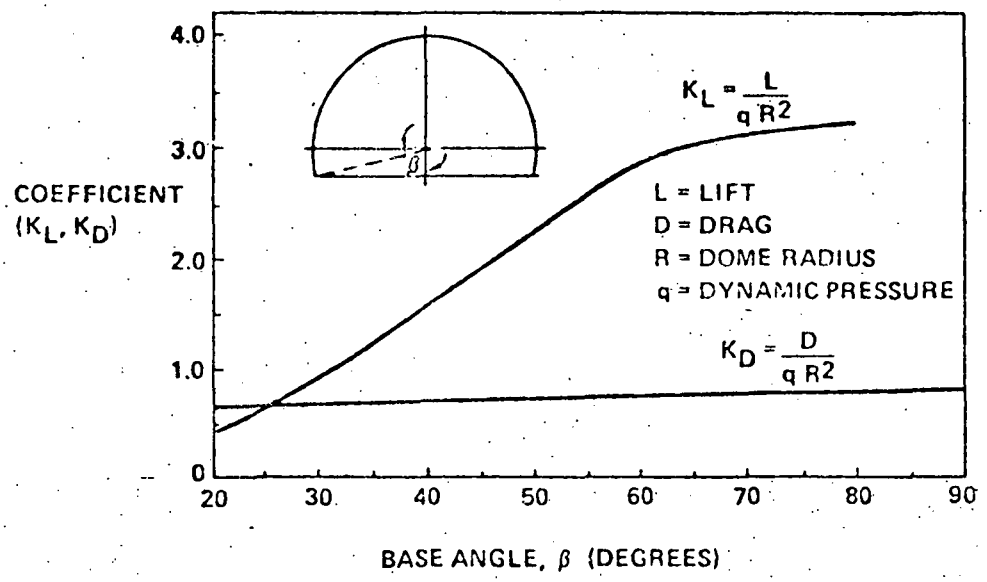

Figure: 3.1-7 Effect of Base Angle on Force Coefficients

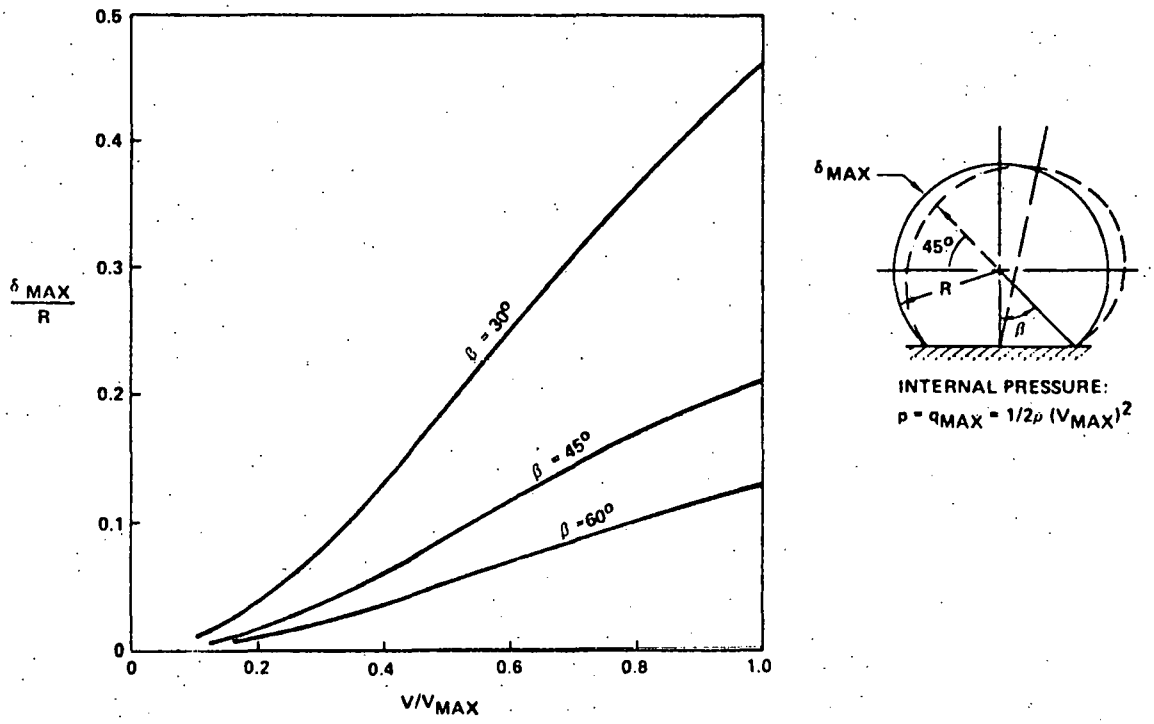

Figure: 3.1-8 Enclosure Deflection vs. Wind Velocity

wind velocity for domes with various base angles. Maximum radial deflection for a 60^{o} base angle at the maximum design wind velocity is 0.125 of the dome radius. Deflections for domes with smaller base angles are unacceptably large. To obtain a reasonable clearance envelope inside the dome for the reflective assembly, a minimum base angle of 60^{o} is specified.

Dome diameter is controlled by wind velocity and allowable stress of the material. The maximum stress in the material, as given in Reference 3.1-1 is:

$$S = 2.1q(\frac{R}{t})$$

where: S is the maximum material stress,
q is the dynamic pressure due to the wind velocity,
R is the dome radius,
t is the dome material thickness

The above equation includes the effect of internal pressure, which is assumed equal to the maximum dynamic pressure to maintain the shape of the dome. The maximum stress given by the equation is a peak stress that may occur locally at any point in the membrane depending on direction of the wind.

As discussed earlier, Tedlar has been selected for the enclosure material. A thickness of 0.10 mm (4 mil), the thickest presently available, was selected to obtain the largest possible dome size. A yield strength for Tedlar of 27.6 MN/m^2 (4000 psi) was used in the design of the dome. Tensile test data from research experiments (see Section 6.2.1) has justified the use of the above yield strength for detail design of research experiment domes.

The design allowable stress is taken as 75 percent of the material yield to allow for reduced joint efficiencies and for local stress concentrations at tiedowns or other discontinuities. The material, when new, has good elongation characteristics, with ultimate tensile strength approximately twice the yield stress. Therefore, local stress concentrations exceeding the above allowance, caused by unexpected design or manufacturing problems or by abnormally high wind gusts, will be accommodated by local yielding of the material, resulting in redistribution of internal loads

to lower material stress levels.

The enclosure size is obtained from data presented in Figure 3.1-9, which shows dome diameter versus effective wind velocity for 0.10 mm (4 mil) Tedlar at different yield stresses. DuPont information and results of research experiment tests indicate that yield stress for Tedlar will not significantly change with exposure until embrittlement is reached. Therefore, the curve for the initial yield stress of 27.58 MN/sq. m (4000 psi) is used. Effective wind velocities versus dome diameter are indicated for three typical locations by the dashed curves on the figure. The Albuquerque, N.M. location is used, which has the most severe environment of the three, giving a dome diameter of 5.18m (17.0 ft.) at an effective wind velocity of 25 m/sec (56 mph).

The effective wind velocity of 25 m/sec (56 mph) requires an internal pressure of .038 N/cm^2 (0.056 psig) to equal the effective dynamic wind pressure. Under design wind environment, maximum velocity at the top of the dome will exceed the effective velocity. However, in this region pressure coefficients are negative (Reference 3.1-1) and identation of the dome will not result. The above internal pressures cause a constant uniform membrane tensile stress of approximately 5.1 MN/sq. m (740 psi). Results of creep tests, presented in Section 6.2-3 indicate that no significant dimensional changes in the dome will occur with time.

Total lift and drag forces calculated conservatively for maximum wind velocity at the height of the dome are 17.81 kN (4004 lb.) and 2.60 kN (584 lb.), respectively. These forces are resisted with adequate margin of safety by the concrete and steel foundation. Foundation stresses are low and minimal reinforcing is required to distribute hold down forces into the concrete. Soil bearing pressures due to foundation weight are less than 9.58 kN/m^2 (200 $lb./ft.^2$) and no soil stabilization requirement is anticipated.

A preliminary earthquake analysis of the dome using the Uniform Building Code approach (Reference 3.1-3) has been made. Using the most conservative values for all coefficients gives an equivalent lateral force of 0.86 g for Zone III earthquake design (Section 3.2.2.2.3). Applying this acceleration to the mass of the dome material plus the mass of the enclosed air results in lateral deflections which are less than the clearances

established for maximum wind deflection. Film stresses for the earthquake loading will be considerably less than for the design maximum wind condition because the large aerodynamic lift forces, which contribute most to the maximum film stress, will not be present.

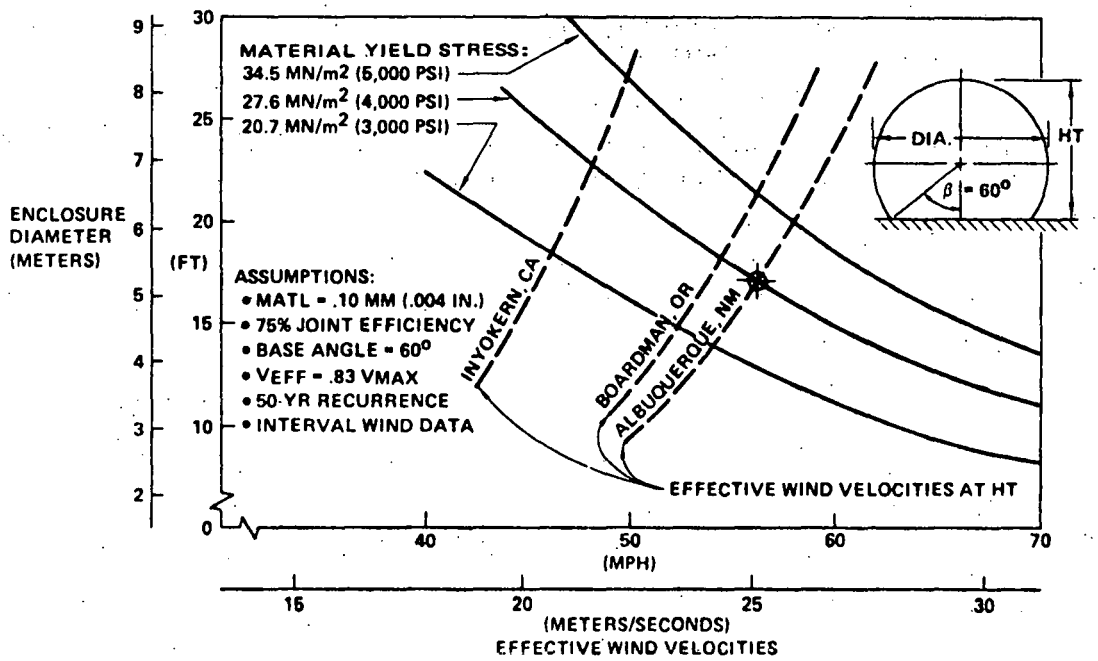

Figure: 3.1-9 Enclosure Diameter vs. Effective Wind Velocity for 0.10mm (4 mil) Tedlar

3.2 REFLECTIVE ASSEMBLY

Design of the reflective assembly involved configuration studies, materials studies and structural design. Results of these studies are discussed in this section.

3.2.1 Configuration

Configuration studies on the reflective assembly were aimed at selecting the most cost-effective shape and support technique for the membrane reflector, consistent with meeting optical performance requirements. The reflective assembly selected for research experiments as a result of these studies is shown in Figure 3.2-1. It consists of a 4.57 m (15 ft.) diameter ring of aluminum tubing with a circular reflective surface of 0.05 mm (2 mil) thick aluminized Mylar bonded to a flat, rigid urethane foam surface, cast onto the ring. The ring is supported at three points by tubular aluminum arms welded to the ring and bolted to a hub plate.

Earlier studies evaluated a reflective assembly which consisted of a hexagonal-shaped aluminized Mylar film, pre-stressed by spring-loaded edge members attached to three 120^{0} spaced sides of the hexagon. Recognizing that a circular reflector could have about 20% more area within a given clearance envelope than a hexagonal reflector, a study was initiated to develop a more effective concept. Nine reflector and support concepts were evaluated for their effective areas, relative costs, manufacturing feasibility, and optical/structural characteristics. Based on these studies, the present concept was selected.

It is essential that the reflector substrate film has a highly specular (smooth) surface, low cost, and sufficient strength to carry a load 6.9-13.8 MN/m^2 (1000-2000 psi) without significant creeping. The film candidates evaluated for this program, their reflectances, respective costs and strengths are shown in Table 3.2-1. From the standpoint of reflectance, strength and cost, Mylar (polyester) was selected for research experiment hardware. Reflectance tests on Mylar showed that various types produced different reflectance values. The highest surface quality material (DuPont designation 200 XM648A) was selected on the basis of these tests. Vacuum deposited aluminum will be applied to the "adherable" side of this material since it has a higher reflectance than the back "non-adherable" side.

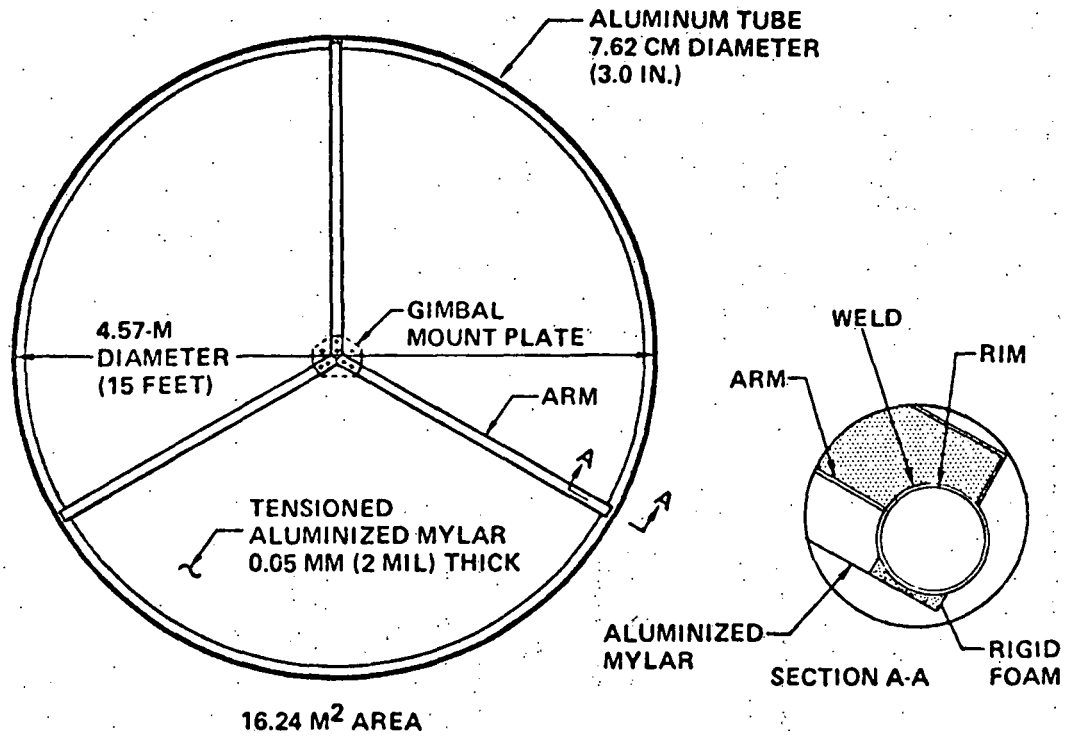

Figure: 3.2-1 Reflective Assembly Design for Research Experiments

Table: 3.2-1 Reflector Material Properties

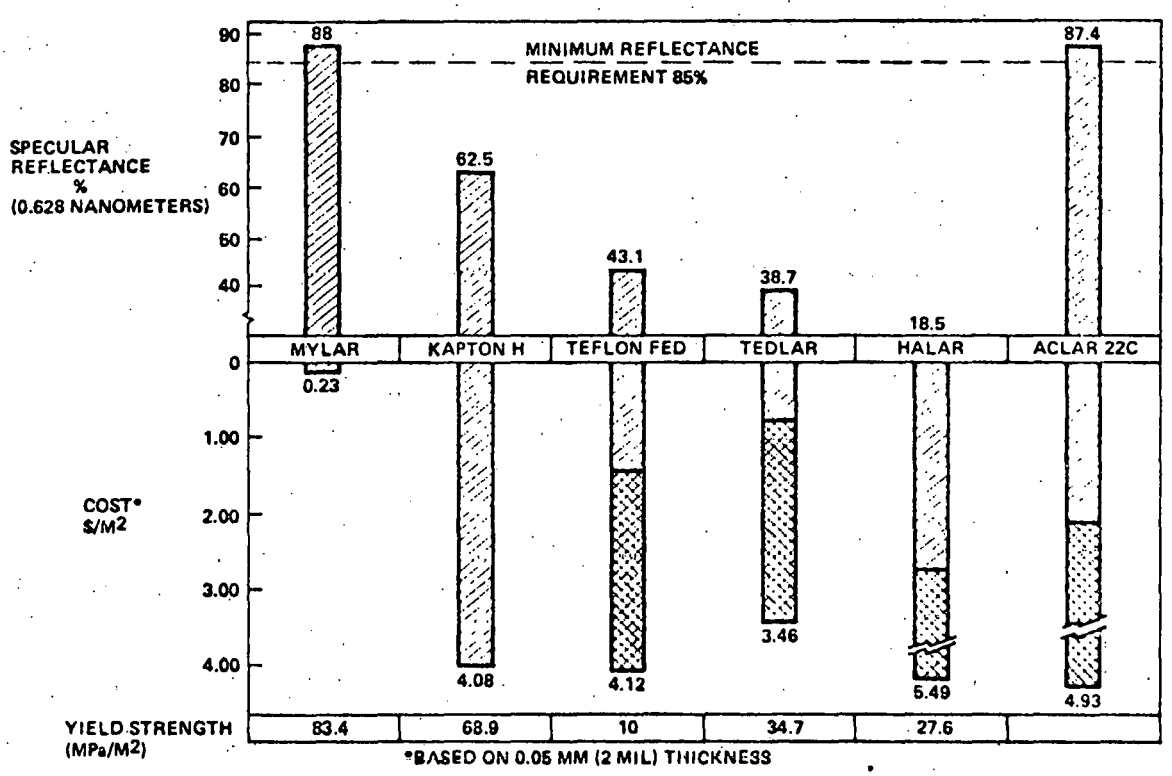

An unprotected aluminum coating has been selected for the research experiment membrane reflector. This selection was made on the basis of cost, solar reflectance, and long-term stability when operating in a protected environment. Candidate coating combinations which were evaluated are shown in Figure 3.2-2. Preliminary cost and reflectance data (including cost of plastic film) were established through discussions with coating manufacturers, publications, and prior experience. Letters of inquiry were sent to five manufacturers, and followed up by telecon discussions.

Long-term stability of the reflective coating is an important consideration because of the costs associated with replacement of membrane reflectors. Data show that the largest change in reflectance during aging (growth of the natural oxide film) occurs in the vacuum ultraviolet wavelength region, and that the rate of change decreases with time. Data from Boeing tests, in which aluminized mirrors were measured after a 9-year period, show that no significant change in reflectance during aging (growth of the natural oxide film) occurs in the vacuum ultraviolet wavelength region, and that the rate of change decreases with time. Data from Boeing tests, in which aluminized mirrors were measured after a 9-year period, show that no significant change in reflectance occurred in the wavelength region larger than about 300 nano-

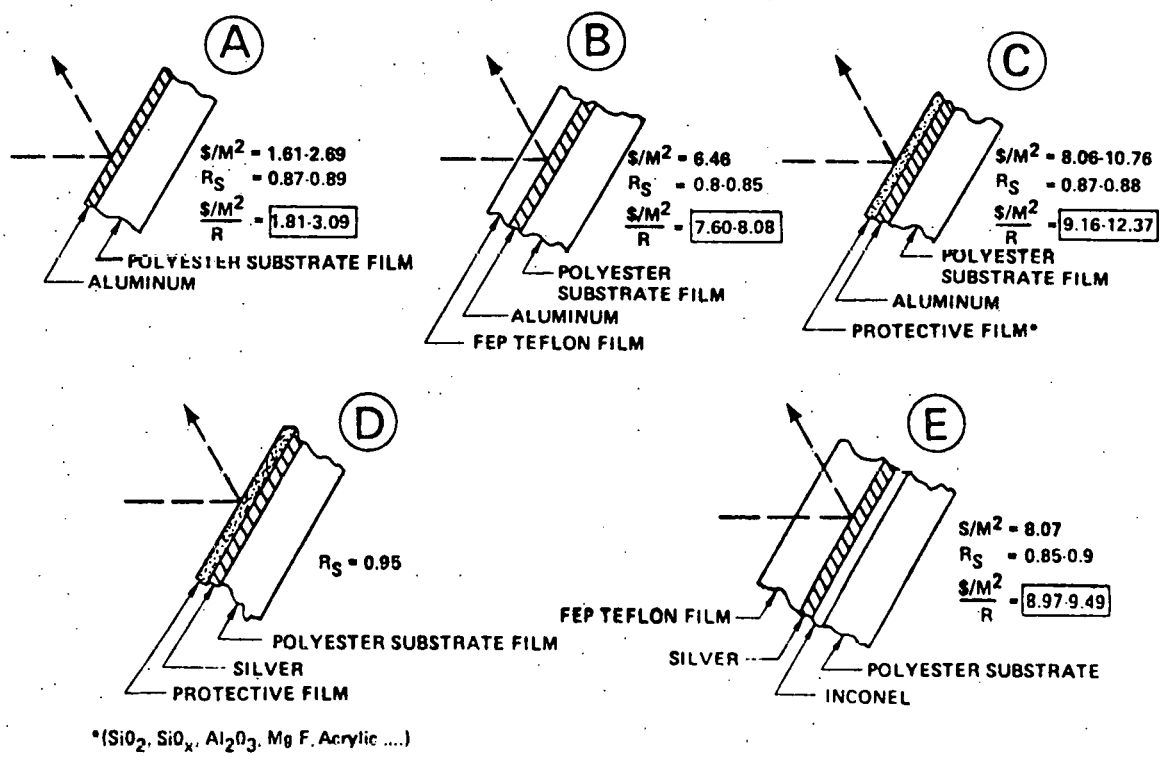

Figure: 3.2-2 Candidate Reflective/Protective Coatings

meters. Specimens had a solar reflectance of about 89.6% in 1966, and values of 89.5, 89.4, and 89.5% in September 1975. It should be noted that the Boeing specimens were stored in an environment of nearly constant temperature, relative humidity 30-50%, and in the dark. Results of research experiments showed that an unprotected aluminized Mylar specimen degraded from approximately 88.8 to 87.5% at a wavelength of 0.628 nanometers, in the accelerated simulated sunlight test. The specimen was exposed for 500 hours in Xenon lamp radiation containing about 9.5 equivalent air-mass 2 ultraviolet suns.

Considering the above data and cost savings, an unprotected aluminum reflector coating was selected. In the event that unforeseen degradation occurs to unprotected aluminum during testing, an oxide or acrylic overcoated front-surface aluminum reflector will be specified in the Pilot Plant PD.

3.2.2 Structural Design

Reflector size is controlled by the size of the transparent dome, less clearance for wind deflection. A nominal radial clearance between the reflector and dome of 0.30 m (1.0 ft.) has been established (Section 3.1.3.2) for the research equipment. This clearance establishes the maximum reflector outside diameter of 4.58 m (15 ft.).

3.2.2.1 Design Loads

The reflective assembly is protected from direct contact with the major elements of the environment (wind, snow, ice) by the transparent dome. There could, however, be some indirect effect of wind on the reflector through unsteady aerodynamic buffeting of the dome. Also, the Pilot Plant specifications call for structural design subject to a Zone 3 earthquake environment. Other design considerations are gravity, temperature, and loads produced by the design concept of the reflector; i.e., tensioning methods and control systems.

The lateral "g" loading for earthquake design is given in Reference 3.1-2 as:

$$g = \frac{V}{W} = ZKCS$$

where

V = total lateral load at the base

W = total dead load

Z = numerical coefficient related to a seismic zone

K = numerical coefficient related to the type of structure

C = base shear coefficient dependent upon the dynamic response of the structure

S = coefficient dependent on soil properties and relative natural period of the soil and structure

Evaluating these coefficients by using the most conservative value for each coefficient results in a design g load factor of 0.86 at the base of the reflective assembly support structure. This value is used for the design of the entire structure.

3.2.2.2 Design Analyses

3.2.2.2.1 Membrane Stress Analysis

As discussed in Section 3.2.1, a passively tensioned circular membrane reflector has been selected. The membrane will be prestretched to a uniform biaxial tension of 6.89 MN/m^2 (1000 psi), and bonded to a circular ring. Mylar material of 0.05 mm (2 mil) thickness was selected for the reflector membrane. This thickness material is less susceptible to damage from handling than thinner films, yet does not require large stretching forces and heavy support structure necessary with thicker films.

Variations in temperature and humidity will cause changes in membrane stress. Differential expansion of the Mylar and the aluminum frame over an extreme temperature range of 89°C (160°F) will result in a change of plus or minus 26 percent from the nominal membrane stress of 6.89 MN/m^2 (1000 psi). The effect of humidity on membrane stress is less pronounced than that of temperature. It will usually tend to reduce the effect of temperature because relative humidity tends to decrease as temperature increases.

Long term creep tests of the Mylar reflector material at 60°C (140°F) were conducted at stress levels of 3.45 MN/m^2 (500 psi) and 6.89 MN/M^2 (1000 psi). No creep was observed at the lower stress level, but at the higher level creep strain stabilized at 0.15% to 0.18% (Section 6.2.3.) These data indicate that loss of membrane tension due to creep relaxation will not have significant effect on reflector performance.

3.2.2.2.2 Gravity Deflection

Maximum gravity deflection of the 4.58 m (15.0 ft.) diameter circular membrane stretched horizontally to 6.89 MN/m^2 (1000 psi) is 0.26 cm (0.10 in.). A more convenient way of expressing this deflection is in terms of the reflec-

tor focal length corresponding to the parabolic deflection mode that the membrane assumes. Figure 3.2-3 shows focal lengths for a uniformly-stretched circular Mylar membrane as a function of membrane stress and angle of tilt of the reflector plane from vertical. Focal length is independent of membrane thickness and diameter. Minimum focal length for the nominal membrane stress of 6.89 MN/m^2 (1000 psi) is 502 m (1647 ft.) when the reflector plane is horizontal. This is approximately the same as the maximum heliostat to target distance for the Pilot Plant. The axis of the deflected parabolic surface remains normal to the plane of the reflector support frame regardless of the angle of tilt. Therefore, gravity deflections will not affect pointing accuracy.

The reflector support structure consisting of the circular ring and three support arms is of tubular aluminum construction. The structure is designed by stiffness, and stress levels are very low. Maximum out-of-plane deflection of the circular ring between supports due to gravity, when horizontal, causes a maximum angular deviation of a small portion of the reflector surface from the nominal reflector plane of 0.05^{o}, which will have negligible effect on reflector performance. The vertical deflection at the ends

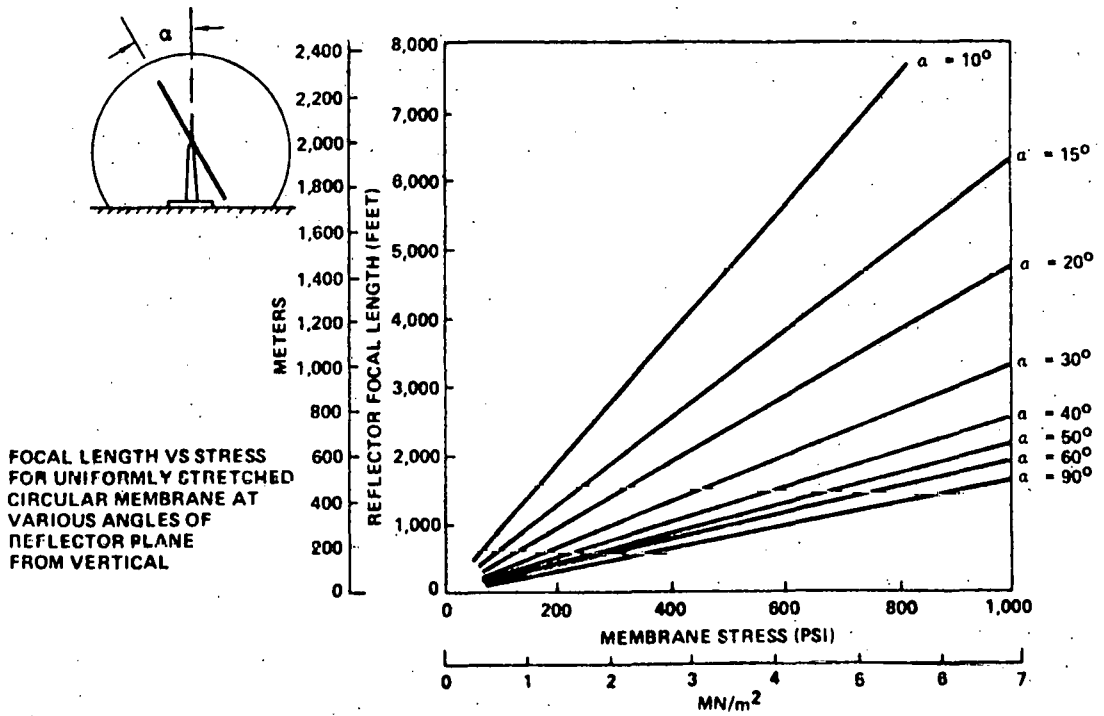

Figure 3.2.3 Membrane Deflection Due to Gravity

of the support arms causes a rigid body downward translation of the ring of 0.74 cm (0.29 in.). Adequate clearance between the reflector plane and the central mounting hub is provided to accommodate the vertical deflection of the ring plus the sag of the membrane so that defocusing will not occur with the reflector in the horizontal position.

3.2.2.2.3 Earthquake Analysis

A conservative estimate of maximum lateral deflection of the reflector support structure has been made. Using the equivalent lateral load of 0.86 g, derived in Section 3.2.2.1 for a Zone 3 earthquake, the maximum lateral deflection of the reflective assembly is 2.5 cm (1.0 in.). Adding this to the maximum earthquake dome deflections (Section 3.1.2.2) gives maximum possible relative deflections of reflector and enclosure which are less than the clearances provided for wind deflection.

3.2.2.2.4 Buffeting Analysis

Although the wind does not impact the reflector directly because of the protection provided by the transparent dome, it could have an indirect effect due to unsteady aerodynamic buffeting of the dome. Buffeting of the dome will produce air movement inside the dome and if the movement is severe enough, buffeting of the reflector will result. The possibility of reflector buffeting is not considered a structural problem, however, buffeting of the reflector could be detrimental to the optical performance of the reflector. Even if significant buffeting exists, the phenomenon will occur at intermittent intervals and, thus, overall efficiency may not be affected significantly. The magnitude of the effect will depend on the response of the dome due to the wind and the subsequent coupling of this response with the reflector. The dynamic response is amplified when the frequency of the structure matches the gust frequency.

The effect of buffeting will be evaluated during full-scale testing; and if a problem does exist, appropriate means will be employed to alleviate the problem, i.e., tiedown interior point of the reflector, increase stiffness of reflector, etc.

3.2.2.2.5 Thermal Stress Analysis

Thermal gradients are small enough that thermal stresses in the aluminum reflector support structure are insignificant. An analysis was made to determine possible thermal stresses due to differential expansion of the

aluminum support ring and the cast polyurethane foam ring to which the reflector film is bonded. Because of the very low modulus of the foam, it was found that an extreme temperature change of 38°C (100°F) from the fabrication temperature would increase the bond shear stress between the foam and the aluminum by only 0.69 KN/m^2 (0.1 lb/$in.^2$).

3.2.2.2.6 Vibration Analysis

The dynamic response characteristics of the reflector system subjected to intermittent step inputs from the stepper motor are presented in Figures 3.2-4 through 3.2-6.

Figure 3.2-4 shows the response of the reflective assembly as a function of the relationship between the duration of the input pulse and the structural frequency. This relationship is expressed as the frequency ratio, B, which has been calculated as 1.21 for the present system. The corresponding amplification of 0.85 means that there will be an initial overshoot amplitude equal to 85% of the input step. The response after the initial step depends on the damping in the system and the phasing of stepper motor input.

Analysis shows that aerodynamic damping available at the velocities experienced during the normal tracking mode of operation is only .05% of critical. Because of the present welded construction of the assembly structural damping is assumed to be negligible. Figure 3.2-5 shows the effect of damping after five seconds (expected minimum period of step inputs during normal tracking). With .05% damping the amplitude of oscillation is still 96.3% of the initial amplitude after five seconds, therefore, damping can be ignored when considering the response of the system to repeated step inputs.

Figure 3.2-6 shows the undamped reflector response (solid curve) to the initial step input (dashed curve) with four alternative phasings for the beginning of a subsequent step. Figure 3.2-7 shows the response of the reflector to repeated steps for these four different phasings. For the worst case (Case I) the amplitude of oscillation will built up to exceed the 0.1° accuracy tolerance after five steps. The responses indicated in Figure 3.2-7 indicate worst conditions which could only occur if the structural frequency is some exact multiple of the stepping rate so that consistent phasing is maintained. This is very unlikely to be the case and the possible amplitude build-ups indicated are not expected to occur. If excessive amplitude build-up is observed in actual operation, additional damping will be incorporated into the system to suppress it.

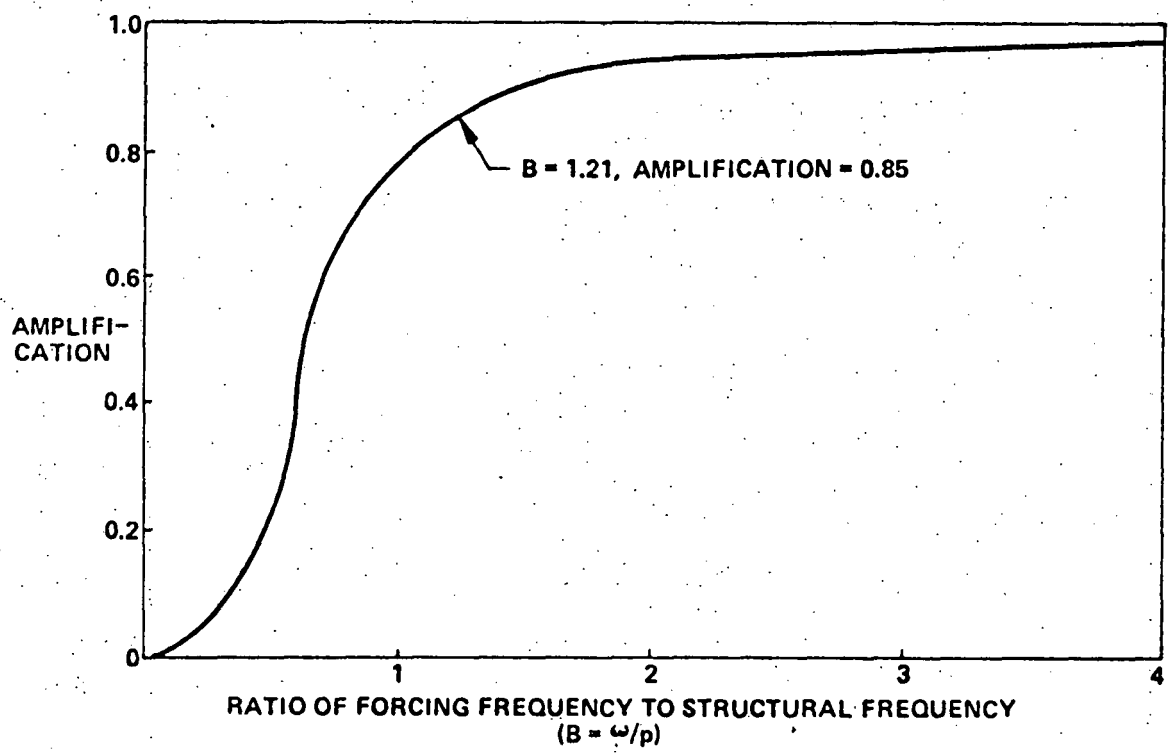

Figure: 3.2-4 Reflector Response to Initial Step versus Frequency Ratio

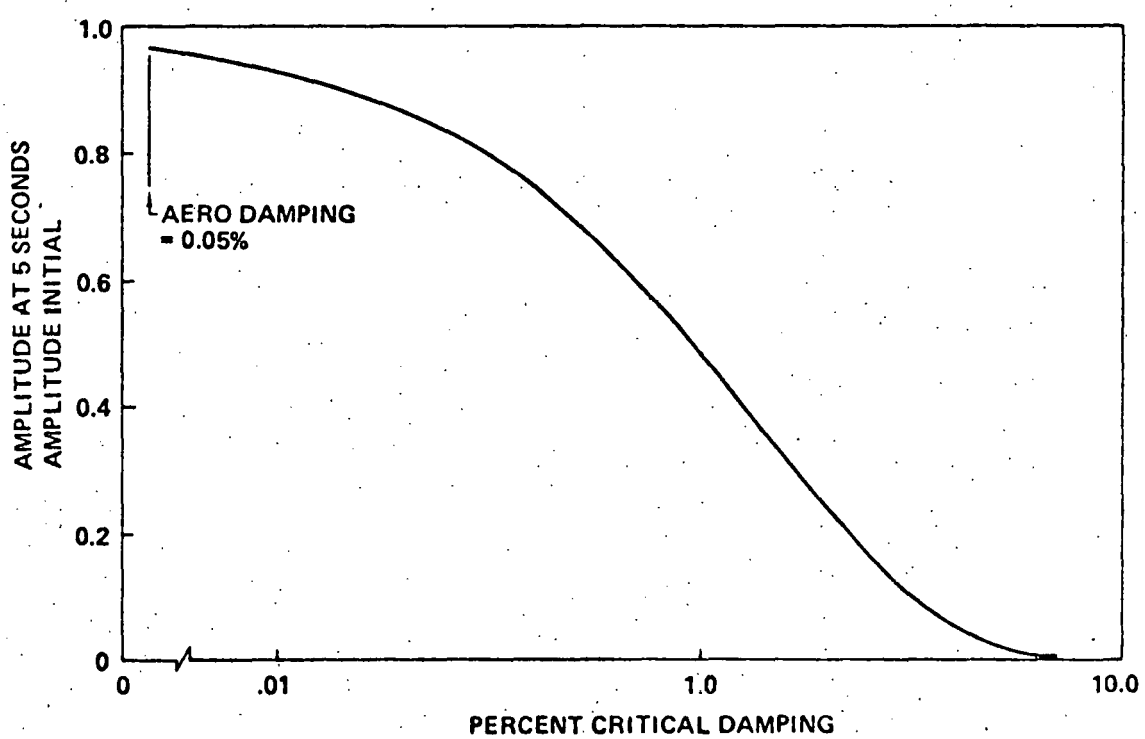

Figure: 3.2-5 Damped Amplitude of Oscillation After 5 Seconds

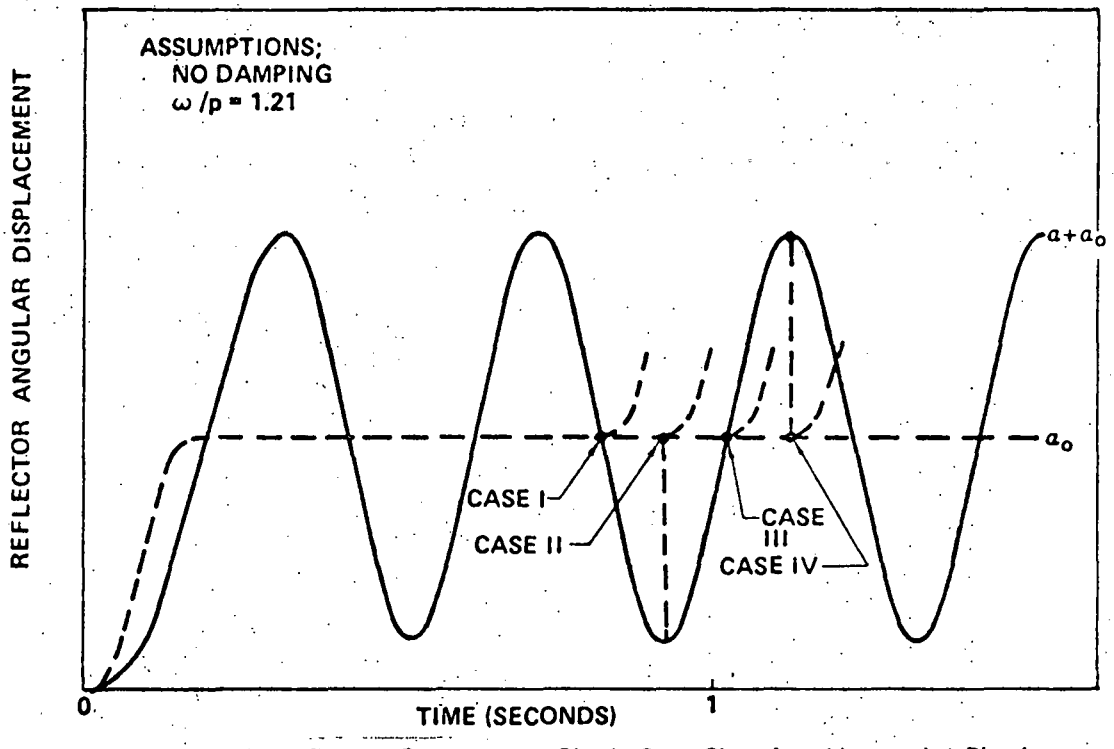

Figure: 3.2-6 Reflector Response to Single Step Showing Alternative Phasings for Beginning Subsequent Step

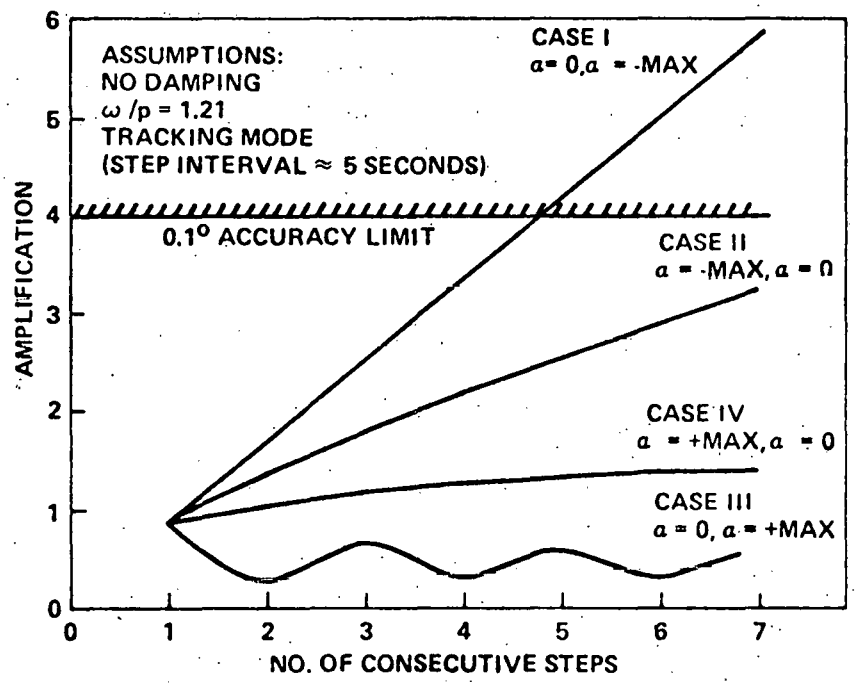

Figure: 3.2-7 Reflector Response versus Number of Consecutive Steps for Different Phasings

The response of the reflector during emergency stow operation is shown in Figure 3.2-8. The response tends to oscillate within a narrow band, never building up to excessive amplitude.

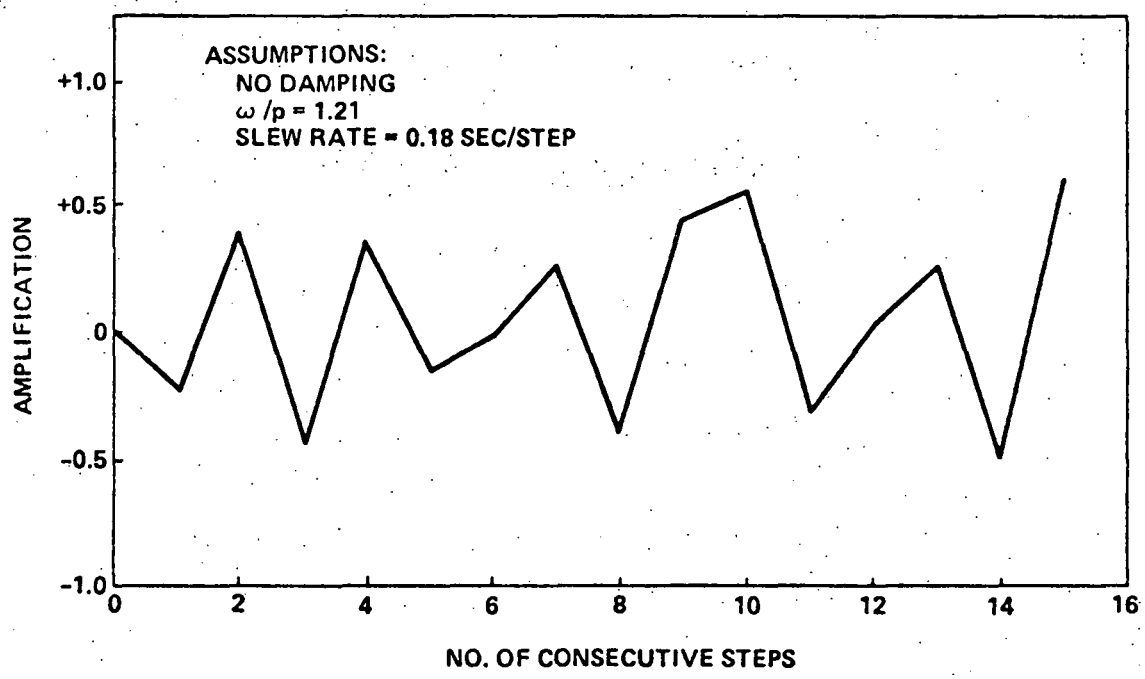

Figure: 3.2-8 Reflector Slew Response

3.3 DRIVE AND CONTROL ASSEMBLY

The primary function of the drive and control assembly is to position the the reflective assembly so that the solar image is reflected onto the central receiver. The sun's rate of progression (to an observer on the earth's surface) through the sky is such that positioning control of the reflector could occur incrementally at intervals of several seconds. Ephemeris data for a particular site may be tabulated or can be computed (with the addition of a correction factor). A proper gimbal mechanism, a small angle-stepped incremental drive actuator, solid state electronics and the solar-reflector-receiver geometric equations form the elements suitable for the development of a digital controller as the solution to this particular problem-application.

3.3.1 Configuration

The general configuration of the research experiments drive and control assembly is representative of the PD baseline assembly design. The research experiments drive and control system schematic (Figure 3.3-1) illustrates the configuration in detail. Included are 3 heliostat assemblies and one field controller with interfacing peripherals. The two drive actuators position the 2-axis gimbal mechanism, which supports the reflective assembly, in elevation and azimuth. The electronic transmission unit receives input commands and provides the necessary electrical power to the drive actuators. The field controller includes a mini-computer and an interface controller for the teletype, the time-of-day clock, the remote panel, the operator panel, and the heliostats. The field controller contains a software program which processes ephemeris data and individual heliostat geometric data to provide input digital step commands for each specific heliostat drive axis.

3.3.1.1 Control Loop Baseline Design

The type of heliostat control is an open-loop system with incremental positional feedback. Open loop control is performed by commanding the reflective assembly to a predicted angle based upon the known geometric relationship between the sun, the heliostat, and the central receiver. The actual control method used provides an additional step update signal to achieve synchronization between the number of steps commanded and the number registered. Figure 3.3-2 illustrates the method of digital step tracking used in the control system.

3.3.1.2 System Operation Capabilities

The requirements were defined in Section 2.0. Pursuant to these requirements, the drive and control assembly is configured with capabilities described in the following. The modes of operation provided are:

(1) Track
(2) Standby
(3) Shutdown
(4) Alignment
(5) Manual

The track mode will accomplish the placement of the reflected solar image upon the receiver target with a 1-sigma orientation accuracy of approximately 0.057^{o}. The standby mode will accomplish the placement of the reflected solar image to a position offset from the receiver target approximately 7 ft. in the azimuth direction. This mode will demonstrate removal of the solar image from the receiver target in the required 40 seconds, and re-acquisition to the track mode. The shutdown mode will accomplish the positioning of the reflective assembly (heliostat) in the shutdown (or stowage position.) A slew rate of 0.125^{o}/sec is employed during the shutdown mode. The shutdown (stowage) position is 0^{o} in elevation (reflective surface horizontal and upward), and 0^{o} (true south) in azimuth. The alignment mode provides the command/control function identification of the heliostat-receiver relative geometry, which is necessary for the original heliostat orientation and subsequent realignment following maintenance procedures.

3.3.1.3 Hardware Design

Table 3.3-1 illustrates the breakdown of the drive and control assembly into major hardware component areas. These areas will be described in the following sections.

3.3.1.3.1 Drive Actuator

The drive actuator function is to provide small angle step increments to a reflective assembly rotational axis. There are 2 drive actuators per heliostat, (as shown in Figure 3.3-3) one for the azimuth rotational axis and the other for the elevation rotational axis. Each drive actuator includes a stepper motor of 1.8^{o}/step, 40 oz-in of output torque, detent torque, and bi-directional capability. The motor weighs 1.6 lbs. (0.7 k g), has a frame diameter of 5.6 cm (2.2 in) and a shaft diameter of 0.64 cm (0.250 in.). The mechanical gearing is accomplished with a harmonic drive unit of 80/1 gear reduction (and torque multiplication) and over 200 in-lbs of output torque capability. Feedback is provided by the actuator-contained optical encoder, which provides 1000 cycle/revolution resolution, with TTL-compatible self-contained electronics. The drive actuator is manufactured as a cartridge assembly and is interchangeable and replaceable on the gimbal mechanism without removal of the reflective assembly or gimbal mechanism.

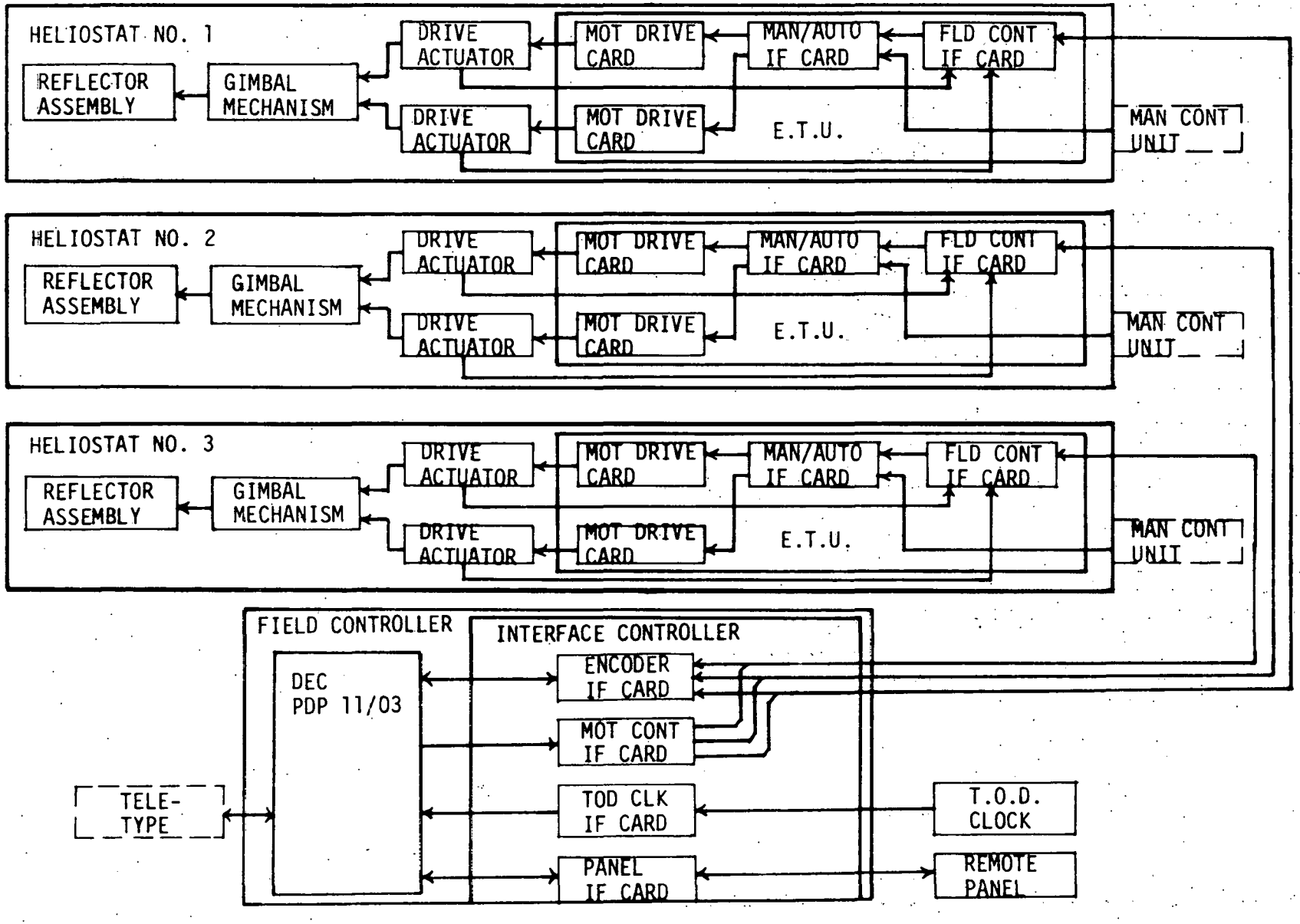

Figure: 3.3-1 Research Experiments, D&C System Schematic

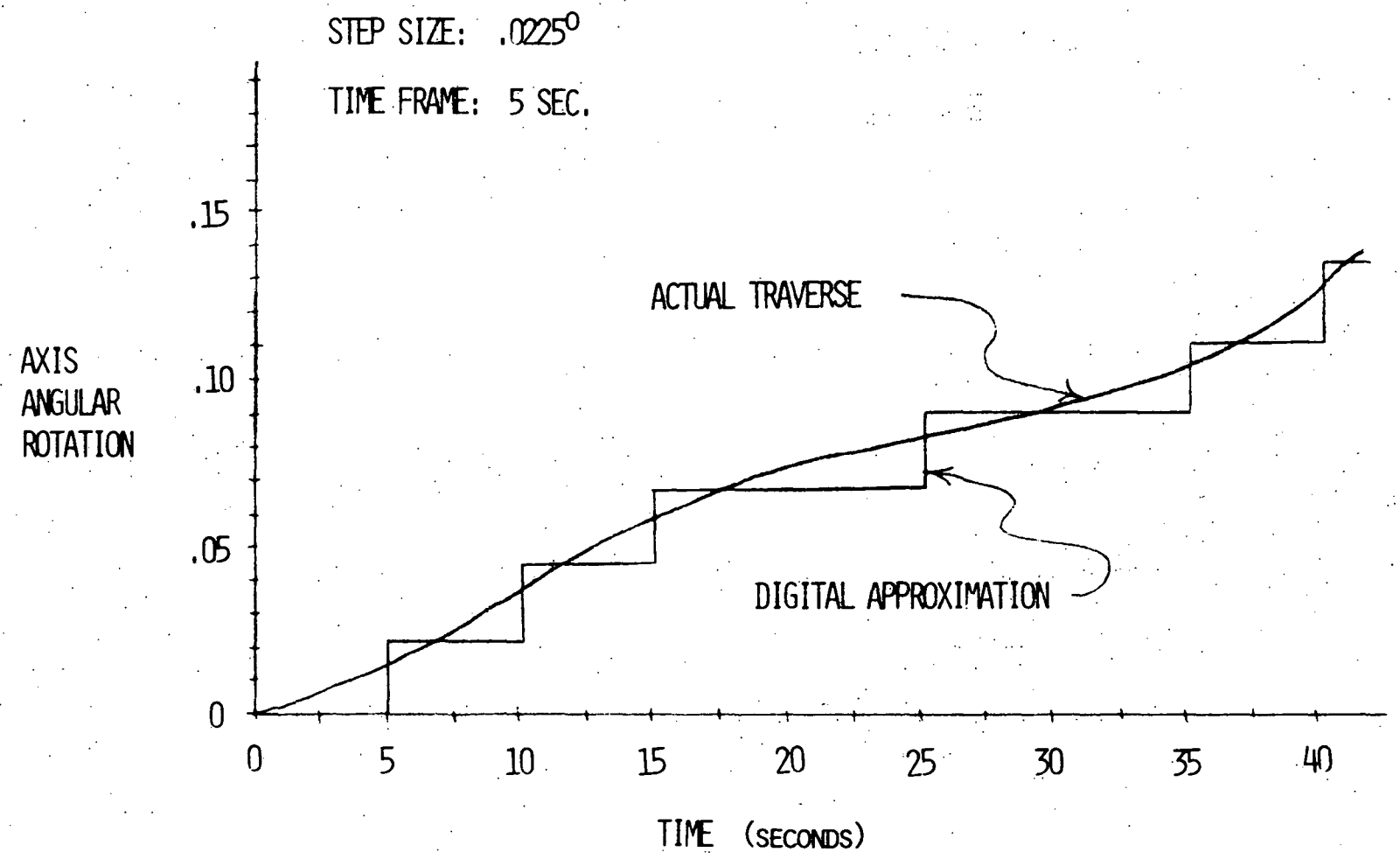

Figure: 3.3-2 Reflector Step Tracking

The drive actuator package provides an output shaft rotational step of 0.0225^{o}/ step. The configuration of the drive actuators is identical to the baseline design.

3.3.1.3.2 Drive Structural Support Mechanism

Figure 3.3-3 illustrates the configuration of the 2-axis gimbal mechanism necessary to drive the reflective assembly. The 2 axes are orthogonal, one for azimuth and one for elevation, and configured for dynamic balance for optimization of endurance and reliability. The gimbal mechanism is configured for ease of replacement or maintenance and is identical for research experiment to the PD baseline gimbal mechanism.

3.3.1.3.3 Heliostat Control Transmission

Figure 3.3-4 illustrates a block diagram of the control transmission interface at each heliostat. The interface consists of a collection of electronic circuit cards and individual DC power supplies housed in an enclosure called an Electronic Transmission Unit. This unit is portable, and lightweight, and is louvered to afford adequate ventilation for the two open-frame power supplies (which contain overvoltage protection). The interface provides for transmission of the reflective assembly positioning commands via the field controller or the manual control unit at the heliostat. The electronic cards will be accessible and easily removal for maintenance purposes.

Table: 3.3-1 Drive and Control Assembly

1. Drive Actuator (2/heliostat)
   - A. Stepper motor
   - B. Harmonic drive actuator
   - C. Drive bearings
   - D. Optical encoder
2. Drive Structural Support (1/heliostat)
   - A. 2-axis gimbal mechanism
   - B. Counterweight
3. Heliostat control transmission (1/heliostat)
   - A. Electronic control box
     1) Motor drive cards
     2) Manual/automatic interface card
     3) Computer decoder card
     4) Power supply modules
   - B. Manual remote control box
   - C. Limit switches
4. Central controls interface
   - A. Field microprocessor controller
     1) Electronic chips: CPU, PROM, RAM, etc.
     2) Power supply modules
     3) Ephemeris data
     4) Processor equations and Programming
   - B. Cabling and wiring
5. Alignment

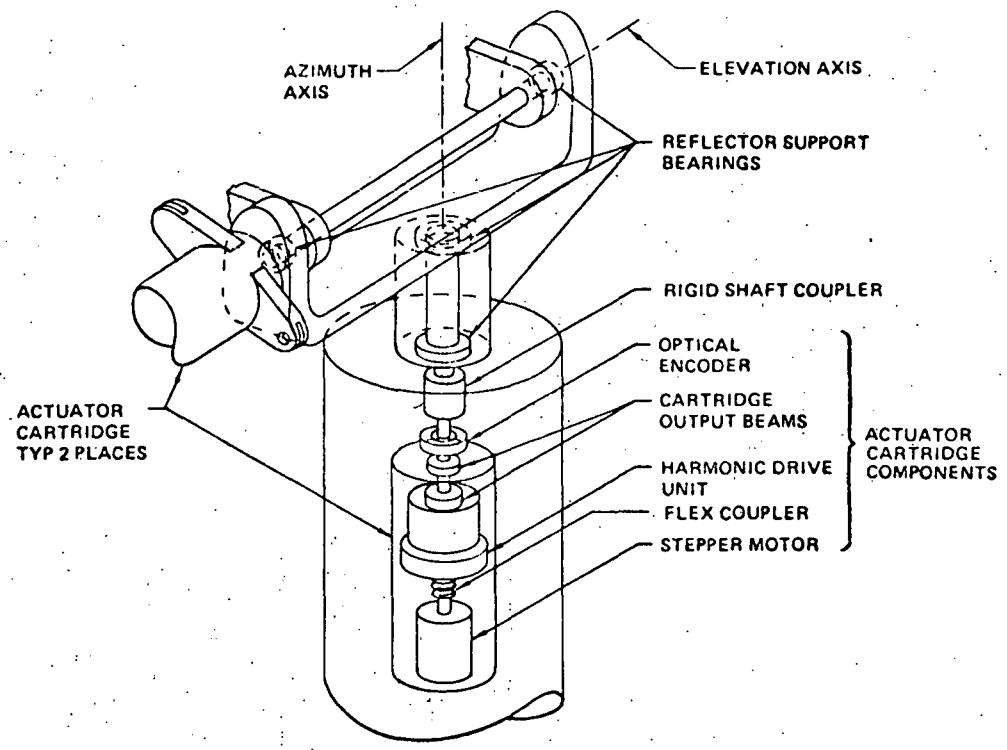

Figure: 3.3-3 Gimbal Configuration

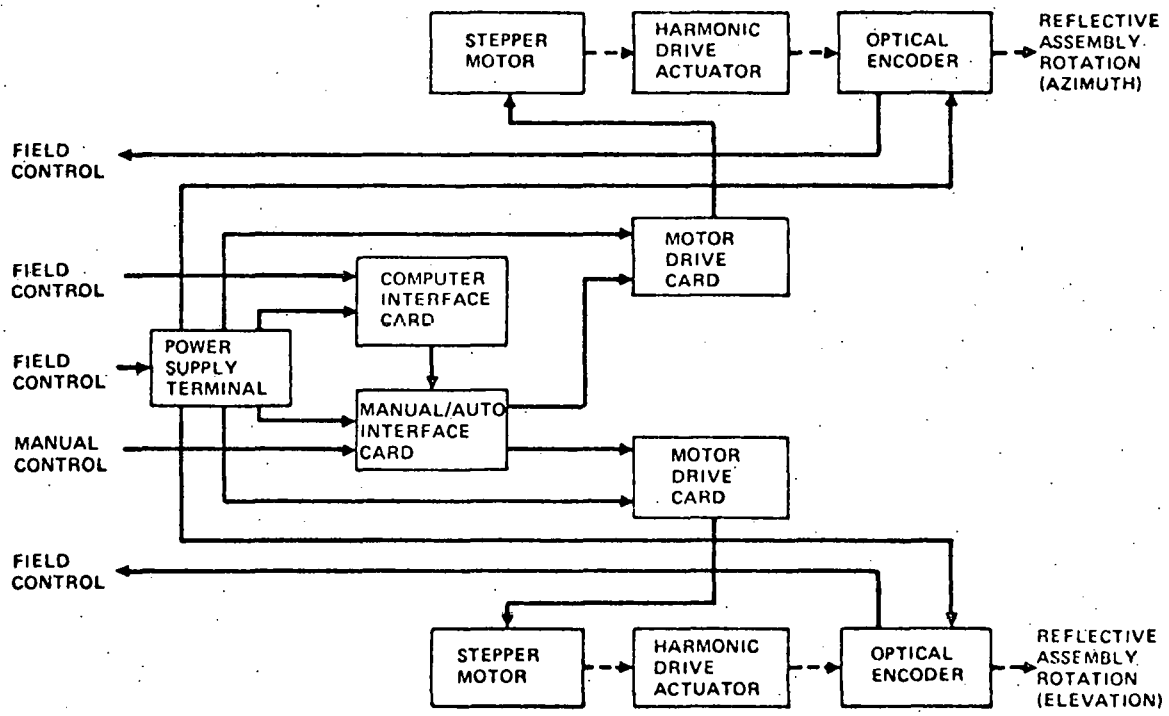

Figure: 3.3-4 Heliostal Drive/Control Block Diagram

The manual control unit is a rugged, lightweight, portable switchbox with a 3.04 m (10 foot) cable and connector which plugs into either of the 3 heliostats to provide manual positioning of any reflective assembly. A 3-position selector switch enables the "automatic", "manual" or "off" control modes. Two spring return-to-center switches enable individual elevation (up/down) and azimuth (left/right) control of the reflective assembly.

There are limit switches on each gimbal axis to secure power to the drive actuators and thereby prevent overtravel, windup, and equipment damage in case of an electronic malfunction.

The heliostat drive and control assembly includes the wire bundle cabling inside the heliostat (which enables easy disconnection of the electronic units) as well as the above mentioned electronics control components.

3.3.1.3.4 Field Controller

The field controller with associated peripheral components is shown in Figure 3.3-5. The field controller hardware includes a PDP 11/03 mini-computer, an interface controller, having computer electronics contained in a chassis separate from the mainframe with a hinged operator's front panel, a time-of-day clock, a remote operator panel, and a teletype. The teletype is not a deliverable item. Connections to the heliostats and peripherals will be through differential drivers and receivers on direct radial channels with dedicated wire cabling.

The interface controller provides all circuitry required to monitor and control heliostat functions. These monitor and control functions include motor commands for 2 axes of 3 operating heliostats, individual encoder monitoring for each axis and limit switch monitoring. All functions are under direct computer control. The computer will issue single step commands for each step and each motor. The computer will read the state of the associated encoder for each step issued, after a pre-determined delay which allows the motor to respond and mechanical oscillations to diminish. Limit switch data is available to the computer upon request.

The heliostat controller interface to the computer is a 16 bit parallel word per transfer via a purchased DEC interface card. The controller will provide one step pulse to the addressed heliostat motor for each computer output transfer of a step command. Heliostat encoder and limit switch data must

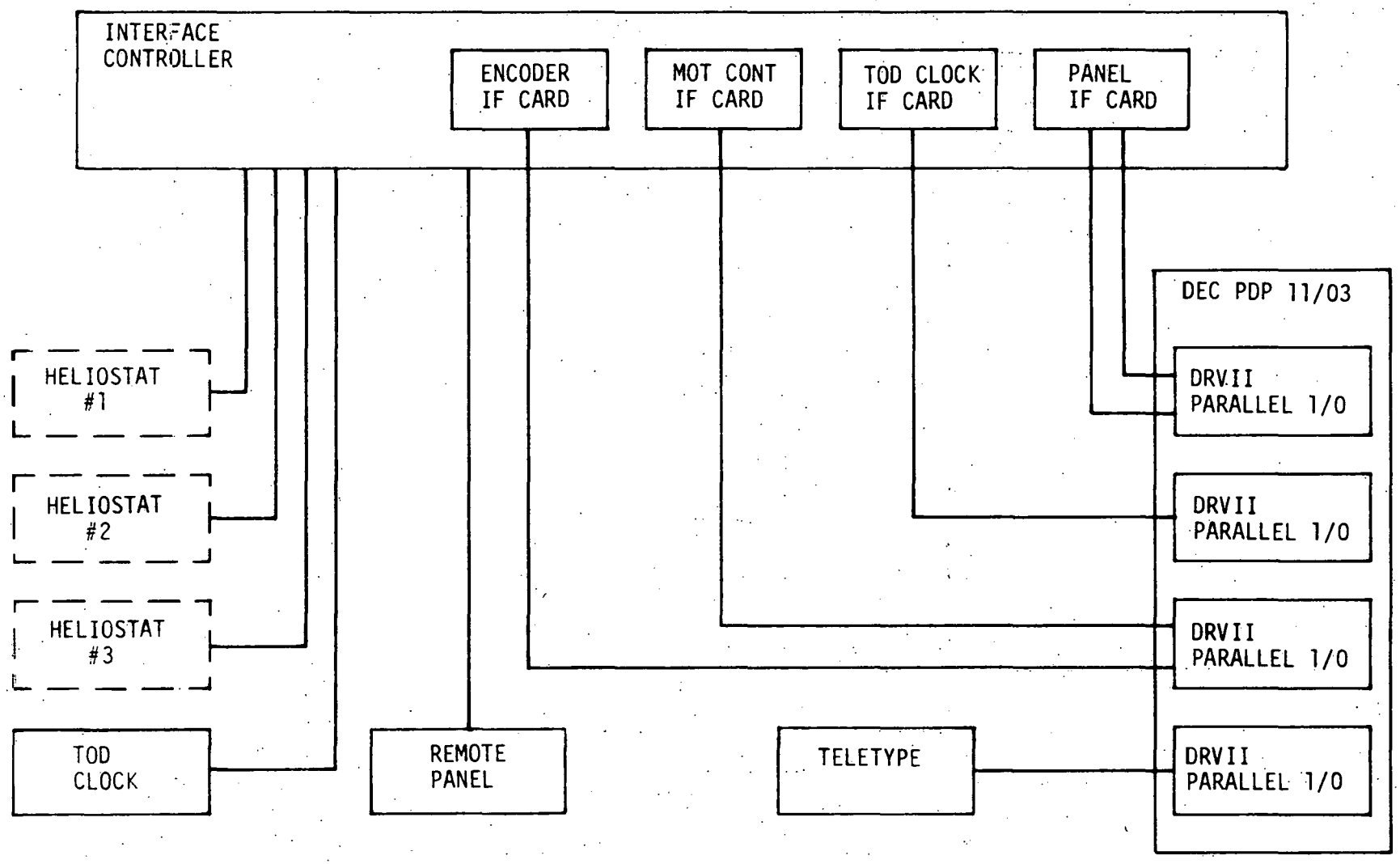

Figure: 3.3-5 Collector Subsystem Field Controller Diagram

D277-10022-1

be selected by the computer and then read. Selection is made by writing into the interface control and status register (CSR) with appropriate CSR bits. All data transfers are on a non-interrupt basis under program control

The time-of-day clock (TOD) controller is the interface between the mainframe and a time clock. The time clock has a parallel BCD seconds-to-day TTL compatible output and a request/reply interface. The computer reads in TOD data under program control. Two 16 bit words are required for complete TOD information. The computer selects the input word via the interface control and status register. New data will be read from the time clock whenever CSR0 changes from a 0 to 1. The clock output register is held (not updated) whenever CSR0 is 1.

Two operator panels will be provided with the associated interface controller. One panel is actually the interface controller chassis hinged cover. This panel contains 16 switches and 16 indicators used for operator control and monitoring, simulating functions normally provided by a central computer. The field controller computer can write to the indicators or read the switches via a DEC interface card. The other panel is a remote control box used to control the heliostats during alignment. This box contains 5 switches that may be read in the same manner as the operator panel switches. Selection of which panel is read is made by bit 0 of the interface CSR register (1 = Operator Panel; 0 = Remote Panel). Actual bit assignments will be made later. Functions required on these panels as presently identified are as follows:

Operator Panel

- o Switches
  - o Standby
  - o Track
  - o Shutdown
  - o Alignment

  } Mode Select Rotary Switch

- o Displays
  - o Standby Mode
  - o Track Mode
  - o Shutdown Mode
  - o Alignment Mode
  - o Fine Align
  - o Course Align

- o Heliostat 1 Failure
- o Heliostat 2 Failure
- o Heliostat 3 Failure
- o Heliostat 1 Selected
- o Heliostat 2 Selected
- o Heliostat 3 Selected

Remote Panel

o Switches

- o Heliostat Select (Rotary 1 of 3)
- o Azimuth/Elevation Select
- o Single Step (Momentary Pushbutton)
- o Alignment Complete

o Displays

(None)

A logic 1 will turn the display light ON or indicate the switch is activated (function selected).

The interface controller will be housed in a 19-inch standard card cage chassis with hinged front panel. As much as possible, all circuitry will be TTL logic and will be mounted on wire wrap cards for ease of fabrication and modification. The backplane will be wire wrap for similar reasons. All cables will be connected via twist loc or screw secured cannon type connectors.

The Remote panel will be a small BUD type box. One cable 250 feet long with connectors at each end will be provided for each heliostat connection. One cable 3 feet long will be provided for the time-of-day clock connection. One cable 100 feet long will be provided for connection to the Remote panel.

3.3.1.4 Software Design

Software design philosophy for the heliostat drive and control assembly is based on simplicity and hardware cost. To lower heliostat-computer interface hardware cost, the following additional functions will be performed by software:

1. Encoder absolute position (.36° increment).
2. Drive stepper motor at one step per 180 ms maximum.
3. Limit switching monitor.

To simplify software design, the computer will have only two interruptable modes, the real time processor interrupts and power failed/auto restart inter-

rupts. When a power failed/auto restart event occurs, upon power return the system enters the Power-On sequence, reinitializes and continues.

The commanding of the stepper motor to step one step at a time will allow the correlation of each .36° increment output from the encoder to a particular command motor step. Hence, if an error existed, a correlation factor can be generated readily. One limitation to this approach is that the maximum number of steps that can be commanded to the motor is fixed.

At this time, the computer time frame has been chosen as five seconds. The calculation time needed per heliostat is approximately 30 ms. Using this number for 64 heliostats, the maximum number of steps that can be commanded is approximately 15 (.337°) steps in one computer time frame.

The primary functions of the software modules are to implement the different modes of operation as required by the collector subsystem. These modes are:

1. SHTDWN (Shut-down)
2. ALIGN
3. STANBY (Standby)
4. TRACK

The first level flow charts for these four (4) major modules are given in Figures 3.3-6 to 3.3-14.

A brief description of the four major modules that accomplish the required modes of operation are given below:

3.3.1.4.1 Shtdwn Module

This module returns all non-failed heliostats to the 'zeroth' step reference position. The program accomplishes the drive to the 'zeroth' reference position as follows:

1. Inhibit Real Time Processor.
2. Determines if mirrors are at 'zeroth' reference position first. If all mirrors are at 'zeroth' reference position, program enters at infinite loop that monitors the input mode command. Exit from this loop can only be accomplished by a mode change (Step 8).
3. If the mirrors are not at 'zeroth' reference position, the program uses the internal apparent mirror position and generates the necessary commands to drive the mirror to its reference position.

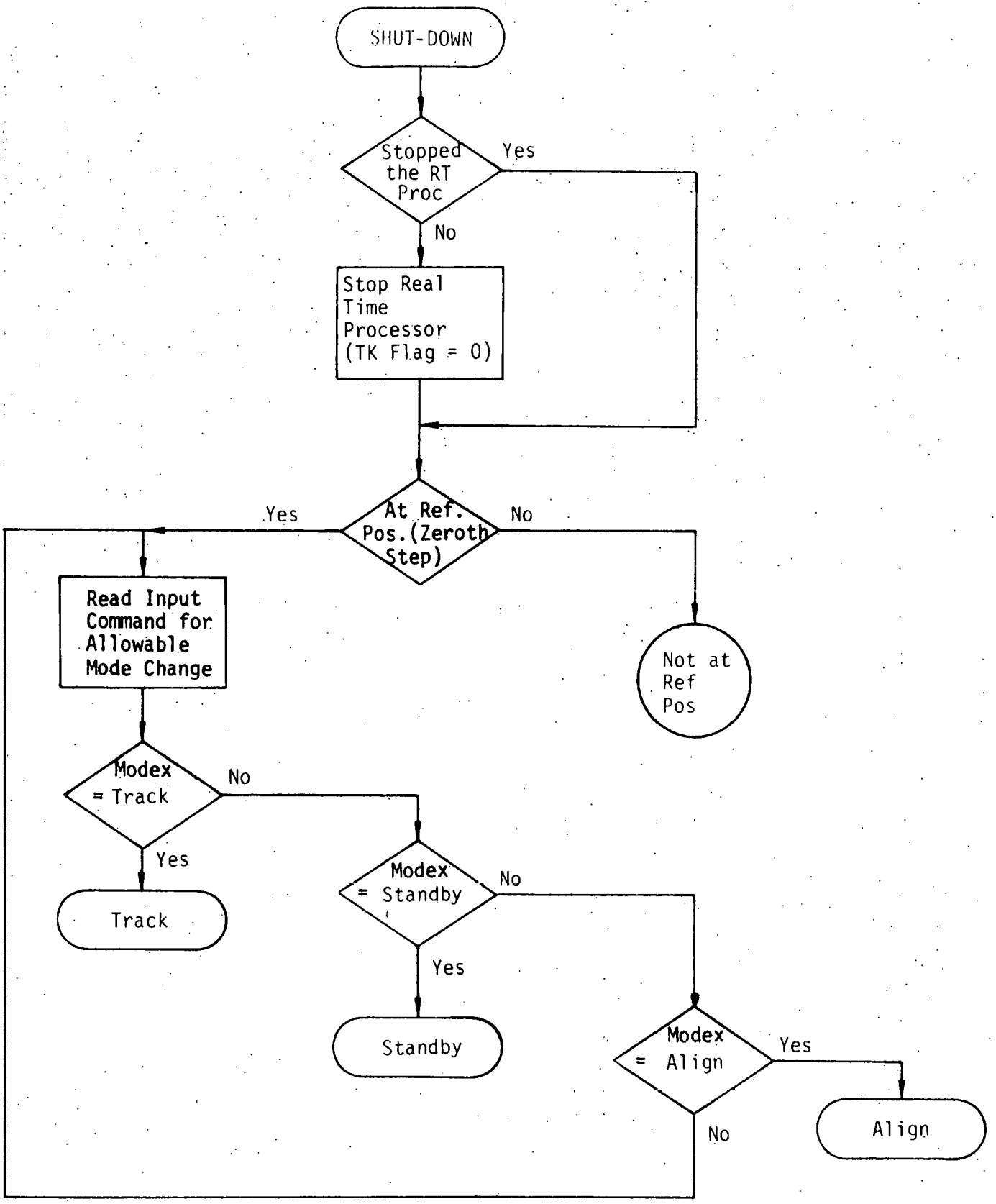
SHUT-DOWN
Stopped the RT Proc
Yes
No
Stop Real Time Processor (TK Flag = 0)
At Ref. Pos. (Zeroth Step)
Yes
No
Read Input Command for Allowable Mode Change
Not at Ref Pos
Modex = Track
No
Yes
Track
Modex = Standby
No
Yes
Standby
Modex = Align
Yes
No
Align

Figure 3.3-6

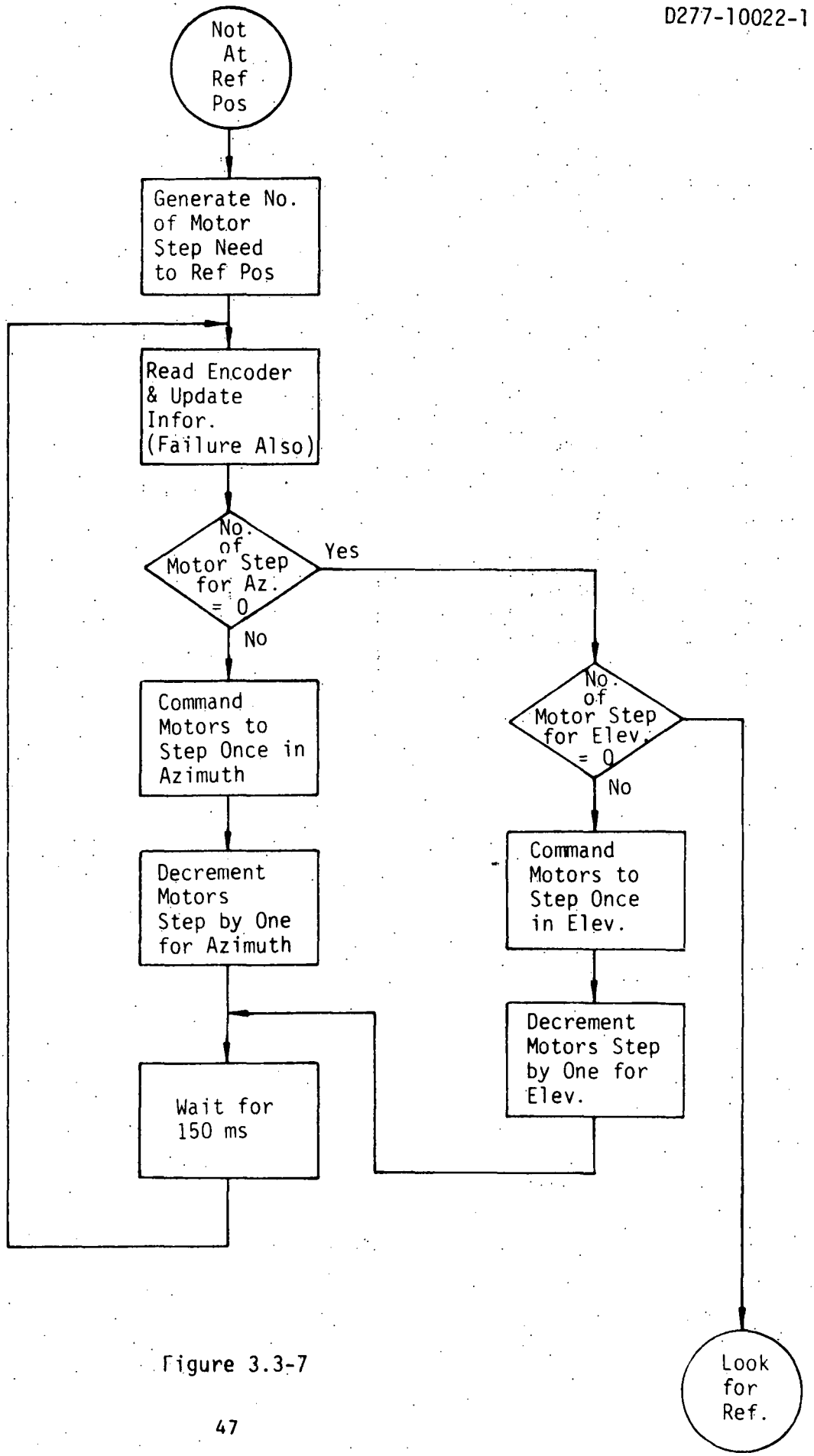
Not At Ref Pos
Generate No. of Motor Step Need to Ref Pos
Read Encoder & Update Infor. (Failure Also)
No. of Motor Step for Az. = 0
Yes
No
Command Motors to Step Once in Azimuth
Decrement Motors Step by One for Azimuth
Wait for 150 ms
No. of Motor Step for Elev. = 0
No
Command Motors to Step Once in Elev.
Decrement Motors Step by One for Elev.
Look for Ref.

Figure 3.3-7

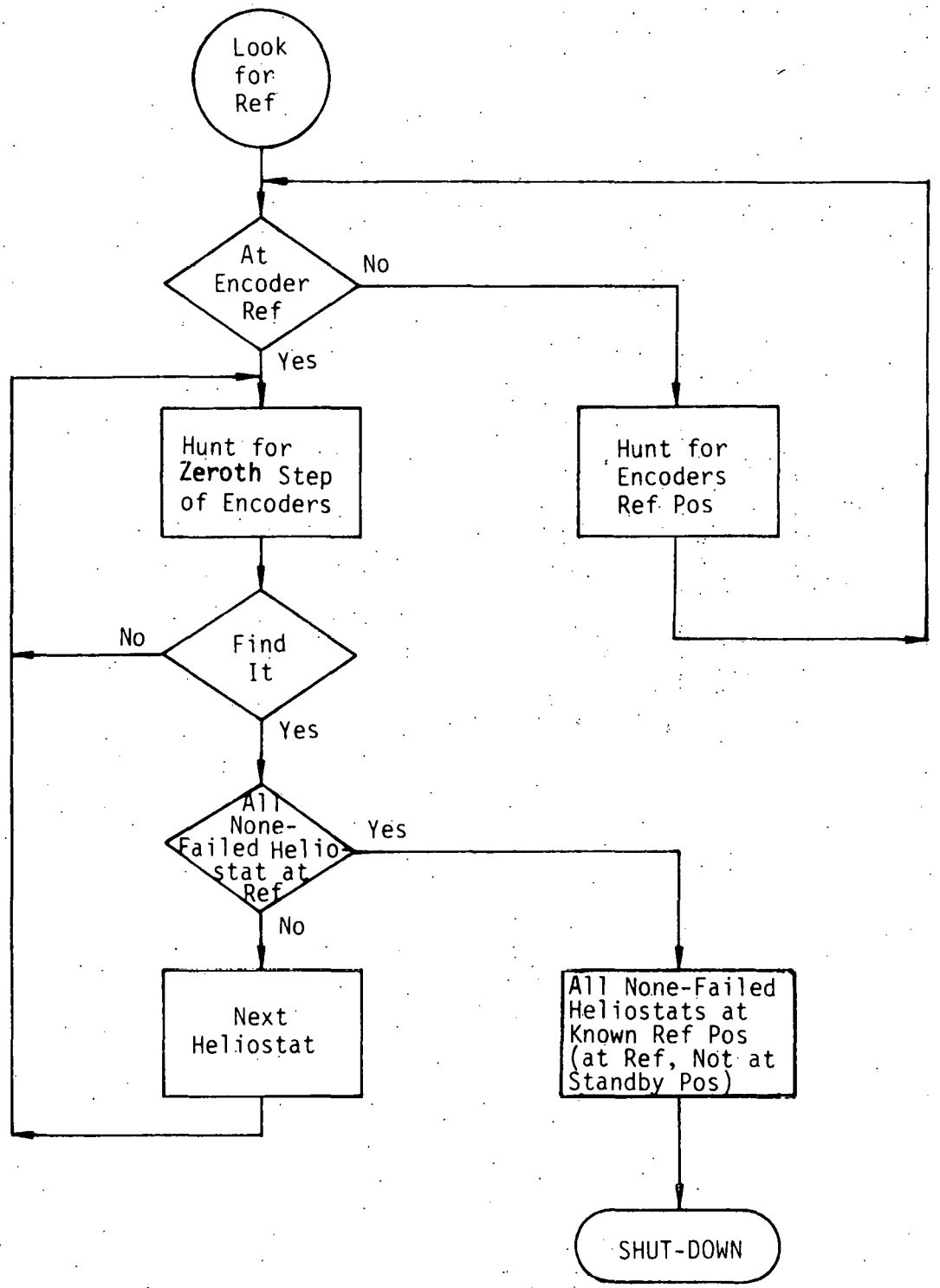
Look for Ref
At Encoder Ref
No
Yes
Hunt for Zeroth Step of Encoders
Hunt for Encoders Ref Pos
Find It
No
Yes
All None-Failed Heliostat at Ref
Yes
No
Next Heliostat
All None-Failed Heliostats at Known Ref Pos (at Ref, Not at Standby Pos)
SHUT-DOWN

Figure 3.3-8

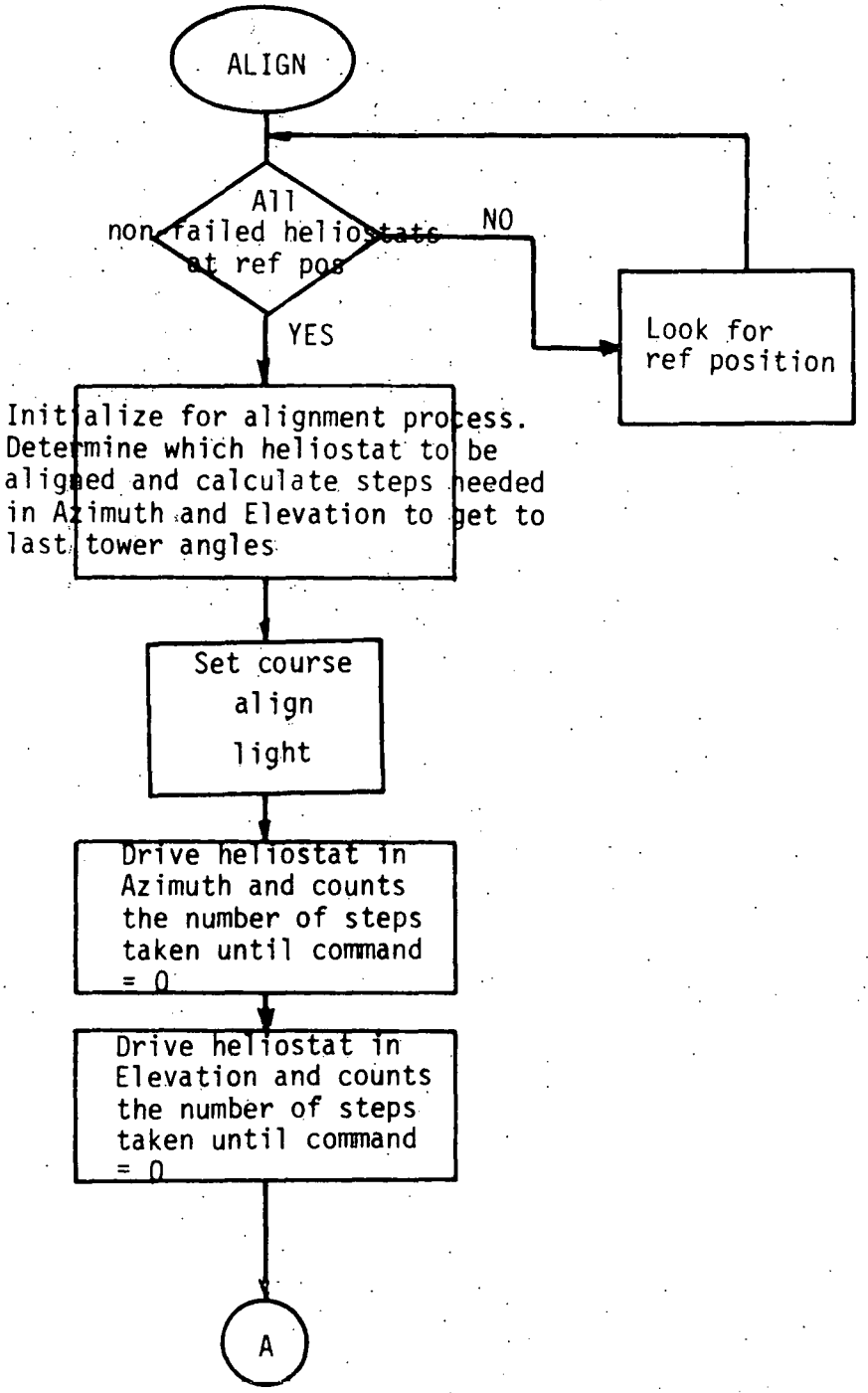
ALIGN
All non-failed heliostats at ref pos
NO
YES
Look for ref position
Initialize for alignment process. Determine which heliostat to be aligned and calculate steps needed in Azimuth and Elevation to get to last tower angles
Set course align light
Drive heliostat in Azimuth and counts the number of steps taken until command = 0
Drive heliostat in Elevation and counts the number of steps taken until command = 0
A

Figure 3.3-9

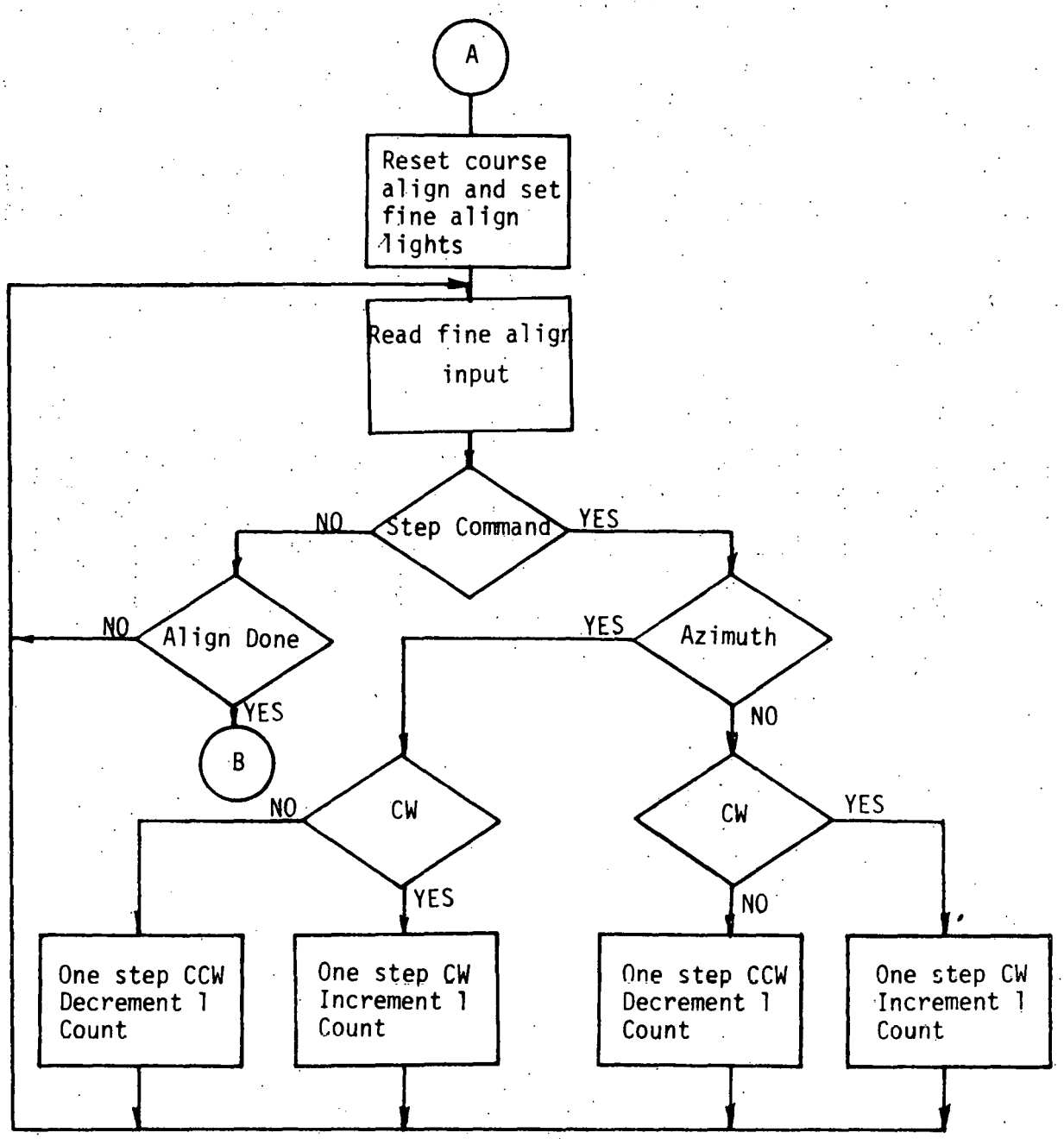
A
Reset course align and set fine align lights
Read fine align input
Step Command
NO
YES
Align Done
NO
YES
B
Azimuth
YES
NO
CW
NO
YES
CW
YES
NO
One step CCW Decrement 1 Count
One step CW Increment 1 Count
One step CCW Decrement 1 Count
One step CW Increment 1 Count

Figure 3.3-10

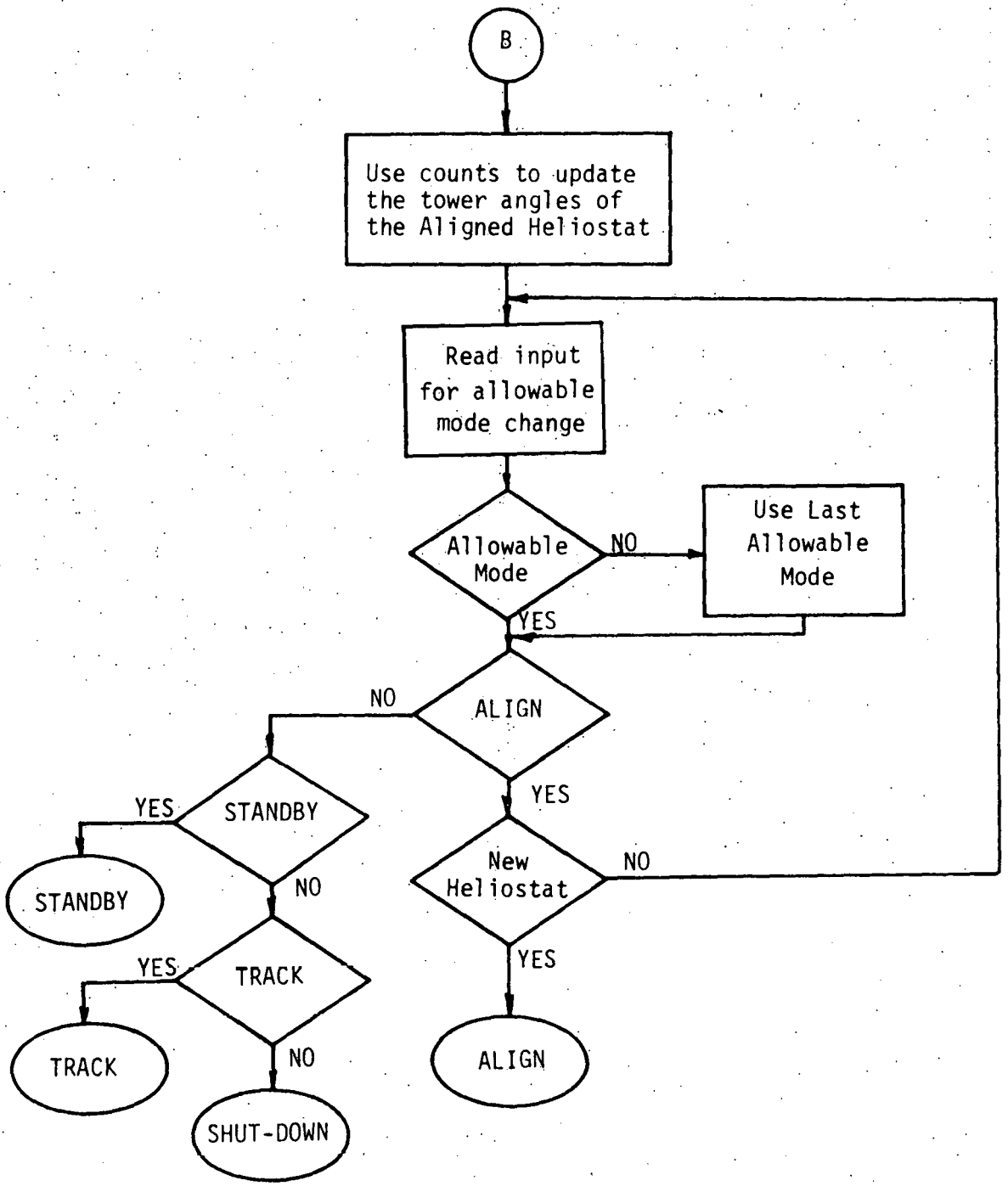
B
Use counts to update the tower angles of the Aligned Heliostat
Read input for allowable mode change
Allowable Mode
NO
Use Last Allowable Mode
YES
NO
ALIGN
YES
STANDBY
YES
STANDBY
NO
New Heliostat
NO
YES
TRACK
YES
TRACK
NO
ALIGN
SHUT-DOWN

Figure 3.3-11

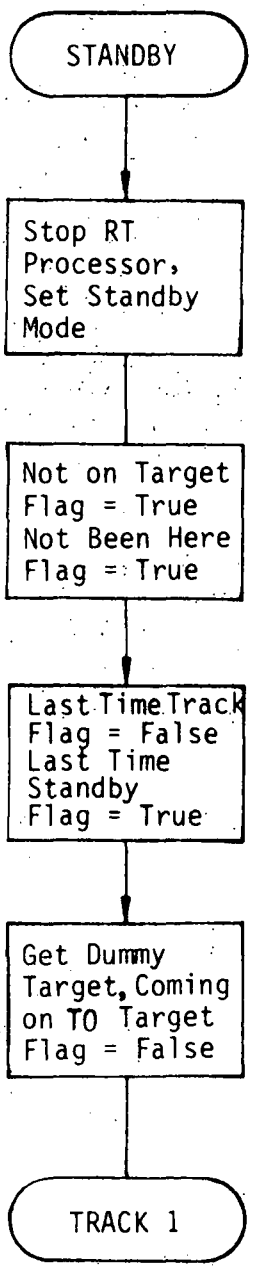
STANDBY
Stop RT Processor, Set Standby Mode
Not on Target Flag = True
Not Been Here Flag = True
Last Time Track Flag = False
Last Time Standby Flag = True
Get Dummy Target, Coming on TO Target Flag = False
TRACK 1

Figure 3.3-12

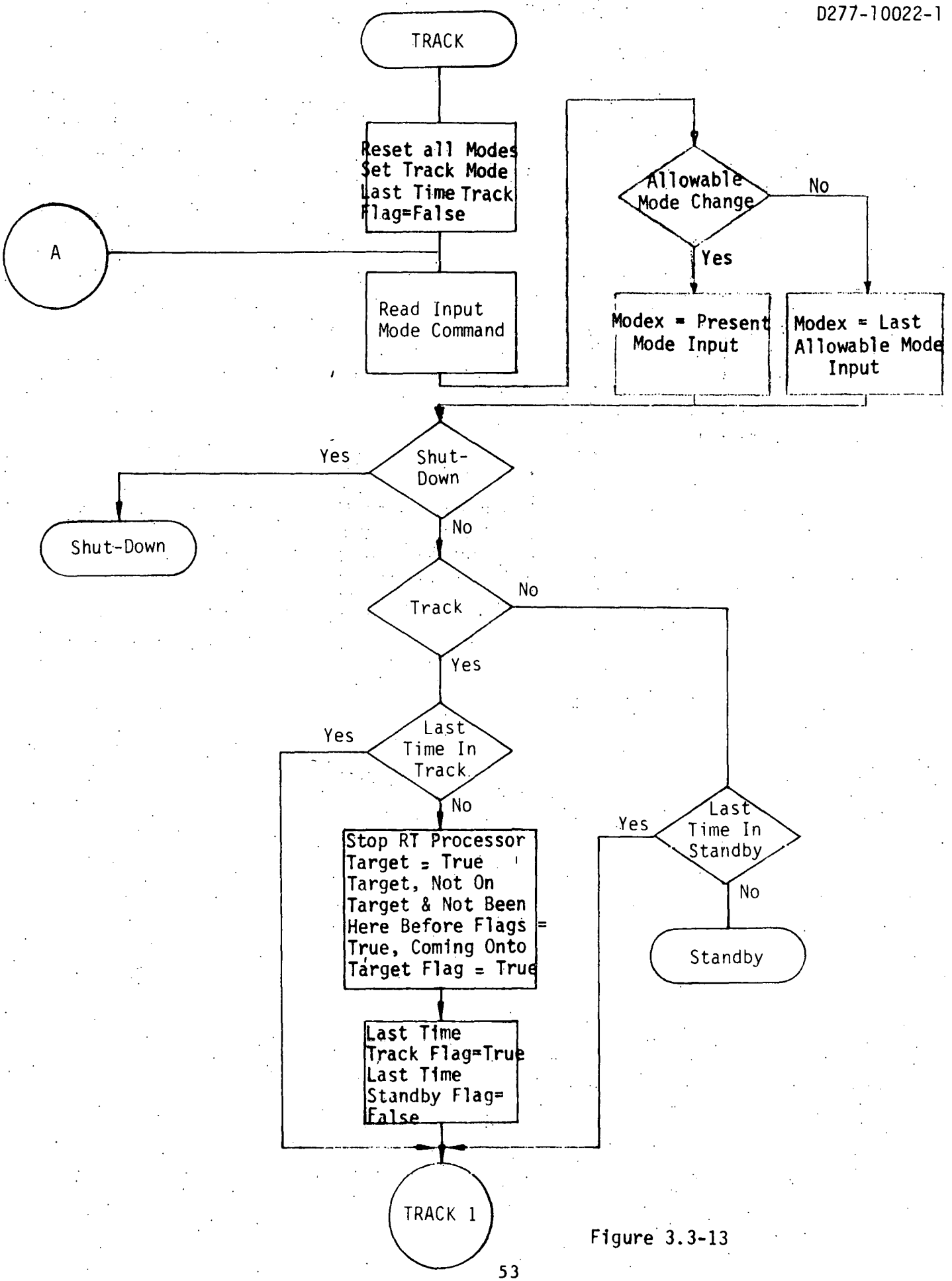
TRACK
Reset all Modes
Set Track Mode
Last Time Track
Flag=False
A
Read Input
Mode Command
Allowable
Mode Change
No
Yes
Modex = Present
Mode Input
Modex = Last
Allowable Mode
Input
Yes
Shut-
Down
Shut-Down
No
Track
No
Yes
Yes
Last
Time In
Track
No
Stop RT Processor
Target = True
Target, Not On
Target & Not Been
Here Before Flags =
True, Coming Onto
Target Flag = True
Last Time
Track Flag=True
Last Time
Standby Flag=
False
Yes
Last
Time In
Standby
No
Standby
TRACK 1

Figure 3.3-13

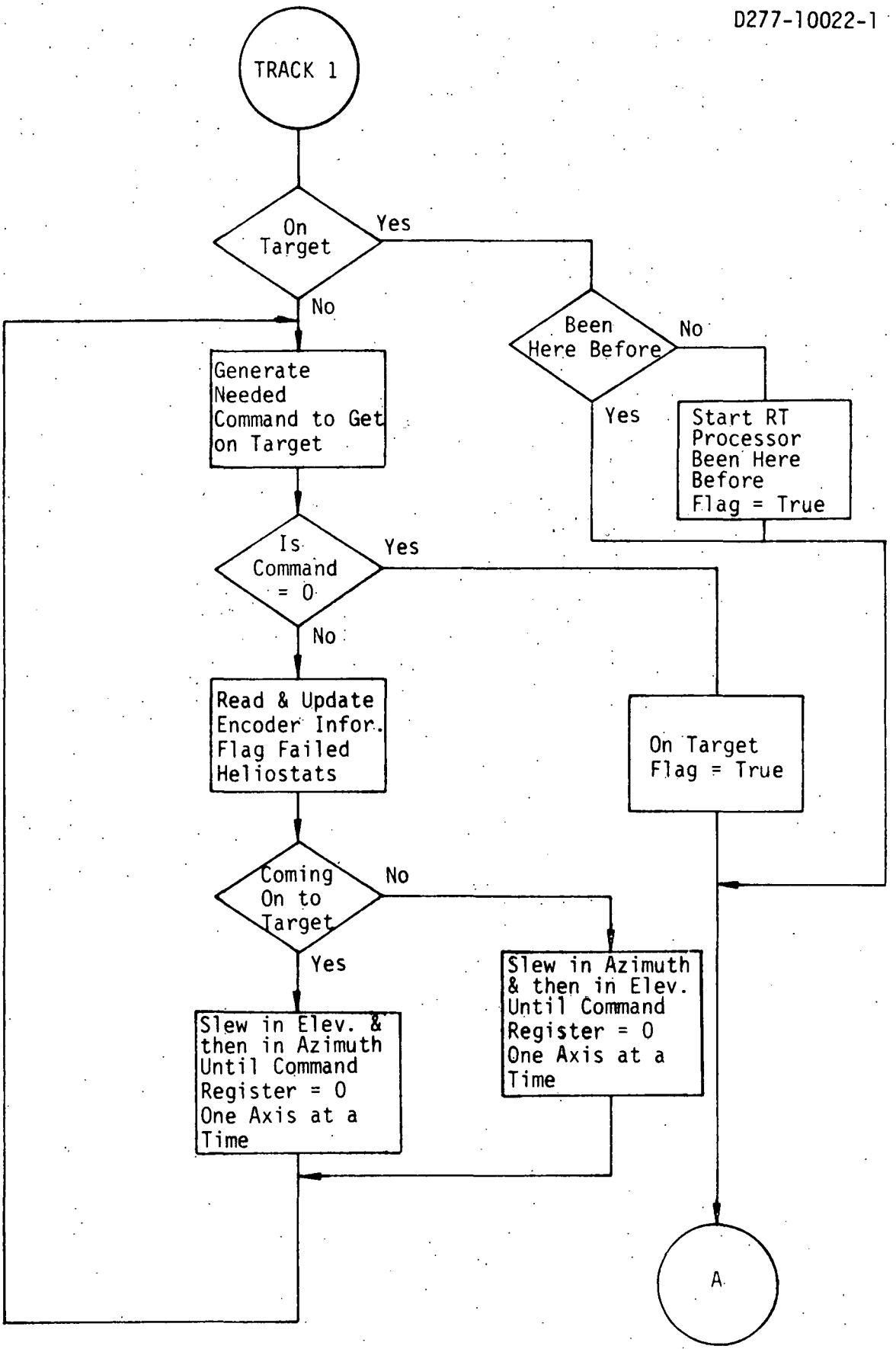
TRACK 1
On Target
Yes
No
Been Here Before
No
Yes
Generate Needed Command to Get on Target
Start RT Processor Been Here Before Flag = True
Is Command = 0
Yes
No
Read & Update Encoder Infor. Flag Failed Heliostats
On Target Flag = True
Coming On to Target
No
Yes
Slew in Azimuth & then in Elev. Until Command Register = 0 One Axis at a Time
Slew in Elev. & then in Azimuth Until Command Register = 0 One Axis at a Time
A

Figure 3.3-14

4. The mirrors are driven in the azimuth direction first and then in the elevation direction. (Drive 1)
5. On completion of all output pulses, the program enters into a loop to hunt for the encoder's reference position. (Drive 2)
6. On completion of Step 5, the program enters another loop to hunt for the first (zeroth) step of the mirror's position. (Drive 3)
7. On completion of the above steps, the program knows exactly where each mirror is at. Flag's internal to the program are set accordingly.
8. Program then enters the infinite loop that monitors mode changes.

The shutdown module can be entered from the track, power-on, and standby modules.

3.3.1.4.2 Align

This module provides a means of updating the heliostat's mirror to collector angles needed in the control law calculations. The function is semi-automatic. That is, an operator must provide manual inputs. The sequence of events for this module is as follows:

1. Drive heliostats to the 'zeroth' reference position if not at zeroth reference position.
2. Drive selected heliostat to the last known tower angles (azimuth first and then elevation).
3. Wait for operator inputs to fine-tune both azimuth and elevation angles or 'Done' command.
4. Update both azimuth and elevation angles on receiving 'Done' command from operator.
5. Wait for operator input to change modes or align next heliostat.

3.3.1.4.3 Stanby

The stanby module provides a dummy target for the system to track the sun. The sequence of events for this module is as follows:

1. Inhibits the Real Time Processor.
2. Initializes system parameters to the standby mode.
3. Supplies a dummy target for tracking.
4. Enters the Track module at (Track 1)

These tasks will enable the heliostats to slew onto the dummy target and then track the sun.

3.3.1.4.4 Track Module

The track module performs the functions of slewing the mirrors onto the target or off the target and initializes the Real Time Processor to track the sun. When in the track module, program can only exit to the shutdown or standby modules.

The track program performs its functions as follows:

1. Determines if a request is made to enter the shutdown or standby modes. Enter that requested mode's module or continue in track.
2. Determines if mirrors are to be driven in the slew mode. If so, set-up for slew mode operation to slew onto target or off of target.
3. Determines if mirrors are on target. If not on target, generate commands to slew onto target in elevation and then azimuth, or to slew off of target in azimuth and then elevation. This process repeats until target has been acquired.
4. Once on target, the Real Time Processor is initialized to track the sun. Flags are set and program continues to loop in this module to monitor for mode change.

3.3.2 Design Analysis

The drive actuator output torsional loads were analyzed to produce the torque requirements of the drive components. This detailed analysis is given in the appendix. The loads on the actuator output shaft include the torques due to: friction, reflective assembly inertia, counterweight inertia, and air mass inertia. The counterweights serve to minimize the static torque load of the reflective assembly. The results of this analysis indicate that a capability of 22.6 Nm (200 in-lbs) is required for positional control of the PD baseline 39 Kg (86 lb) reflective assembly. Since the research experiments reflective assembly is much lighter than the PD baseline, a design margin is inherent in the design, which is configured to baseline requirements. As the harmonic drive provides an 80/1 torque amplification, the stepper motor output torque of 0.20 Nm (1.81 in-lbs) was calculated as the minimum required to perform functional operations. The stepper motor selected has an output torque capability of 0.28 Nm (2.5 in-lbs), which thus provides an additional margin in capability and performance.

The drive and control assembly error budget analysis is illustrated in Table 3.3-2. The total error for any sigma value (normal distribution) is the root sum of the squares of the listed component errors. This value is for the single-axis positioning accuracy of the reflective assembly, (commonly called pointing accuracy). The alignment and drive actuation errors are the two major contributors of system error as indicated in the table.

	3σ (99.73%)	2σ (95.4%)	1σ (68.27%)	.67σ (50%)
REFLECTOR TRACKING	.01125°	.0107°	.0077°	.0056°
REFLECTOR STEP SYNCHRONIZATION	.01125°	.0107°	.0077°	.0056°
STEP RESPONSE	.0225°	.022°	.015°	.0112°
ENCODER	.0178°	.0118°	.0059°	.004°
DRIVE ACTUATION	.108°	.072°	.036°	.024°
EPHEMERIS DATA	.009°	.006°	.003°	.002°
GIMBAL PLACEMENT	.045°	.030°	.015°	.010°
COMPUTER CALCULATIONS (16 Bit)	.006°	.004°	.002°	.0014°
ALIGNMENT (TOTAL, ESTIMATE)	.1119°	.0746°	.0373°	.025°
TOTAL (RSS)	.165°	.112°	.057°	.038°

Table: 3.3-2 Drive and Control Assembly Error Budget

3.3.3 Alignment

The purpose of the alignment task is (1) to initially set the "alignment position" of each heliostat mirror and (2) to define the angular displacement of the "alignment position" from a predetermined "reference position" for input to the solar tracking control actuator. This task will be accomplished using a spherical coordinate laser measuring system developed by The Boeing Company.

The measuring system consists of a laser ranging device mounted on a high precision two axis yoke/rotab assembly shown in Figure 3.3-15. The ranging function is accomplished (See Figure 3.3-16) by transmitting an amplitude modulated CW laser beam to a small target area, collecting a portion of the reflected light in a receiver telescope where an electrical signal is generated, and determining the phase delay, at the modulation frequency, between the transmitted light and the received light. The phase delay provides a very accurate measurement of the distance to the target. The absolute distance measurement accuracy of this system has been certified to $\pm$ 0.016 inch (two sigma) over a range of 10 to 100 feet using a laser interferometer as a standard. For lack of a longer calibration range, accuracy over longer distances were not evaluated. Under optimum conditions, the laser measuring system has been used to measure distances of up to 5 miles.

The angle measuring function of the laser measuring system is accomplished by two high precision angle encoders, one for measuring elevation angle and one for measuring azimuth angle. These encoders are built into the two axis yoke/rotab assembly in the proper locations to sense the appropriate movement. The resolution of each system is 0.36 seconds of arc.

The proper alignment of the heliostat mirrors (Figure 3.3-17) is dependent on the definition and establishment of reference directions relative to the solar system's coordinate system. These references are (1) true vertical from the earth's surface and (2) true south. The references are established in the following manner. The gimbal axis drive is initially set to a vertical position by placing an electronic level ($\pm$ 1/5 second resolution) on the mirror interface plate and adjusting its orientation to horizontal. The mirror is then attached to the interface plate using predetermined shims to assure parallelism between the mirror surface and gimbal plate. The actuator encoder/drive mechanism is then fine adjusted and locked.

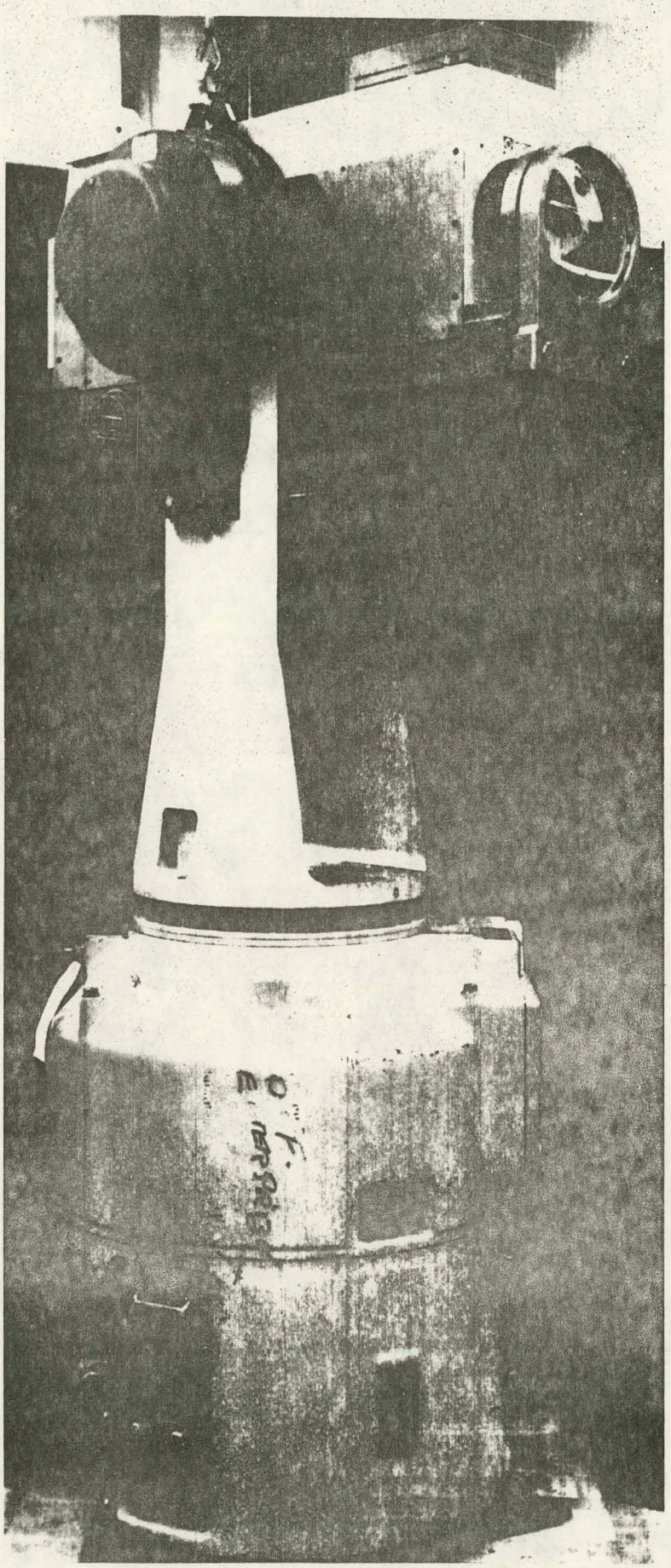

Figure: 3.3-15 Laser/Geodolite Photo

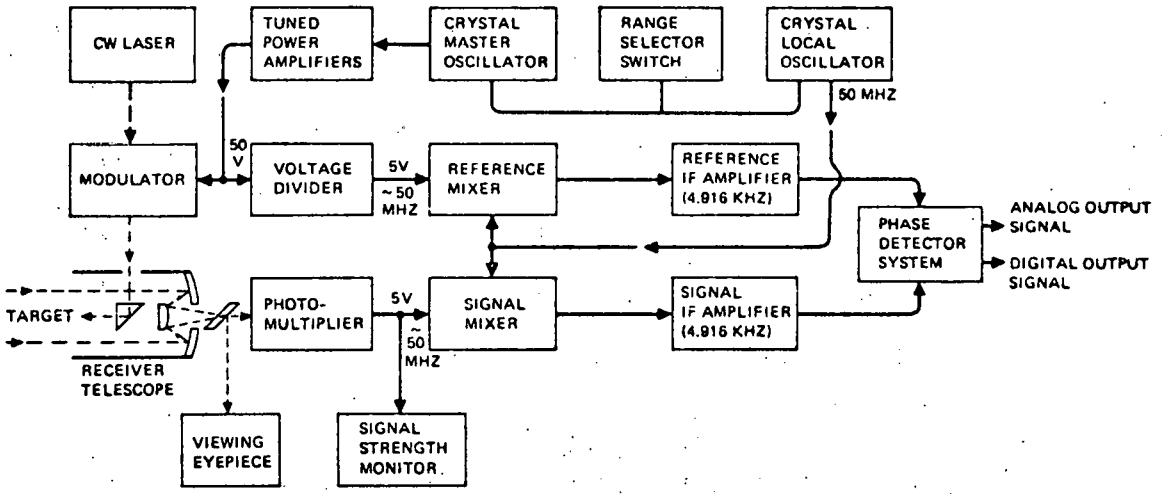

Figure: 3.3-16 Schematic of Geodolite

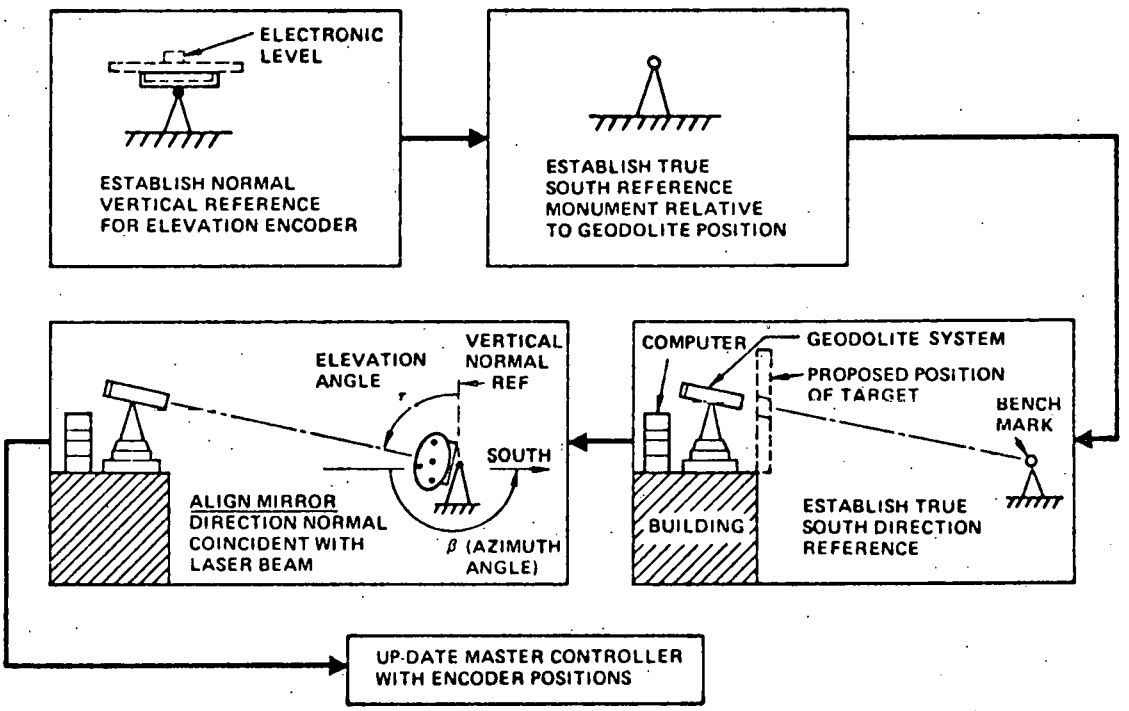

Figure: 3.3-17 Alignment Procedure

The true south direction relative to the laser measuring system is defined by a precision direction finder and marked with an existing benchmark monument bearing.

With the laser measurement system in measurement position behind the solar collector target, the laser beam is rotated and tilted until it illuminates the bench mark. The azimuth angle of the laser system's rotab is set at zero for later calculation of mirror gimbal azimuth setting.

The actual alignment of the heliostat mirror commences by first pointing the face of the mirror toward the laser measuring system relative to true normal vertical and a predetermined azimuth angle position. The laser system then ranges on each of two sets of two targets which are positioned diametrically opposed to each other and in line with gimbal axes of rotation. The targets are installed during the fabrication of the mirror. Azimuth and elevation adjustments are made by the laser measuring system operator via a remote control box until the distances to all of the diametrically opposed targets are the same. At this stage, the alignment position has been established; i.e., the elevation angle, γ, relative to the true vertical reference, and azimuth angle relative to the predefined azimuth position are known, but the azimuth angle, β, relative to true south is not known. The position actuator controller is then signalled that this position is the alignment position.

To determine angle β, the laser system is positioned such that the beam is incident on a center target installed during mirror fabrication. The angle measured by the laser system azimuth angle encoder is used to calculate the azimuth angle the mirror must rotate to obtain the true south reference orientation. The laser system operator then directs the heliostat azimuth gimbal actuator to move the β angle while monitoring pulses relative to the predefined azimuth position. At this orientation the azimuth true south reference position is obtained and established in the position actuator controller.

Re-checks of the heliostat alignment positions can be accomplished by causing the position controller to move the mirror to the alignment position. The laser measuring system can re-measure the target distances and associated angles to determine whether the alignment position has changed. Adjustments can be easily updated to re-establish new alignment position using portions of the above procedure.

3.4 THERMAL DESIGN

3.4.1 Thermal Control System Description

The thermal environment requirement imposed on the collector subsystem is survival of ambient temperature variations from -30 to 49°C. The baseline temperature control approach is essentially passive, depending on the use of materials with acceptable thermal radiative properties. Radiation is the dominant heat transfer mechanism of the heliostat. Natural convection accounts for the remaining heat transfer within the heliostat. Use of the pressurization air for cooling is not considered at present; however, the air source can be used to force cool the electronics if the need arises.

Assumptions of materials, finishes and geometry used in calculations are detailed below. Recognize, however, that thermal analyses were performed during conceptual design studies and that some design changes were made during detail design. The physical heliostat model and major components used in calculations are shown in Figure 3.4-1. For the present, the aluminum reflector frame and frame skeleton will use the as-received mill finish. The vertical mast was assumed to be a galvanized steel post with an access hole cut in the side to expose the azimuth gimbal drive actuator. Both the azimuth and elevation gimbal drive actuators were presumed to have a hard anodized protective finish. The ground liner and dome support walls were presumed to be concrete, although a steel sidewall has been incorporated in detail design. The electronics module associated with the control system was presumed to rest near the liner, dissipate an average 50W and has a painted protective finish on the case.

The analyzed protective enclosure is a 5.18M (17-foot) diameter dome made from 0.15 mm (6 mil) Tedlar with high specular transmittance. The reflector was assumed to be a hexagonal film of 13.2 sq. m. made from a 0.05 mm (2 mil) Mylar aluminized and overcoated with SiO_x on the first surface. The dome is truncated and mounted to the foundation with a 60° base angle.

The current design differs thermally from the configuaration described above to the extent that 1) the reflector surface is now circular and 2) no overcoat is specified for the metalized reflector surface. The change to a circular reflector will produce a larger reflector area relative to the dome cross-section with a trend to slightly lower reflector temperatures because a larger fraction of direct solar insolation will be reflected out.

3.4.2 Thermal Control Analysis

3.4.2.1 Analysis Model

The physical heliostat configuration, shown in Figure 3.4-1 with its principal components was interpreted in terms of its essential thermal properties resulting in a modular thermal model. This model, with appropriate boundary conditions, was then submitted for computer solution using the "Boeing Engineering Thermal Analyzer" program described in Reference 3.4-1.

3.4.2.2 Thermal Properties

Thermal optical properties have the greatest effect of all relevant thermal properties in controlling temperatures of the heliostat. A summary of the optical properties used in the analysis are shown in Table 3.4-1. Among the sources from which these values were derived are those contained in Reference 3.4-2, 3.4-3, 3.4-4, and 3.4-5.

3.4.2.3 Thermal Analysis

Thermal analysis involved predicting transient thermal behavior based on actual temperature and insolation profile data for assumed Inyokern and Albuquerque sites. The basic thermal difference between the PD baseline heliostat and the research experiment heliostat is that the Pilot Plant heliostat is surrounded by identical heliostats at the same temperature. Since heat rejection to space by the enclosure surface is a significant mechanism, the Pilot Plant heliostat will therefore run hotter than its research experiment counterpart. This analysis is based on a heliostat located internally in the heliostat field.

The insolation and temperature profiles for the Inyokern and Albuquerque sites were abstracted from data tapes obtained from the Aerospace Corporation, Reference 3.4-6. One profile each for Inyokern and Albuquerque, containing the extreme high temperature recorded in 1962 - 1963, are shown in Figures 3.4-2 and 3.4-3. Each profile covers the 24-hour day containing the record temperature and consists of the ambient temperature, direct and diffuse insolation values. (Profiles based on peak insolation occurred in late autumn or early spring, and the thermal consequences were less severe.) The third profile shown on Figures 3.4-2 and 3.4-3 was obtained from the Inyokern data by averaging the insolation and temperature data by hour for a period of 15 days before and after June 21st.

The diffuse component of the solar insolation was obtained indirectly from the tape data using the published "Direct" and "Total" insolation quantities.

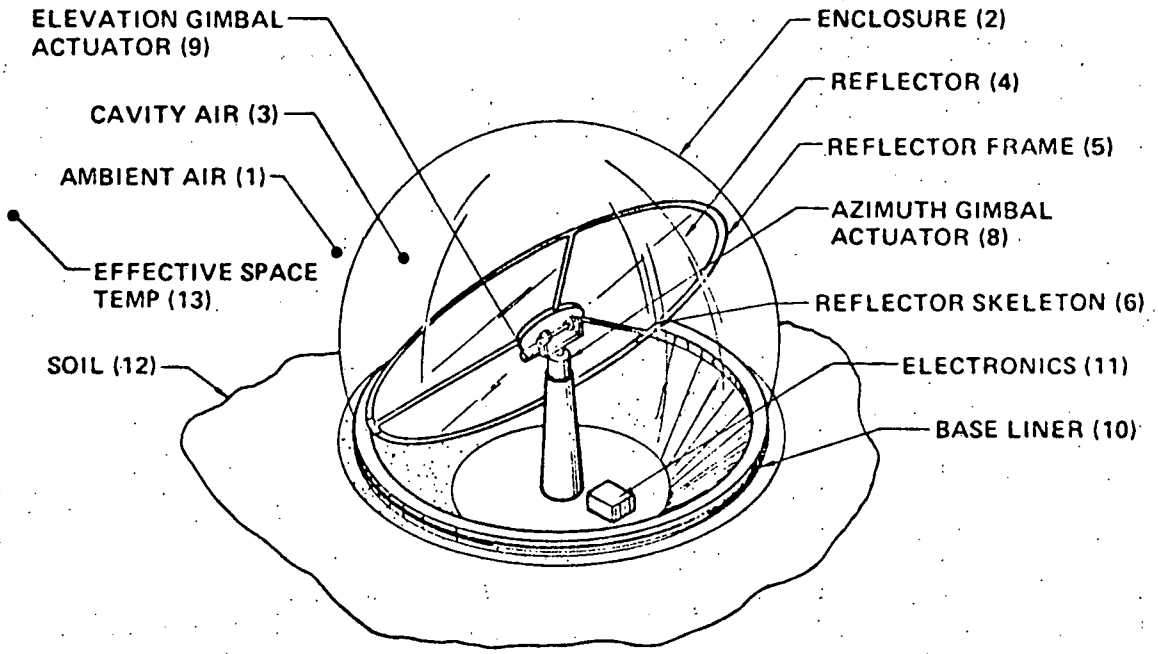

Figure: 3.4-1 Thermal Model

Table: 3.4-1 Optical Properties

COMPONENT	α SOLAR	τ SOLAR SPEC	τ SOLAR DIFF	τ SOLAR TOTAL	ρ SOLAR	ϵ IR	τ' IR	ρ IR
DOME MATERIAL	.03	.87	.04	.91	.06	.35	.50	.15
REFLECTOR MATERIAL								
Front Side with Coating	.14			.0	.86	.10	0	.90
Front Side W/O Coating	.08			.0	.92	.03	0	.97
Backside						.85	0	.15

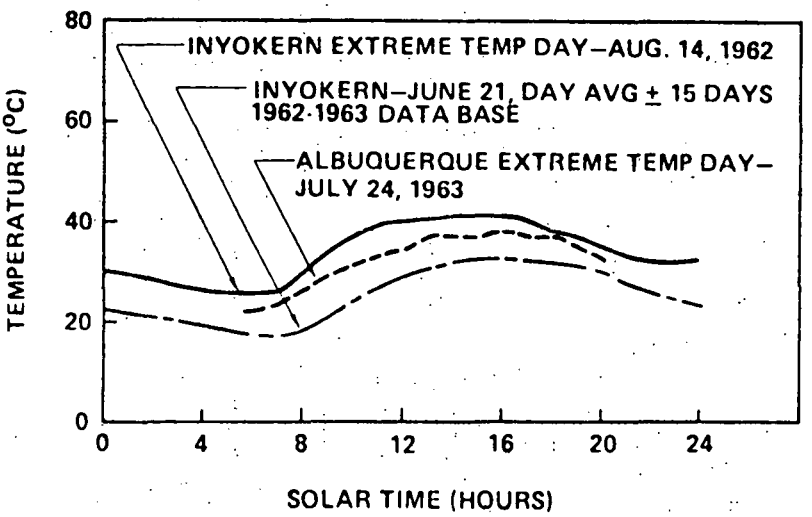

Figure: 3.4-2 Model Ambient Temperature Profiles

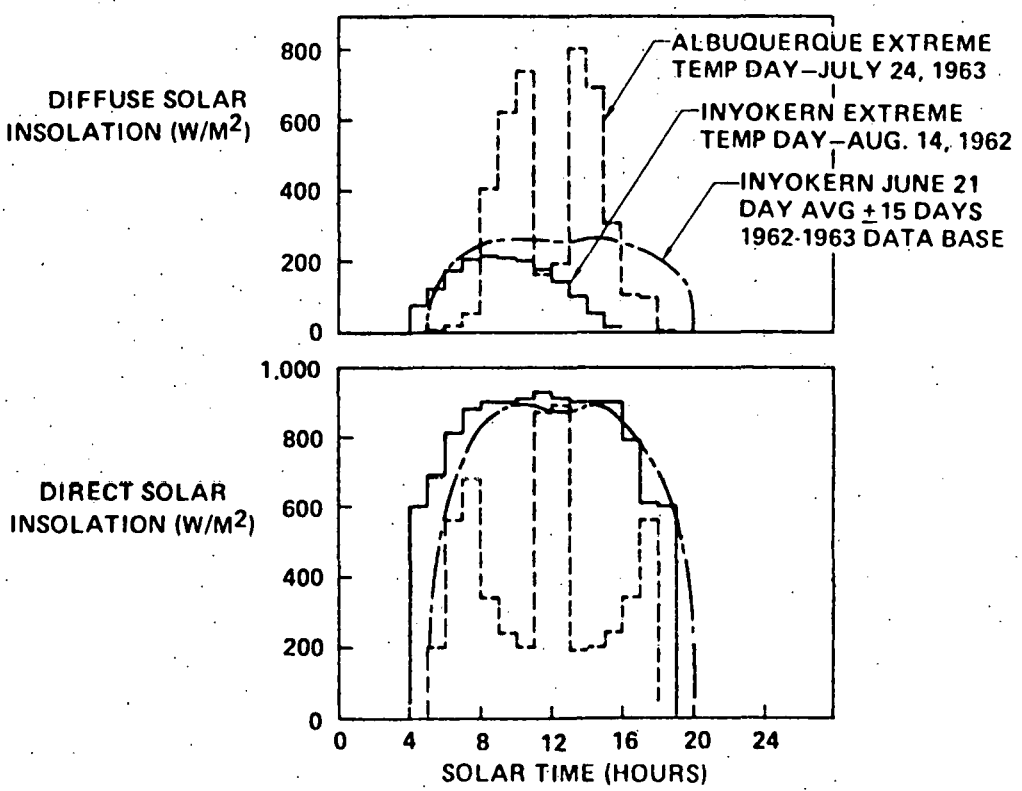

Figure: 3.4-3 Model Solar Insolation Profiles

Since the "Total" insolation value is equivalent to the total insolation of a flat horizontal surface, the "Diffuse" quantity was obtained from the following relationship:

$$I_{diffuse} = I_{total} - I_{specular} \quad \text{Sin } \emptyset$$

where $\emptyset$ is the apparent sun inclination angle.

3.4.3 Results and Conclusions

The temperature relationships between various components in the heliostats for component temperature variations throughout a daily cycle are shown on Figures 3.4-4 and 3.4-5 for the "Inyokern June 21st," "Maximum Temperature Inyokern Day" and "Maximum Temperature Albuquerque Day," respectively. Comparison of these temperatures with analyses of larger heliostats located in a close-packed array (Pilot Plant configuration), has indicated that components in research experiment heliostats will run 5 to 6°C cooler.

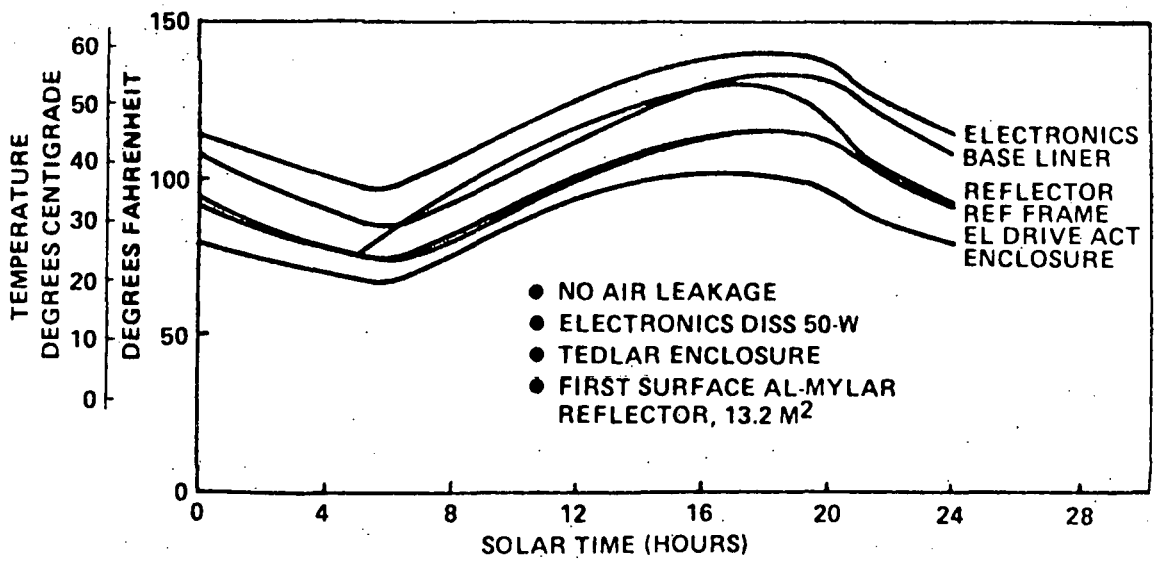

Figure: 3.4-4 Component Temperatures of Research Experiment Collector Located at Inyokekn, California - June 21 Profile

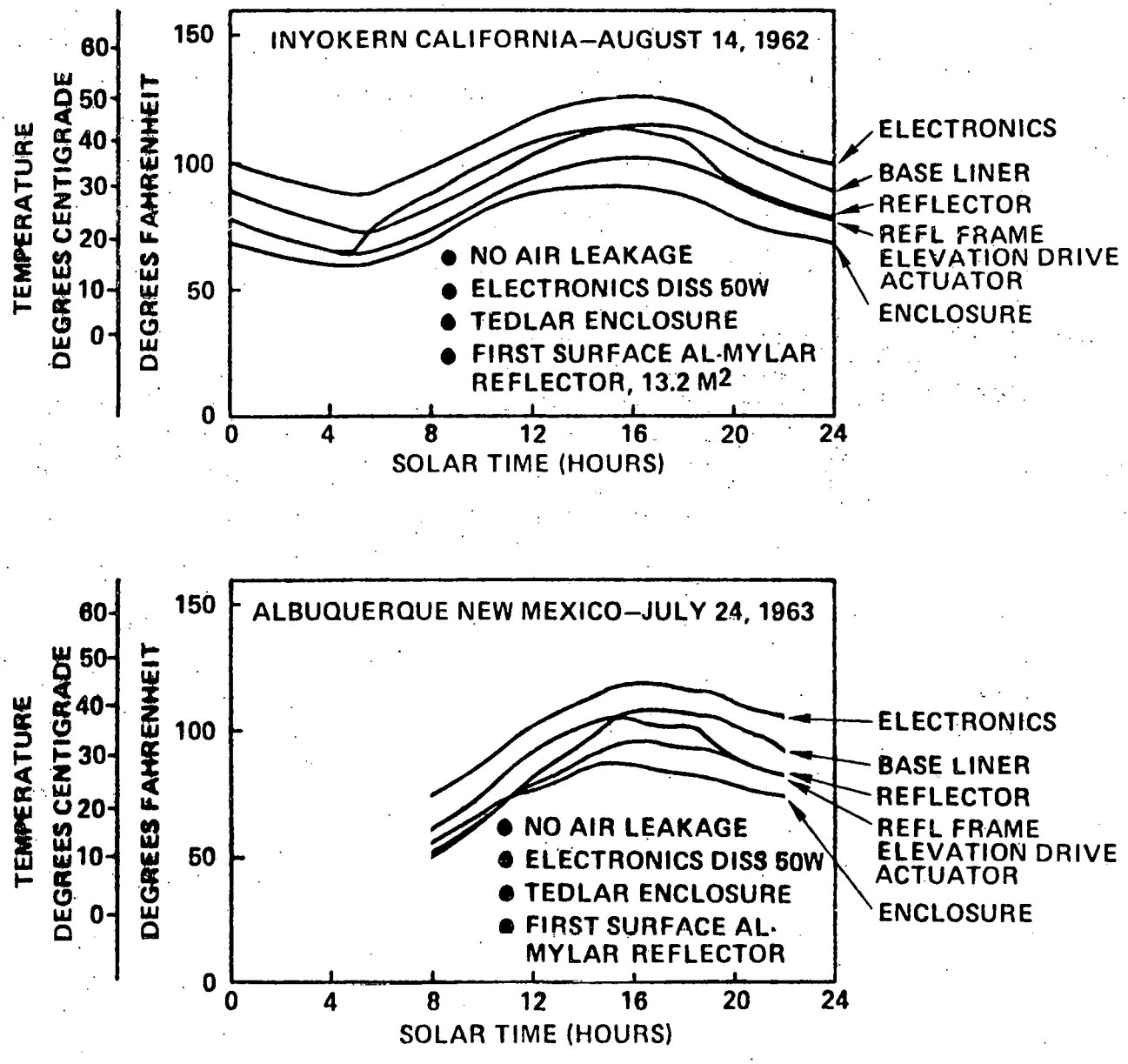

Figure: 3.4-5 Component Temperatures of Research Experiment Collector for Site Extreme Temperature Day

3.5 SAFETY

A summary of potential safety hazards and precaution or corrective action incorporated in the detail design is given in Table 3.5-1.

HAZARD	PRECAUTIONS OR CORRECTIVE ACTION
INSTALLATION	NORMAL SAFETY PROCEDURE FOR EXCAVATION & CONCRETE HANDLING WITH HEAVY EQUIPMENT. PREVENTION OF PUBLIC ACCESS. NORMAL HARD-HAT SAFETY PROCEDURES AND EQUIPMENT FOR OVERHEAD CRANE INSTALLATION OF EQUIPMENT.
ELECTRICAL	MANUAL CONTROL STATION AT EACH HELIOSTAT WITH CAPABILITY TO BLOCK CONTROL COMMANDS FROM CENTRAL AND TO SHUT OFF ALL POWER TO HELIOSTAT. PROVISIONS IN CENTRAL CONTROL TO SHUT OFF POWER TO INDIVIDUAL HELIOSTATS.
LIGHTNING	GROUND CENTER POST. GROUND ENCLOSURE HOLD DOWN SEGMENTS. GROUND REFLECTOR STRUCTURE DIRECTLY TO CENTER POST
FLOOD	DO NOT SITUATE FIELD IN A FLASH FLOOD AREA. IF SOIL CONDITION IS CONDUCIVE TO FORMATION OF SURFACE WATER IN CLOUDBURST CONDITION PROVIDE DRAINAGE IN PATHWAYS BETWEEN DOMES.
FIRE	PROVIDE ADEQUATE CO_2 EXTINGUISHER WITH INSTALLATION AND MAINTENANCE CREWS. EACH PERSON ENTERING AN ENCLOSURE MUST HAVE PERSONAL EQUIPMENT TO CUT OUT THROUGH ENCLOSURE.
WIND	EACH PERSON ENTERING AN ENCLOSURE DURING HIGH WIND CONDITIONS SHOULD HAVE A HARD HAT AND PERSONAL EQUIPMENT TO CUT THROUGH ENCLOSURE.
SOLVENT, VAPORS, OXYGEN CONSUMING EQUIPMENT	THE DOME AIR PRESSURE SYSTEM MAY NOT PROVIDE ADEQUATE AIR FOR PERSONNEL. ADDITIONAL VENTILATION IS MANDATORY FOR PROLONGED STAYS OR IF OXYGEN CONSUMING EQUIPMENT SOLVENT OR VAPORS ARE PRESENT IN ENCLOSURE. LOCK DOOR TO PREVENT UNAUTHORIZED ENTRY.

TABLE 3.5-1

SUMMARY OF SAFETY CONSIDERATIONS

THIS PAGE

WAS INTENTIONALLY

LEFT BLANK

4.0 MANUFACTURING

Manufacturing processes and tool designs have been selected for the fabrication of the transparent enclosure and reflector. All of the processes have been proven by the fabrication of tests, parts and subscale prototypes.

4.1 TRANSPARENT ENCLOSURE FABRICATION

The enclosure will be fabricated from polished Tedlar film using 18 gores and one polar cap. The joints will be heat sealed to form the spherically shaped enclosure.

4.1.1 Fabrication Steps

The fabrication sequence for the transparent enclosure is shown in Figure 4.1-1. The gores are first trimmed using a template and then the base seams are made. These gores are joined to form the dome shape. The polar cap is then trimmed and heat sealed in place.

It was found to be cost effective to use 18 gores because it eliminated the need to thermoform the polished Tedlar film and allowed more effective use of the available film width. With 18 flat gores the shape of the dome around the circumference will be less than 1.5% out of round. A special thermoforming technique is required with the polished Tedlar film. The polishing process imparts an unequal shrinkage of the film in the machine direction. This will cause wrinkles to form during the heating cycle unless the film is pre-tensioned.

4.1.2 Dome Seam Fabrication

All joining of the Tedlar film will be by heat sealing. This requires a temperature of 205 to 218°C (400 to 425°F) and 20 psi pressure at the joint. The pressure is required during both the heating and cooling cycle to restrain the film and prevent localized shrinkage. Two methods have provided satisfactory heat seals; ultrasonic and impulse sealers.

4.1.2.1 Ultrasonic Sealing

The ultrasonic sealer generates heat and pressure at the tip of a vibrating horn. The film is positioned between this horn and a relatively massive, hard surfaced anvil. A spot weld is made by a timed pulse of sonic energy to the horn. A continuous joint can be made by either moving the film in relation to the vibrating horn and anvil or by moving the vibrating horn over the fixed

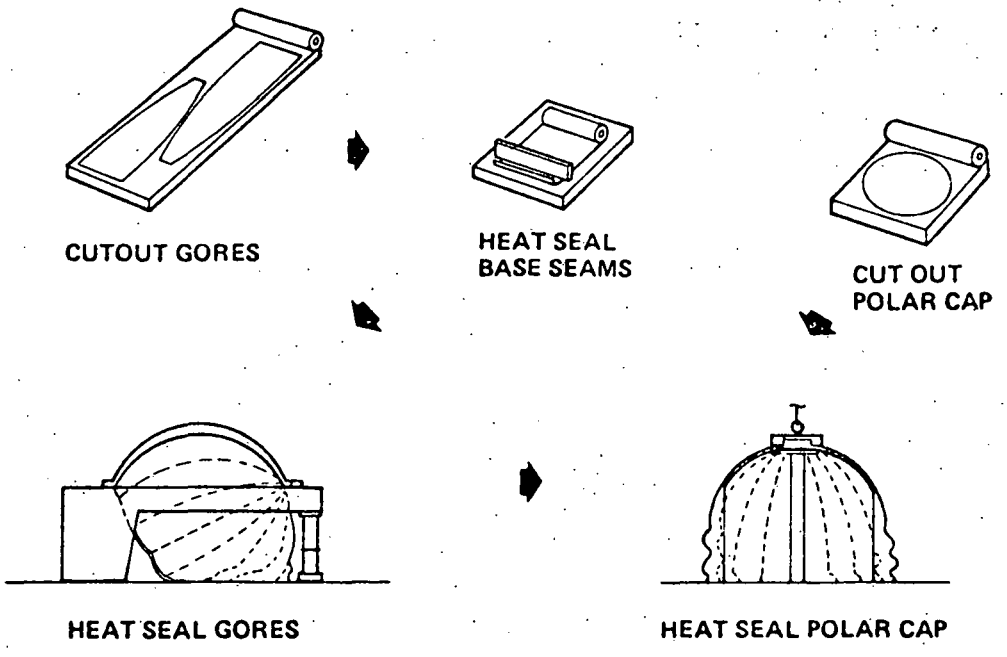

Figure: 4.1-1 Transparent Enclosure Fabrication Steps

film and anvil. During movement, the distance between the horn and anvil must be maintained within a very close tolerance. For 4 mil film the tolerance is ± .0012 inches. Also, the rate of movement must be uniform for any given machine setting. Satisfactory seals at speeds up to 6.1 meters per minute (20 feet per minute) have been made.

The ultrasonic sealer being used to fabricate a 1.07 meter (42 inch) diameter dome is shown in Figure 4.1-2. The film and anvil are being moved under the vibrating horn to make a gore seam. The same technique was used to attach the polar cap with the addition of spot welds being used in the overlap areas where three layers of Tedlar were heat sealed.

4.1.2.2 Impulse Sealing

An impulse sealer consists of a resistance ribbon and a pressure source which runs the full length of the joint being made. The heat is generated by a short (1 to 5 sec) impulse of electric energy to the ribbon. The pressure must be continuous to prevent bridging. A silicone rubber pad is used to distribute the pressure. Kapton film is used over the heating element to assure a smooth surface on the Tedlar heat seal and as a parting film.

Satisfactory impulse seals have been made on up to 4 layers of Tedlar film. A curved impulse sealer 4.9 meters (16 feet) in length with a 2.6 meter (8.5 feet) radius has been made. Satisfactory seals have been made with this heat sealer. Heat seals can be reworked with an impulse sealer by overlapping existing seals.

The heating ribbon and support structure for an impulse sealer is shown in Figure 4.1-3. This sealer produces flat seals up to .86 meters (34 inches) in length. It can be used to make the gore base seams.

4.1.3 Tool Design

The major tools required to fabricate the dome are a gore seam tool and a polar cap seam tool. Concepts of these tools are shown in Figures 4.1-4 and 4.1-5. Both of these tools are designed to use impulse type heat seals. This type of heat seal was selected to reduce tooling costs for the research experiment domes. Ultrasonic heat seals are still expected to be used in localized areas.

Two templates, one for gores and one for the polar cap will be required along with layout and storage surfaces. The base seams will be done in the flat to eliminate any special tool requirements.

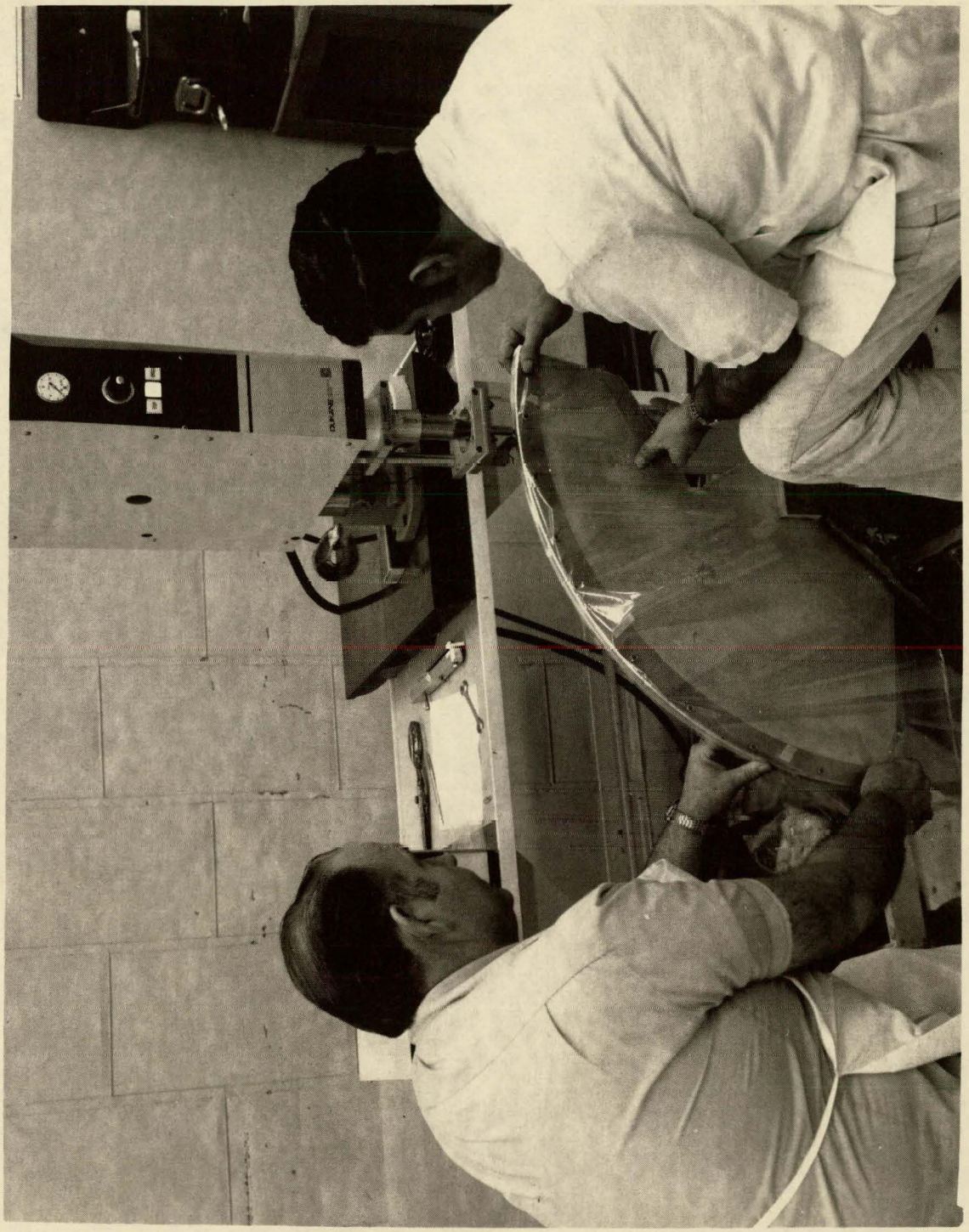

Figure: 4.1-2 Ultrasonic Sealer

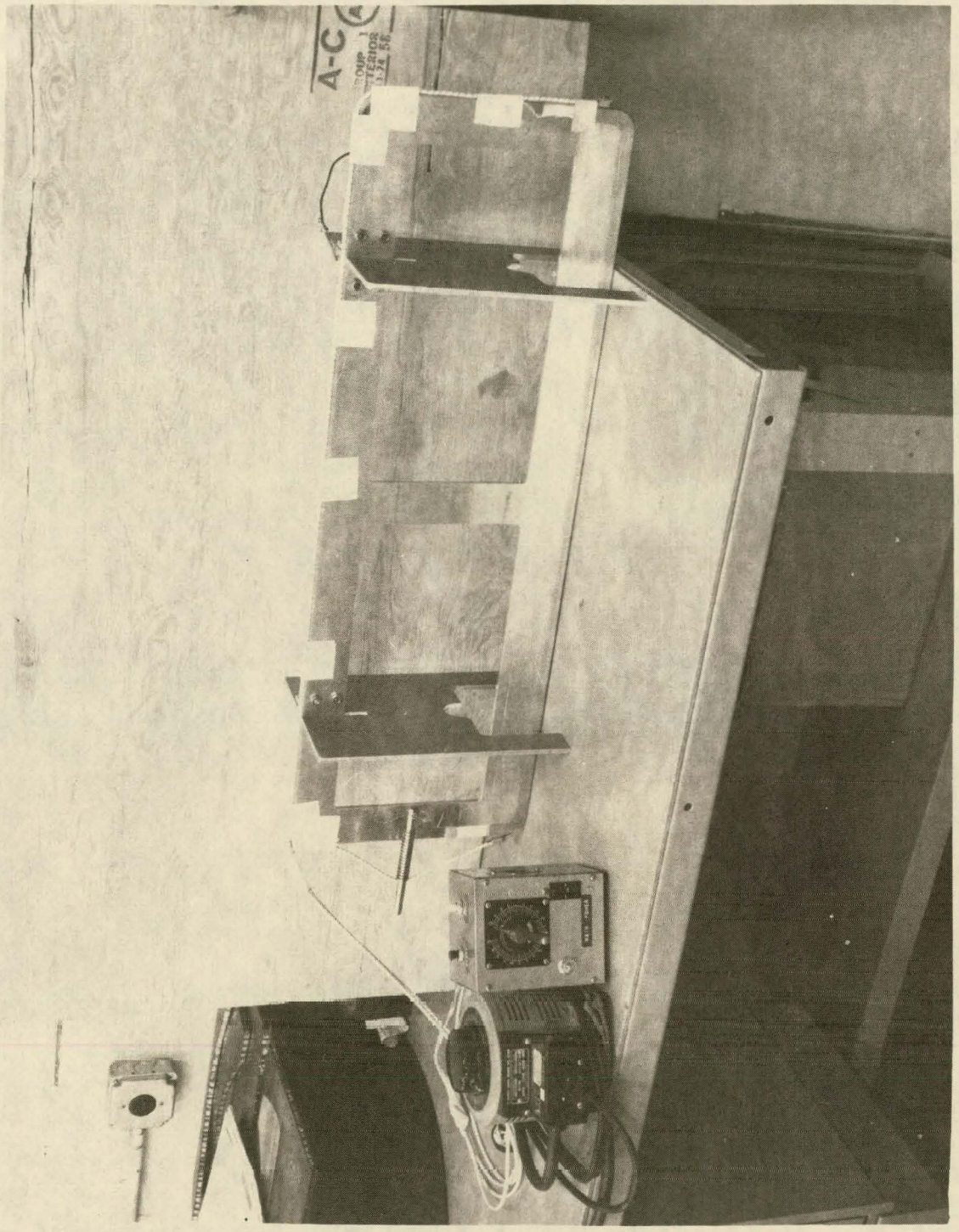

Figure: 4.1-3 Impulse Sealer

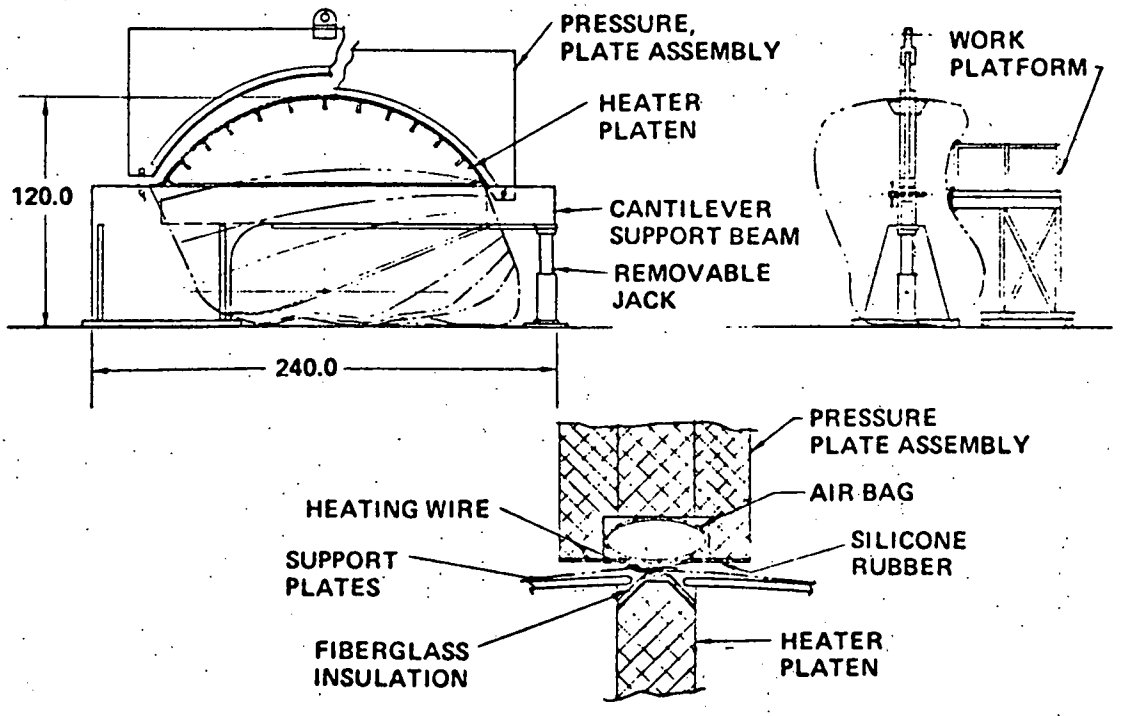

Figure: 4.1-4 Gore Seam Tool Concept

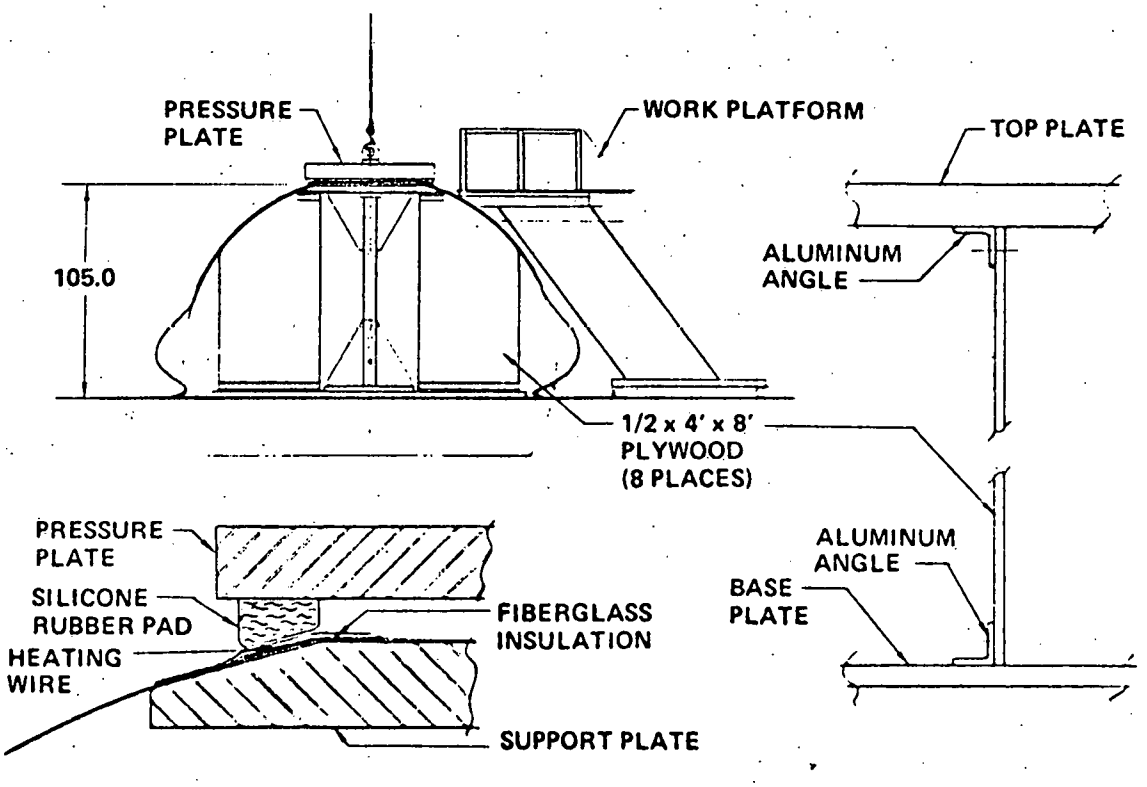

Figure: 4.1-5 Polar Cap Seam

4.2 REFLECTOR FABRICATION

The reflector consists of pretensioned aluminized Mylar bonded to a circular ring made of welded aluminum tubing. The bonding surface of the ring will be a foamed surface, flat within 0.76 mm (0.030 inch).

4.2.1 Fabricating Steps

The fabrication steps for the reflector are shown in Figure 4.2-1. The aluminum tubing will be rolled to shape and then welded to form the ring. The in-plane bonding surface will be formed by foaming a surface on the aluminum tubing against a flat reference surface. The aluminized Mylar sections will be bonded and then placed in a tensioning ring. The reflector membrane will be tensioned and bonded to the support ring by first applying adhesive to the foam surface, positioning the membrane in the tensioning ring on the foamed surface, and then tensioning by adding weights to the tensioning ring. The tensioning ring will have a larger diameter than the reflector ring. The tension on the membrane will be maintained until the adhesive is cured. The reflector will then be trimmed to shape and the tensioning ring removed.

4.2.2 Reflector Seam Fabrication

The aluminized Mylar will be bonded together with a polyester adhesive using a butt joint with an overlapping tape on the back side. The adhesive is a solvent dispersion that is either brushed or sprayed onto the Mylar. Masking can be used to prevent the adhesive from covering non-bonded areas. To obtain the bond, the dried adhesive must be heated to 135° to 162°C (275° to 325°F). This melts the adhesive so that it will adequately wet the Mylar surface. If the Mylar is restrained during this localized heating it will not wrinkle, thus eliminating the need for an additional heat treatment. A vacuum bag will provide sufficient restraint.

A curing agent is added to the adhesive to provide improved environmental resistance to the bond area. This is a room temperature cure which takes several days to complete. It does not appreciably improve bond strength but does improve thermal resistance.

4.2.3 Foamed Surface Fabrication

The flat surface of the reflector ring will be obtained by foaming between the aluminum tubing and a flat in-plane reference surface. The foam used will be a two part Urethane self-skinning foam. It will be constrained during foaming to produce the density required and the surface skin. The

normal cure will be 16 hours at room temperature, however, it can be removed from the mold within 30 minutes. The cure rate can be accelerated with elevated temperatures.

Tensile and creep tests have indicated adequate strength of the foam and of the foam to aluminum bond. A subscale reflector has been fabricated successfully using the foam in an independent research program at Boeing.

4.2.4 Bonding the Pre-Tensioned Reflector

The Mylar reflector film will be bonded to the foam surface with a 2 part Urethane adhesive. This is a room temperature curing 100% solids adhesive. A layer of the adhesive is placed on the foam and then the reflector film is placed on the surface. The film is then tensioned while the adhesive is in the uncured state. Sufficient pressure on the bond line is obtained from the weights used to provide the tensioning. The tensioning must be maintained until the adhesive has cured. Elevated temperatures will accelerate the cure.

4.2.5 Tool Design

The reflector fabrication will require only one major tool to foam the in-plane surface and tension and bond the film to this surface. A concept of this tool is shown in Figure 4.2-2. Other fabricating aids will be a template for rolling the ring segments, a welding jig, and a layout table that can be vacuum bagged.

4.3 SMALL SCALE PROTOTYPES

A subscale heliostat has been fabricated with a 1.07 meter (42 inch) diameter dome and a .91 meter (36 inch) diameter reflector in an independent research program at Boeing. The dome consisted of 11 gores and a polar cap with heat sealed joints. The reflector had a rolled aluminum ring with a cast-in-plane surface. The aluminized Mylar was pre-tensioned and bonded to this ring. Figure 4.3-1 shows the bonding and tensioning operation.

In the same program, a 1.32 meter (52 inch) diameter reflector was fabricated with 2 bonded seams in the film. The Mylar used had been used in the Tedlar polishing step and was not aluminzed. The seams were bonded with polyester adhesive. Polyurethane foam was used to obtain the in-plane surface and polyurethane adhesive was used to bond the film to the foam. A picture of this reflector is shown in Figure 4.3-2.

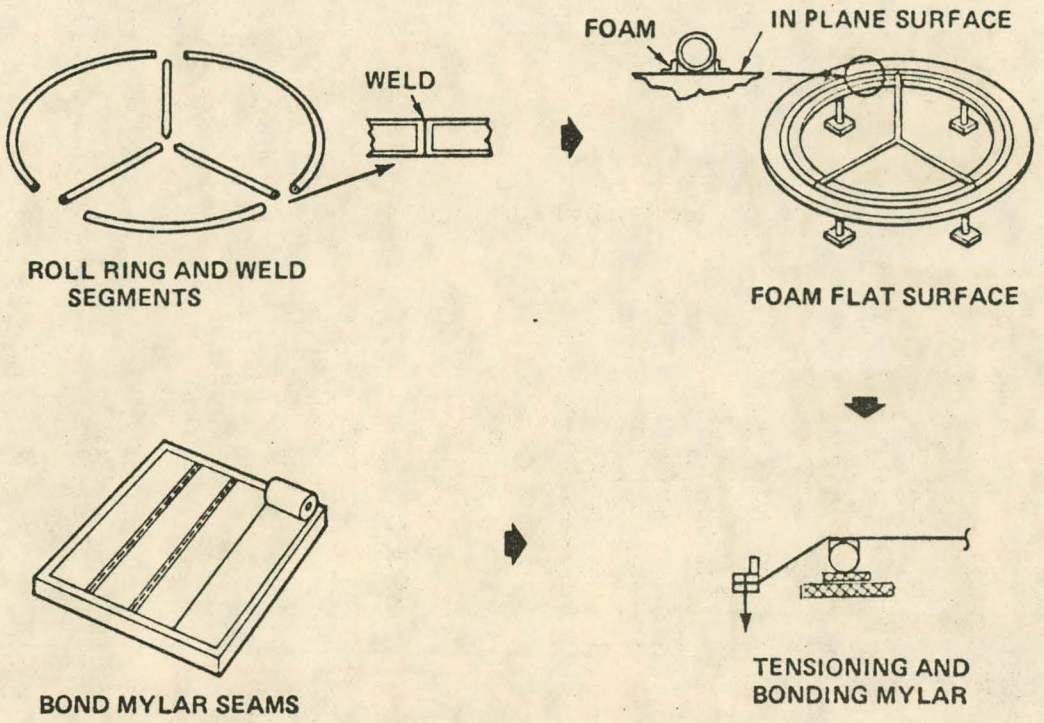

Figure: 4.2-1 Reflector Fabrication Steps

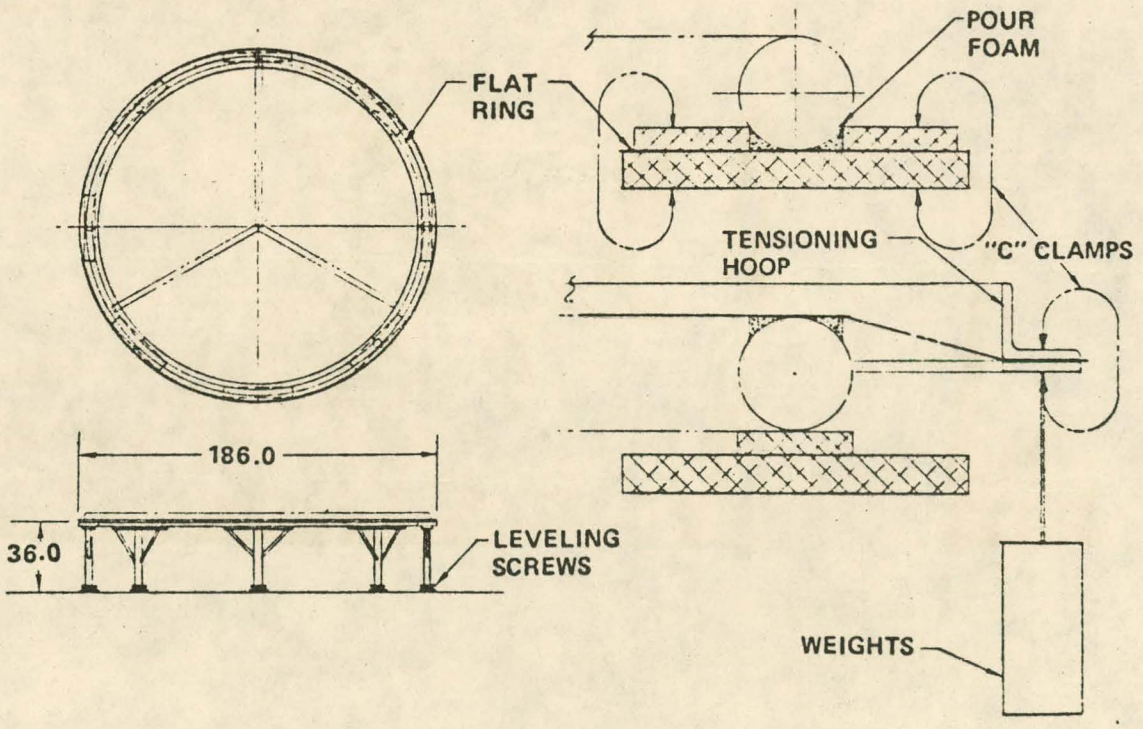

Figure: 4.2-2 Foaming and Tensioning

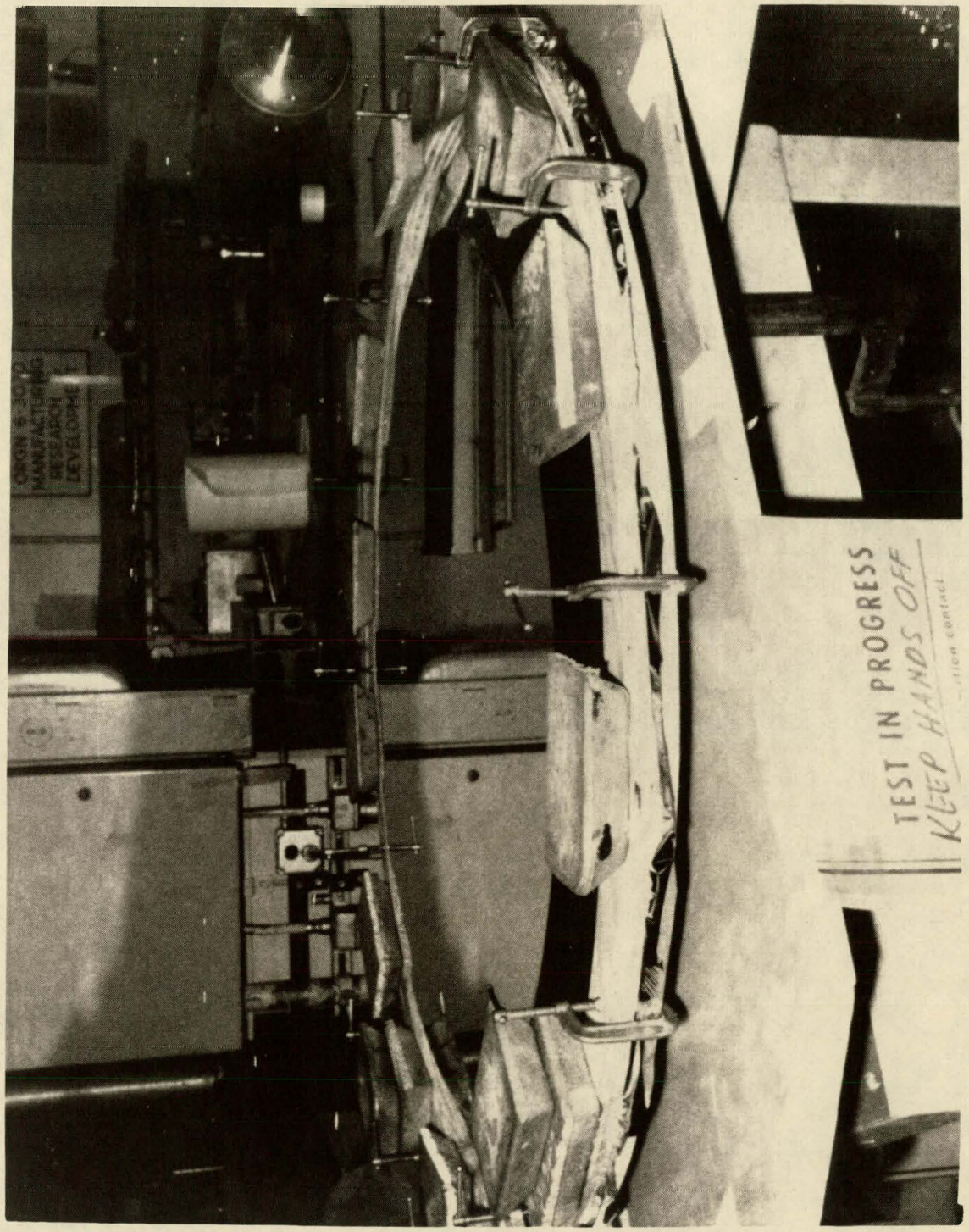

1/5 SCALE REFLECTOR 10-28-75 SMP 20080

Figure: 4.3-1 Subscale Heliostat Reflector Bonding and Tensioning Operation

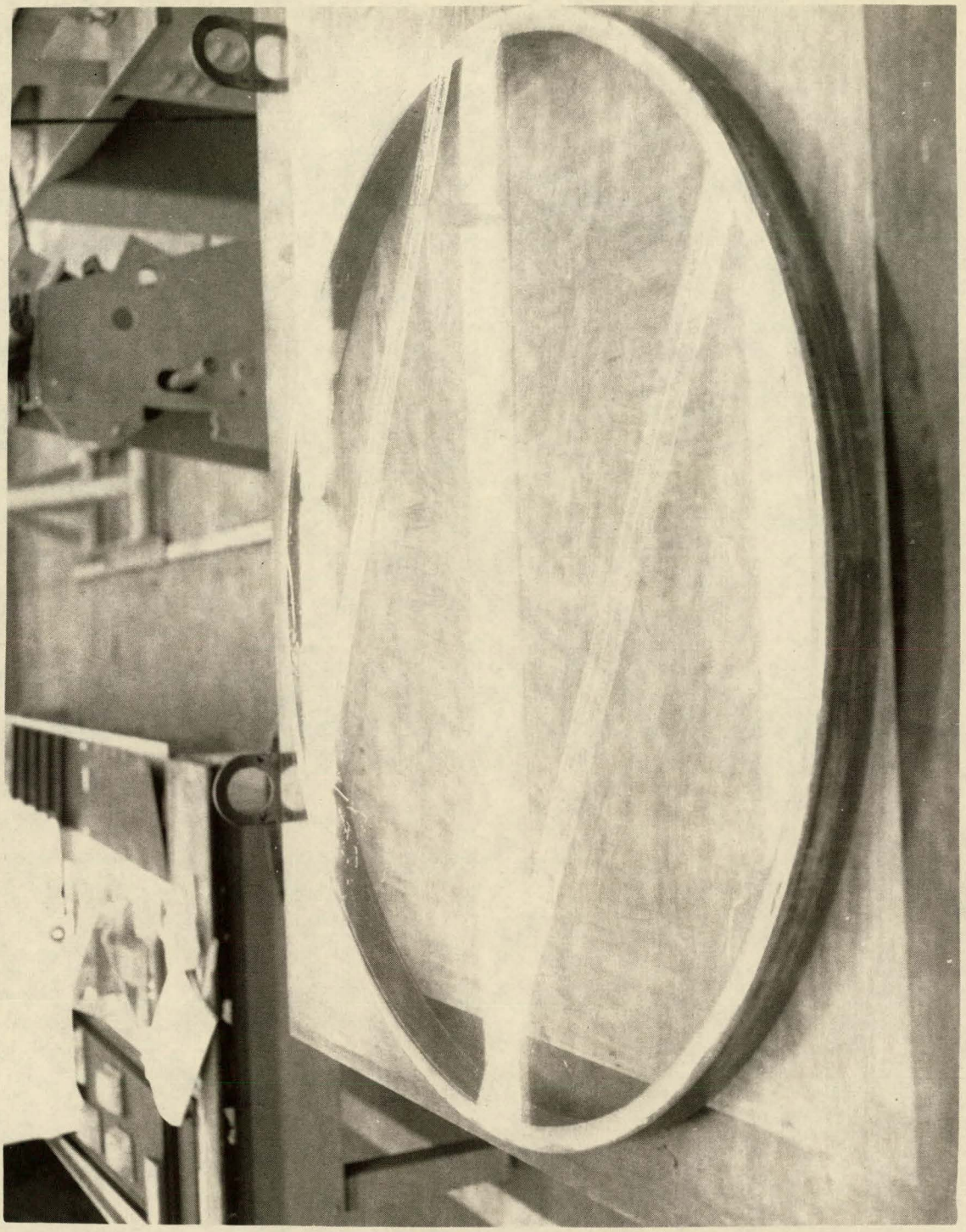

Figure: 4.3-2 1.32 Meter Subscale Reflector

THIS PAGE

WAS INTENTIONALLY

LEFT BLANK

5.0 RESEARCH EXPERIMENTS TEST PLAN

5.1 INTRODUCTION AND SUMMARY

This section of the document describes the assembly, integration, and array tests planned for the Collector Subsystem Research Experiment (CSRE) and Preliminary Design of a Pilot Plant - Phase I and was prepared in accordance with the requirements of CDRL Item 6. It provides a list of planned tests, a description of each test, states the test objectives, and shows the sequence of testing and schedule for test performance.

Table 5.1-1 summarizes the planned tests along with individual objectives.

5.2 ASSEMBLY TEST PLANS

The planned tests are intended to verify satisfactory performance of the transparent enclosure, reflective, and drive and control assemblies when subjected to a variety of environmental conditions and to generate structural and electrical/mechanical data required for design refinement.

The overall objectives of these tests are:

1. Collect technical design data;
2. Collect qualitative handling and maintenance data;
3. Expose assemblies to environments simulating those anticipated during plant operation;
4. Assure assemblies are adequate in performance and configuration for subsequent integration tests.

5.2.1 Transparent Enclosure Tests

5.2.1.1 Pressure and Leak Rate Test

Purpose

a) Verify design pressure is adequate to support enclosure and provide desired surface quality. (.056 psi internal pressure)

b) Verify ability of total enclosure to withstand design allowable stress. (.236 psi internal pressure)

c) Evaluate seam and seal quality for leakage.

Configuration

The test configuration will consist of a transparent enclosure installed on a foundation without reflective assembly or drive and control assembly. Enclosure support will be provided by a blower and/or manifolded compressed gas supply.

TABLE 5.1-1 PLANNED TESTS

TEST TYPE	TEST TITLE	OBJECTIVE
ASSEMBLY Transparent Enclosure	PRESSURE	Qualify enclosure for maximum operational stress to be expected on portions of the dome.
	LEAK RATE	Measure enclosure air leakage at operational pressure.
	ENVIRONMENTAL EXPOSURE	Verify survival of enclosure under 3 seasons of desert weather conditions.
	MAINTAINABILITY HANDLING	Develop and demonstrate handling/ installation and repair/cleaning techniques.
ASSEMBLY Reflective Assembly	DYNAMICS (Nat. Frequency)	Measure dynamic characteristics.
	MAINTAINABILITY & HANDLING	Develop and demonstrate handling/ installation and repair/cleaning techniques.
ASSEMBLY Drive & Control Assy.	ASSEMBLY TESTS	Verify functional performance for all modes.
	THERMAL TEST	Verify performance before, during, and following exposure between temperature extremes.
INTEGRATION	REFL. ASSY/ D&C INTEGRATION	Verify fit and clearance.
	REFL. ASSY/DRIVE & CONTROL/TRANS. ENCL./INTEGRATION	Verify fit and clearance.
ARRAY	OPTICAL TEST	Measure energy collection performance. Measure heliostat transmittance. Measure heliostat reflectance.
	DRIVE & CONTROL TESTS	Demonstrate calibration & alignment. Demonstrate operational modes.
	EXTENDED OPERATION DEMONSTRATION	Demonstrate continuous array operation.

Test Description

The transparent enclosure will be inflated to and maintained at design pressure while a walk around inspection is made to locate major leaks or configuration problems. Photographs will be taken at selected seam and tiedown locations and of the overall setup.

The air supply apparatus will be valved off and a pressure vs. time profile taken.

Next, the enclosure will be repressurized gradually until the maximum test pressure is reached (design pressure + TBD margin). Strain gages located at selected locations will be monitored during pressurization. The air supply apparatus will be valved off and a pressure vs. time profile taken. Figure 5.2-1 shows the setup and pressure time history schematic.

5.2.1.2 Environmental Exposure

Purpose

a) Verify ability of enclosure to survive 3 seasons (summer, fall, winter) of real-time desert-like weather conditions, including sand abrasion, ultraviolet degradation, thermal cycling, rain, snow, hail, ice, and wind loading.

b) Measure performance of enclosure under wind loading.

c) Demonstrate foundation installation.

Configuration

The test configuration will consist of 2 transparent enclosures with foundations and blowers installed at the Boardman, Oregon, test site. The setup will include instrumentation and recording equipment that needs minimal attendance.

Test Description

The transparent enclosures will be exposed to the weather for 3 seasons to assure that a wide variety of typical desert conditions are experienced. Meteorological data will be recorded during the exposure.

The enclosure will be instrumented with thermocouples, deflection indicators, strain gages, and accelerometers to measure the structural properties under wind loading. The following will be measured:

a) Deflection vs. wind velocity

b) Membrane stress vs. wind velocity

c) Natural frequency and mode shapes

d) Dynamic response due to wind
e) Selected time/temperature histories
f) Internal relative humidity

Data will be continually recorded and time indexed to allow later correlation to meteorological data.

Figure 5.2-2 depicts the environmental exposure setup.

5.2.1.3 Handling and Maintainability

Purpose

a) Document enclosure's resistance to permanent wrinkling, scratching, or other damage during fabrication, storage, transportation, and installation.
b) Develop cleaning and repair procedures.

Configuration

a) Configurations shall be those resulting from normal tooling, packaging, transportation, and erection methods developed in the manufacturing and installation program.
b) An erected enclosure will be used to verify cleaning and repair procedures. The enclosure should be visibly dusty (or dirty).

Test Description

Optimum handling shall be determined during the course of manufacturing operations. Folding techniques, protective cloth or paper, storage and transportation containers will be evaluated. Handling operations during fabrication and installation will be developed, documented, and photographed. Special attention will be given to the avoidance of creasing or scratching the material or seams.

Using the cleaning methods and materials developed from coupon level testing, the enclosure will be cleaned. The cleaning apparatus will be of sufficient scale to demonstrate technique.

Demonstrate ingress and egress by entering and exiting enclosure with heliostat tool kit. Observe visually, any change in enclosure shape and height due to pressure losses during entry or exit.

Repair of the transparent enclosure material will be demonstrated at the coupon level. In the event a puncture, tear, or seam failure occurs during handling, installation or field operation repair will be demonstrated.

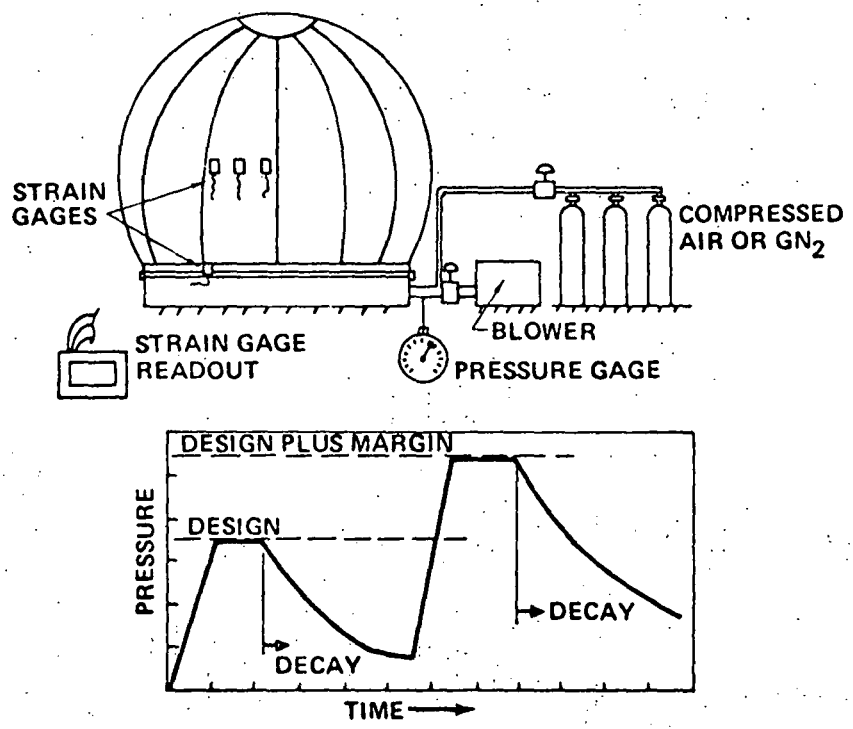

Figure: 5.2-1 Pressure and Leak Rate Test

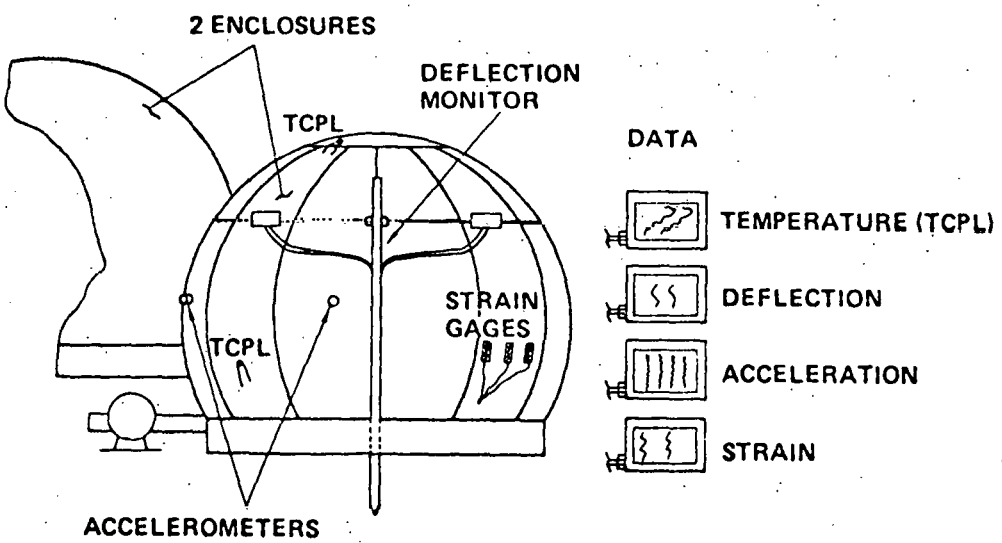

Figure: 5.2-2 Environmental Exposure - Boardman Site

5.2.2 Reflective Assembly Tests

5.2.2.1 Dynamic Tests

Purpose

a) Determine natural frequency of assembly

b) Determine simple mode shapes of assembly

c) Measure dynamic response of assembly to drive motor inputs.

Configuration

The test configuration will consist of a reflective assembly including reflector, support boom, and gimbal assembly with drive modes. The gimbal must be complete to the extent that representative pulses can be input to the reflector by a partial drive/control assembly or simulator. The support boom will be rigidly mounted to the laboratory floor or the portable heliostat base.

Test Description

The support boom and the reflector will be instrumented with accelerometers at TBD locations. Readout equipment shall consist of a CRT display and a multichannel strip chart recorder (visicorder). Dynamic responses to manual inputs at various locations and drive motor inputs (tracking and emergency stow) will be measured and recorded. (See Figure 5.2-3)

5.2.2.2 Handling and Maintainability

Purpose

a) Document reflector's resistance to permanent wrinkling, scratching, or other damage during fabrication, storage, transportation, and installation.

b) Develop cleaning and repair procedures.

Configuration

a) Configurations shall be those resulting from normal tooling, packaging, transportation, and erection methods developed in the manufacturing and installation program.

b) An erected reflector will be used to verify cleaning and repair procedures.

Test Description

Optimum handling shall be determined during the course of manufacturing operations. Protective cloth or paper, storage, and transportation containers will be evaluated. Handling operations during fabrication and

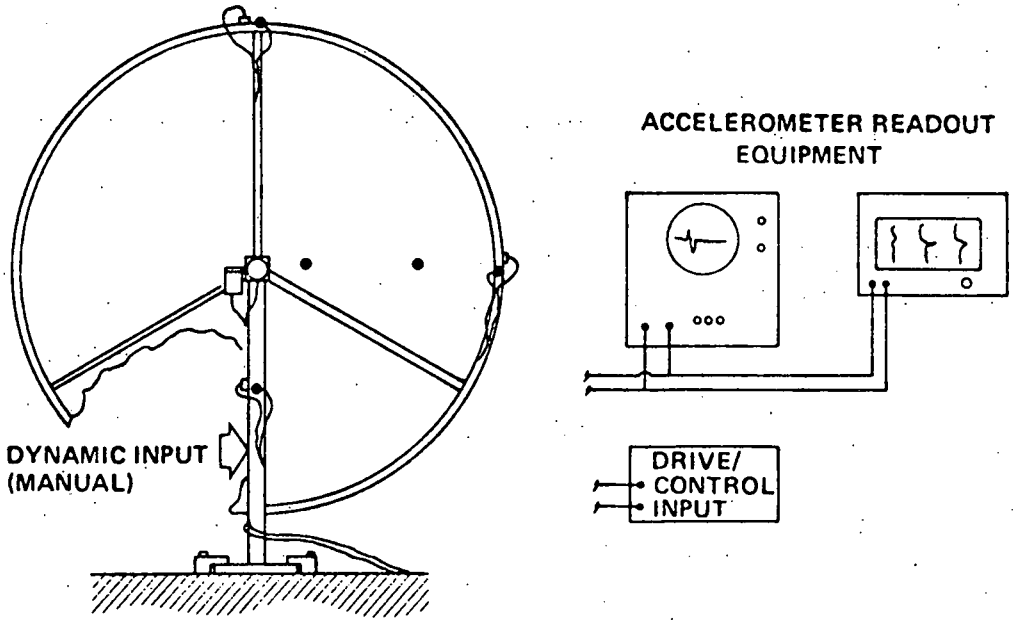

Figure: 5.2-3 Reflector Dynamics Test

installation will be developed, documented, and photographed. Special attention will be given to the avoidance of creasing or scratching the material or seams.

Using the cleaning methods and materials developed from coupon level testing, the reflector will be cleaned. The cleaning apparatus will be of sufficient scale to demonstrate technique.

Repair of the reflector material will be demonstrated at the coupon level. In the event a puncture, tear, or seam failure occurs during handling, installation or field operation repair will be demonstrated.

5.2.3 Drive & Control Assembly Tests

5.2.3.1 Drive & Control Assembly Integration Tests

Purpose

Verify functional operation of drive and control assembly including field controller and one heliostat set of drive and control components.

Configuration

The test configuration will consist of the field controller and one heliostat set of drive and control components.

Test Location

Tests conducted in an electronics test lab at Boeing Kent.

Test Description

Integrate electronic trans. unit 182-12711, manual control unit 182-12713, drive actuators 182-12715, and gimbal mechanism 187-12717, verify operational performance of components.

Perform field controller hardware functional checkout.

Perform field controller software functional checkout.

Perform field controller hardware/software functional checkout.

Integrate field controller and one heliostat set drive and control components. Verify functional operation of control modes, including:

- o Normal tracking
- o Shutdown
- o Standby
- o Alignment

5.2.3.2 Thermal Test

Purpose

Verify performance of drive and control assembly before, during, and following exposure to the temperature extremes called out in the

requirements specification.

Configuration

The complete drive and control assembly, in operational condition, will be tested. The following components are included:

Drive Actuators
Gimbals
Heliostat Electronic Transmission Unit
Heliostat Manual Control Unit
Heliostat Wiring System
Field Controller

Test Description

The assembly will be installed inside a thermal test chamber. The field controller will be situated outside the chamber, as it must be maintained in the range of +5 to +50°C. Thermocouples will be attached to individual components and continuously monitored on a strip chart recorder. The drive and control assembly will be subjected to the following conditions:

1) Chamber and components at ambient temperature - verify functional performance
2) Chamber at +49°C (+120°F) components temperature stable - verify functional performance
3) Chamber at -20°C (-4°F) components temperature stable - verify functional performance
4) Chamber at -30°C (-22°F) components temperature stable - survival - non-operational
5) Chamber and components at ambient temperature - verify functional performance

Performance shall be verified visually thru a window in the test chamber and by monitoring encoder responses.

5.3 INTEGRATION TEST PLANS

Integration testing is performed to assure that the 3 major assemblies (reflective assembly, transparent enclosure assembly and drive and control assembly) are compatible in function and fit. This testing allows the systematic stepwise buildup and checkout of a complete heliostat on a portable foundation inside a laboratory high bay prior to the commencement of field testing.

5.3.1 Integration of the Reflective Assembly and the Drive and Control Assembly

5.3.1.1 Fit and Clearance Verification

Purpose

Verify that the reflective assembly, drive and control assembly and heliostat base interfaces are compatible and mutual clearances exist that are per drawing and adequate for all operational modes.

Configuration

A complete drive and control system (or prototype), a reflective assembly and the portable heliostat base will be utilized for the integration. The work will be performed in a laboratory high bay where minimal air currents exist and an overhead crane is available.

Test Description

The drive and control assembly support post with gimbal mechanism will be installed on the portable heliostat base per drawing. The reflective assembly will then be attached at the gimbal interface. The drive and control assembly will be operated thru all azimuth and elevation configuration to verify mechanical clearances, non-interference of wiring harness, and operation of limit switches.

5.3.2 Integration of Transparent Enclosure, Reflective Assembly and Drive and Control Assembly

5.3.2.1 Fit and Clearance Verification

Purpose

Verify transparent dome interfaces with reflective assembly and heliostat portable base per drawing and with adequate clearance for all operational modes.

Configuration

The test configuration will consist of the drive and control assembly integrated with the reflective assembly on the portable base. A transparent dome and blower apparatus will be available for integration in this test. Work will be performed in the laboratory high bay with the use of an overhead crane.

Test Description

Blower apparatus will be installed and functionally checked out for fit, clearance and capacity. The transparent dome will then be lowered over the reflector and attached at the base interface following installation

procedures previously developed. All details will then be completed such that a complete heliostat configuration exists. The drive and control assembly will be operated thru all azimuth and elevation attitudes to verify fits and clearances of the transparent dome are per drawing and adequate.

5.4 ARRAY TEST PLANS

Array testing will be performed at the Boeing Boardman Test site near Boardman, Oregon. The objective of array testing is to demonstrate overall operation of a collector subsystem, using a 3 heliostat array.

The array setup will be accomplished by complimenting the 2 base/enclosure setups erected earlier for environmental exposure (assembly level) with a 3rd base/enclosure setup, installing 3 reflective assemblies and 3 drive and control systems.

Also included at the test site are a 11.0m x 11.0m x 13.4m high test stand (36 ft x 36 ft x 44 ft high), a power and control room where the field processor and electrical power (including D.C. backup power bank) are located, the target with scanning and fixed radiometers, solar tracking radiometer, laser alignment equipment, support equipment and a meteorological station nearby.

Plan and elevation schematics of the array test layout are shown in Figures 5.4-1 and 5.4-2.

5.4.1 Optical Tests

5.4.1.1 Energy Collection Performance Test

Purpose

The purpose of this test is to measure the integrated energy collection efficiency, the uniformity of irradiance and focusing effect of the projected solar image for each heliostat and for the array.

Configuration

The configuration for this test includes the complete array arranged with respect to the tower as shown in Figures 5.4-1 and 5.4-2. The drive and control system will be aligned and fully operational.

Test Description

The projected solar image of each heliostat will be mapped using the scanning apparatus on the tower. The scanner, which is equipped with many solar sensors, can map the entire image in a few minutes while direct solar measurement is being taken with an equatorial mounted

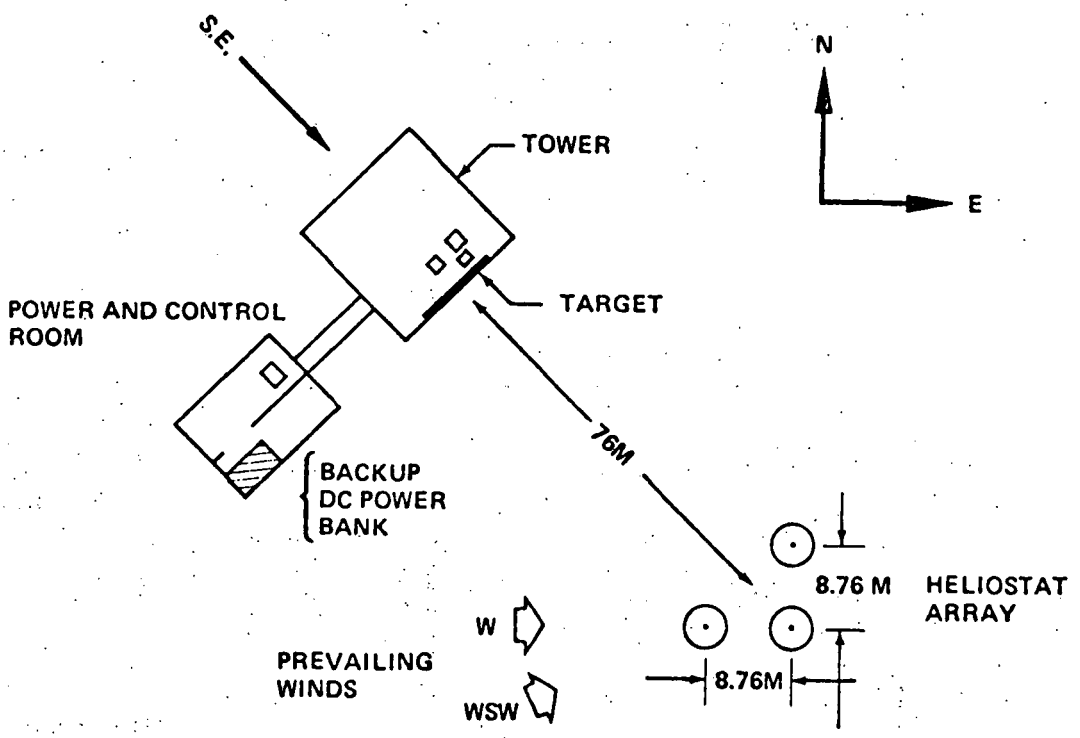

Figure: 5.4-1 Heliostat Array Test—Plan View

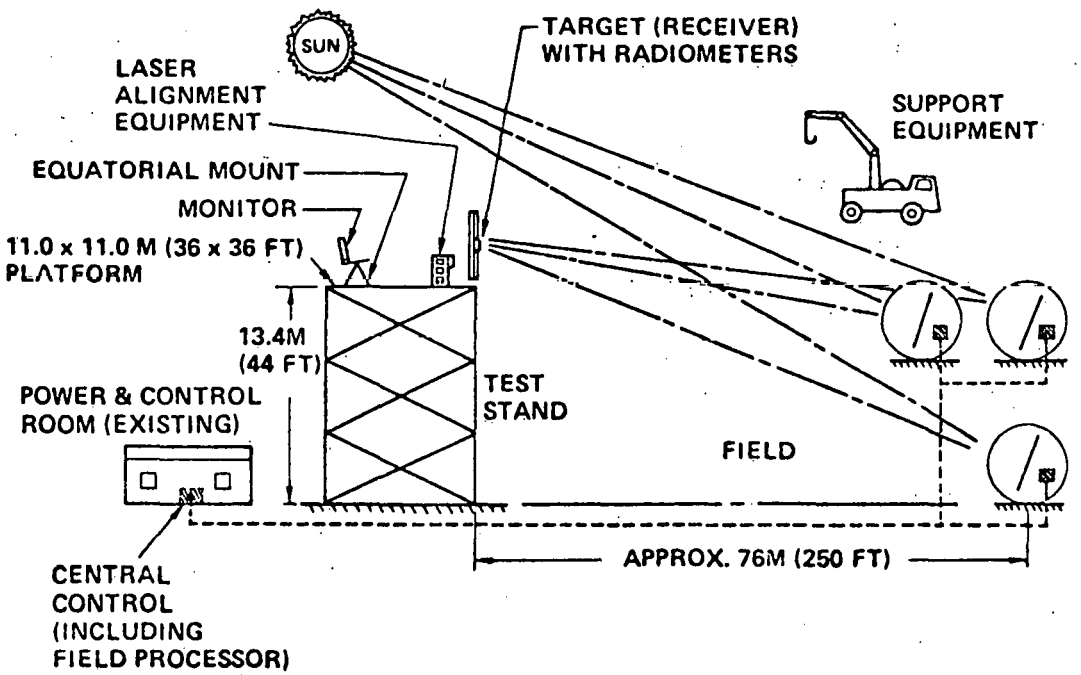

Figure: 5.4-2 Heliostat Array Test—Elev. View

tracking radiometer. The total energy measured by the scanner will be compared with the energy measured by the direct reading solar monitor to obtain overall collection efficiency. The iso-solar map provided by the scanner will also be used to evaluate non-uniformities and focusing effects that may result from non-flatness in the reflector. Scans will be taken at several different times of the day to evaluate reflector flatness and image shape as a function of reflector attitude.

The above scanning will be repeated with all 3 heliostat images being projected on the tower simultaneously.

5.4.1.2 Heliostat Transmittance Tests

Purpose

The objective of these tests is to establish the solar transmittance of fabricated domes for both comparison with coupon level test data and use in collector subsystem performance calculations. This data will compliment coupon level data because it accounts for wrinkles, dust, and the real solar spectral distribution.

Configuration

The configuration will consist of a complete heliostat with the reflector stowed approximately vertical and parallel to the sun's rays as shown in Figure 5.4-3. This configuration allows transmittance measurements inside and outside the dome without obstruction from the reflector.

Test Description

Data transmittance tests will be performed using an EPPLEY Normal-Incidence pyrheliometer as shown in Figure 5.4-3. This instrument measures the incident radiation subtending an angle of 5.73°. Transmittance scans across the dome cross-section will be made with the pyrheliometer located both inside and outside the dome. For reference purposes, solar intensity will be measured outside the dome during each scan. Data taken with the pyrheliometer located within the dome will be useful for calculating transmittance losses of the heliostat (without shadowing or blocking). Data taken with the pyrheliometer located outside the dome will provide data for calculating losses due to shadowing and blocking by adjacent domes. Transmittance data will be correlated to position and angle of incidence on the dome.

Dome transmittance measurements will be made at the beginning and end of the 7 month exposure period at Boardman.

5.4.1.3 Heliostat Reflectance Tests

Purpose

The objective of these tests is to determine the effective reflectance of a heliostat considering both reflectance and transmittance losses.

Configuration

The configuration will consist of a complete heliostat with the reflector positioned as required to allow the measurements described in Figure 5.4-4 and below.

Test Description

Similarly to dome transmittance tests, the normal incidence pyrheliometer will be used to measure the reflected sunlight at various angles of incidence of sunlight on the mirror. A schematic of the test apparatus for this measurement is shown in Figure 5.4-4. Heliostat reflectance tests will be made at the beginning and end of the 3 month period in which mirrors will be operating in domes.

5.4.2 Drive and Control Assembly Tests

5.4.2.1 Operational Modes Demonstrated

Purpose

The purpose of these tests is to demonstrate the ability of the drive and control assembly to perform in the following modes:

A) Track (Normal)
B) Shutdown
C) Standby
D) Manual

Calibration and alignment mode demonstration was outlined in Section 3.3.2.5. Individual heliostat as well as array control will be demonstrated.

Configuration

The required configuration is the fully operational heliostat array (3 units) described in paragraph 5.4 above. Included in the control room will be:

- Field Controller
- PDP-11/03 Computer
- Interface Box
- Operator Panel
- T.O.D. Clock
- Teletype

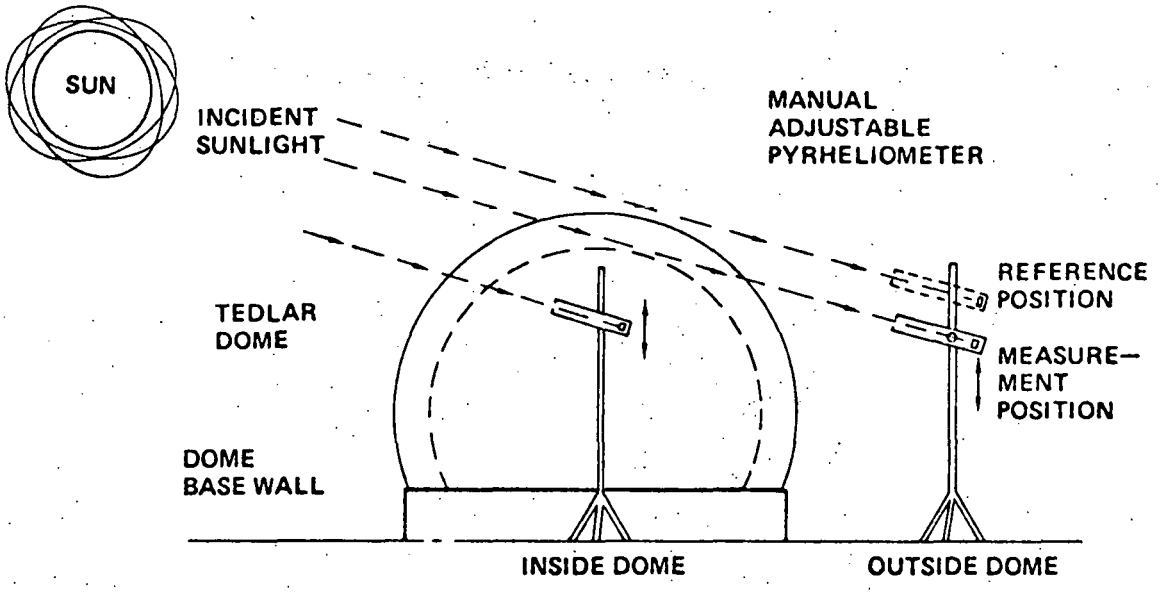

Figure: 5.4-3 Dome Transmittance Test

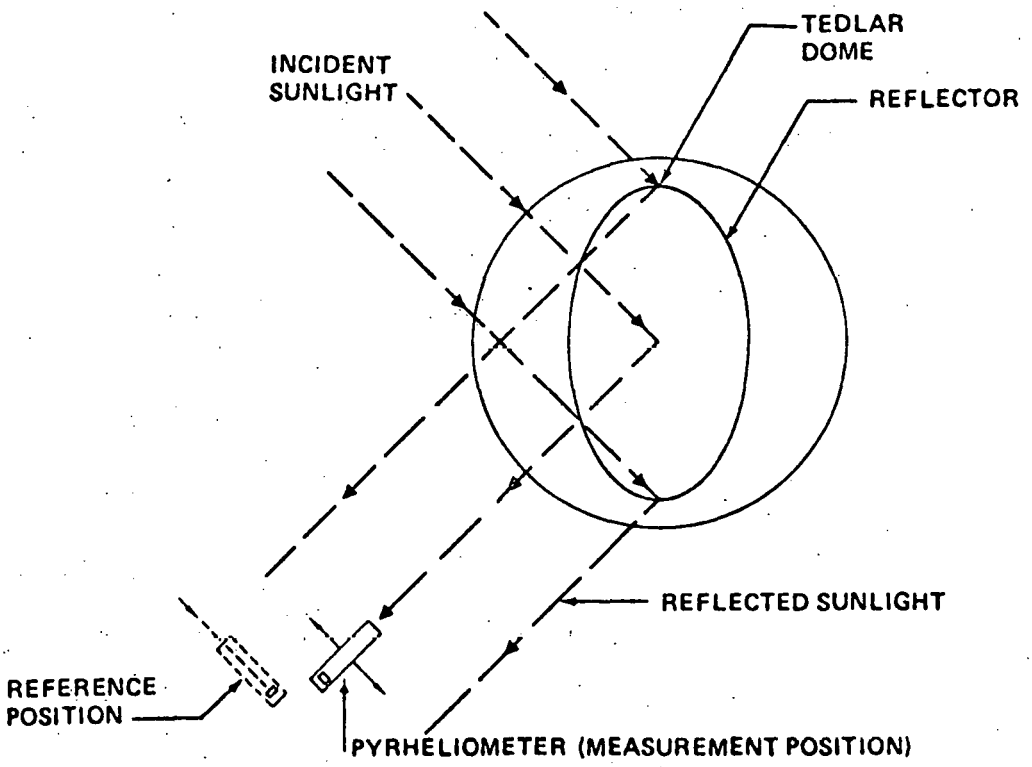

Figure: 5.4-4 Heliostat Reflectance Tests

Description

A) Tracking will be demonstrated by commanding the drive and control system to reflect the solar image onto the test target. Visual observations and image scans will be made at the target periodically to verify image position is located within predetermined spatial limits and to estimate the σ-value for alignment. Tracking accuracy will be evaluated from this test.

B) Emergency shutdown mode will be performed by initiating shutdown command at operator panel and verifying that the image departs from the target in the prescribed horizontal motion, and that it can be removed from an imaginary receiver in less than 40 secs.

C) The standby mode will be demonstrated by initiation of the standby command at the operator panel and verifying that the image is reflected onto the appropriate target position. If proper operation is performed, the image will be projected along a line 1-2^{o} off azimuth axis. This will be visually observed and scanned periodically. The target will be marked to aide in observing the offset image.

D) Demonstration of the manual control mode will be performed by plugging the portable manual control unit into the desired heliostat receptacle and verifying:

1) Control of reflector thru all azimuth and elevation attitudes
2) Limit switch operation
3) Field controller disable operation

The above will be repeated for all three heliostats.

5.4.3 Extended Operation Demonstration

Purpose

The intent of this testing is to gain confidence in the array design and hardware by demonstrating continuous semi-unattended operation of the array for approximately 3 months.

Configuration

The configuration for this test includes the complete array arranged with respect to the tower as shown in Figures 5.4-1 and 5.4-2. The drive and control system will be aligned and fully operational.

Test Description

Subsequent to installation, alignment and checkout, the 3 heliostats will be operating in the tracking mode for approximately 3 months. Interruptions will occur when the array tests described in above

paragraphs are performed. Fixed solar monitors on the test tower will provide continuous verification that the reflectors are properly tracking the sun.

5.5 SCHEDULE

Figure 5.5-1 is the test schedule for the entire test program.

5.6 TEST EQUIPMENT REQUIREMENTS

Table 5.6-1 is a matrix of the equipment required for the indicated tests and the availability status.

Those items that are shown in the status column as"fabricate"are considered project-peculiar deliverable hardware. Equipment that is shown as available such as voltmeters, accelerometers, solar measuring equipment, are considered as Non deliverable.

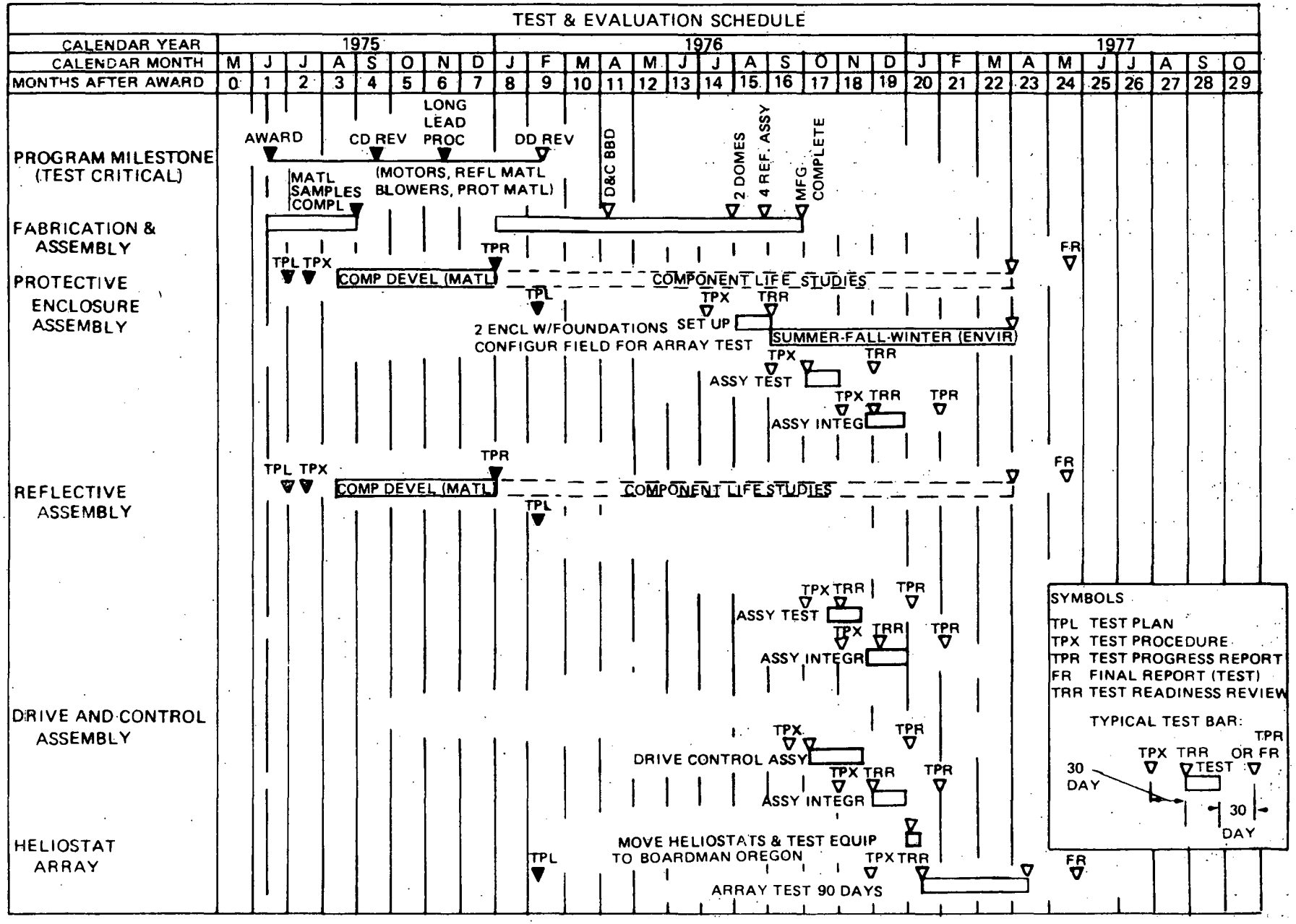

Figure: 5.5-1 Test and Evaluation Schedule

Table 5.6-1

TEST EQUIPMENT REQUIREMENTS

Test	Required Equipment	Status: Fabricate Available
Enclosure Pressure Test	- Gas Pressurization Values, Regulator, etc.	Available
	- Simple Test Fixture	Fabricate
	- Strain Gages and Readout Equipment	Available
	- Deflection Instruments	Available
Enclosure Environmental Exposure	- Meterological Instrumentation	Available at Boardman Site (Portland General Electric Station)
	- Strain Gages and Readouts	Available
	- Deflection Instruments and Readouts	Available
	- Thermocouples and Readouts	Buy
	- Accelerometers and Readouts	Available
	- Foundations (3)	Fabricate
Reflective Assy. Dynamic Test	- Accelerometers	Available
Drive and Control Environmental Test	- Thermal Chamber	Available
	- General Purpose Test Equipment	Available
	- Thermocouples	Available
Reflector/Drive/ Control Integration	- Portable Foundation	Fabricate
	- Gen. Purpose Test Equipment + Tools	Available
Reflector/Enclosure/ and Control Integration	- Portable Foundation	Available (from above)
	- Gen. Purpose Test Equipment and Tools	Available (from above)

Table 5.6-1 (Contd)

Test	Required Equipment	Status: Fabricate Available
Array Test	- Geodolite Laser Alignment Equipment	Available
	- Foundations (3)	Available (from above)
	- Beam Scanner	Fabricate
	- Solar Measuring Equipment	Available
	- Normal Incidence Pyroheliometer	Available
	- Gen. Purpose Test Equip.	Available
	- Central Control Simulator	Available
	- Meterological Instrumentation	Available
	- Washing Equipment	Fabricate
	- Truck with Boom	Available
	- Surveyors Equipment transit, tape, rod, etc.	Available
	- Portable Scaffolds	Available
	- Stepladders	Available
	- Mechanical Tools	Available
	- Electrical Trouble-shooting Tools	Available

6.0 RESEARCH EXPERIMENTS TESTS AND RESULTS

This section of the document is a presentation of results of materials testing to-date. Included are test descriptions and results of optical tests, mechanical tests, environmental exposures and washability tests.

6.1 OPTICAL PROPERTIES

6.1.1 Specular Transmittance

Special specular transmittance apparatus assembled for these measurements utilizes an existing Beckman DK-2A spectrophotometer and a Gier-Dunkle integrating sphere to provide specular transmittance within an acceptance cone angle of 0.5°, as a function of wavelength from 250 to 2500 nanometers. All tests were conducted at 0.5° cone angle and 12° incident angle.

Transmittance properties for transparent dome candidates are presented in Tables 6.1-1 and 6.1-2.

Tedlar, with no additives, produced transmittance in the range of 85-90%. Teflon FEP (0.25 mm) similarly produced transmittances in the range of 85-90%. All other candidates either fail to meet the transmittance/thickness requirements (86%) or have been eliminated for reasons discussed in Sections 3.1 and 3.2.

6.1.2 Specular Reflectance

Specular reflectance tests are performed with a modified bi-directional reflectometer utilizing a 628 nanometer wavelength laser light source. Apertures defining various solid angles are placed at the entrance port to the integrating sphere/detector to determine the distribution of energy in the reflected beam.

Reflectance data for reflector substrate film candidates are presented in Table 6.1-3. All samples were coated with 1000 Angstroms of aluminum by vacuum deposition prior to tests. All, except as noted, were coated in a single batch.

At the cone angle of interest for Pilot Plant design (0.28°), only Mylar (200XM648A) and Aclar 22A meet the reflectance requirements with 90% and 87% reflectance, respectively. The terms "mate-Co.P" and "non-mate Co.P" refer to Mylar that has been co-polished with Tedlar, and "mate" means that surface of Mylar that is next to the Tedlar in the polishing operation. The co-polishing process appears to affect the Mylar surface such that when aluminized there

6.1-1 Specular Transmittance—Other Transparent Films

Identity	Description	Actual thickness (mm)	Transmission %
7825	Standard Tedlar — DuPont roll polish	.099	81.1
7825	Standard Tedlar	.099	81.2
7826A	No epon	.093	87.9
7826B	No epon (less solids)	.091	86.3
7826B	No epon (less solids)	.093	87.9
7827	Standard Tedlar	.097	85.3
8806	No epon (less solids)	.097	90.1
8152-1	Standard Tedlar — Dunmore roll polish (DuPont mill roll No. 7827)	.099	86.4
8152-1	Standard Tedlar	.100	84.7
8152-2	Standard Tedlar	.099	84.8
8152-2	Standard Tedlar	.099	84.8
8152-2	Standard Tedlar	.099	85.9
8152-3	Standard Tedlar (unpolished) (Virgin No. 7827)	.093	38.2
8377	Standard Tedlar — DuPont press polish	.107	78.3
8378	(UV screen and no epon)	.093	87.5

(50 pt calc., 0.5 cone angle and 12° incident angle)

Table: 6.1-2 Specular Transmittance—Other Transparent Films

Sample description	Nominal thickness mm	Actual thickness mm	Transmission %
Aclar 22C (as received)	.13	.124	63.3
Aclar 22C 10 min, 350-375°F, 200 psi	.13	.114	88.4
FEP 10 min, 246°C-260°C, 1.38 mn/m^2	.51	.518	80.3
(as received)	.51	.513	79.1
(as received)	.25	.249	86.3
(as received)	.13	.124	90.6
(as received) UV control	.25	.257	86.2
(as received) UV control	.25	.254	88.1
Halar (as received)	.19	.203	39.2
(20 min, 240°C, 1.38 mn/m^2, slow cool)	.19	.152	72.9
(5 min, 240°C, 1.38 mn/m^2, quick cool)	.19	.152	78.4
(10 min, 240°C & 1.38 mn/m^2)	.25	.119	73.0
CTFE rich (5 min, 232°C, 0.34 mn/m^2)	—	.132	78.5
No antioxident	—	.348	66.8
Standard	.05	.051	84.6
Standard	.19	.206	72.7
Standard	.25	.259	68.3
(8 min, 240°C, 0.69 mn/m^2)	.25	.191	80.6
Korad A-CV (as received)	.05	.046	75.6
Korad A-CV (as received)	.08	.079	64.6
Tefzel 1000 AE (as received)	.25	.254	77.0
500 AE (as received)	.13	.117	84.1

(12° incident, 0.5 cone, 50 pt)

Table 6.1-3 Reflectance Data

Material Description	Cone Angle 0.28	Cone Angle 0.59	Cone Angle 1.53	Comments
	%	%	%	
ACLAR 22A, Polished	87.4	89.3	90.5	Metalized as one batch
(5 MIL), Unpolished	64.9	85.9	88.8	
FEP "A", Polished	43.1	81.2	82.6	
(20 MIL), Unpolished	10.7	34.7	70.1	
HALAR, Polished	18.5	48.4	81.4	
(7.5 MIL), Unpolished	0.9	4.5	20.1	
KAPTON "H" Glossy Side	62.5	80.9	90.4	
(1 MIL) Dull Side	7.1	13.0	31.1	
KAPTON "F" Side 1	6.6	21.2	50.1	
(2 MIL) Side 2	24.9	46.0	66.5	
TEDLAR Polished MILL ROLL #7825 (4 MIL)	38.7	69.6	82.4	
MYLAR MATE-CO.P	74.2	79.8	84.3	
(CO. POL. #7825) NON-MATE CO. P	74.3	78.4	82.5	
MYLAR 200XM648A, Non-Adherable	90.0	90.1	90.3	
AS RECEIVED, Adherable	83.7	84.8	85.3	
MYLAR (200SM648A) MATE-CO. P	84.5	91.5	93.3*	
(CO. POL. 8152-2) NON-MATE CO. P	80.3	83.9	84.9*	
MELINEX (442) AS RECEIVED (2 MIL)	86.7	87.2	87.8	Metalized at Boeing with 1000Å Aluminum

*Cone angle 1.43^{o} instead of 1.53^{o}
**Front surface vacuum-deposited, 12^{o} incident angle from normal

is about a 5% loss in reflectance at the 0.28° cone angle.

6.2 MECHANICAL PROPERTIES

6.2.1 Tensile

Tensile properties were determined for Tedlar, Mylar and Teflon FEP, as shown in Table 6.2-1. Tests were conducted at 21°C (70°F) in accordance with ASTMD882 using a 2.54 cm wide specimen, 15.24 cm gage length and a strain rate of 83% per minute, except as indicated in test variable column. It should be noted that ultimate strength and elongation for several of the batches may be conservative due to the number of "grip" and "near-grip" failures. These conservative values could not be discarded from the average as they were as high, and sometimes higher, than "center-of-test-section" failures. Averages are based on 5 samples per test, except as noted.

Tedlar, 400SG20TR, has an average yield strength of 33.1 MN/m^2 (4800 psi) in both the machine and transverse directions. Its yield strength is not affected by leaving out the commercial additives and is not affected by the polishing process. Mylar, 200XM648A, has an average yield strength of 85.7 MN/m^2 (12.4 Kpsi) in both the machine and transverse directions. The yield strength reduced by 6% due to co-polishing with Tedlar.

Teflon FEP has an average yield strength of 10.0 MN/m^2 (1450 psi) in both machine and transverse directions and appears to be relatively unaffected by co-polishing.

Tensile properties as a function of temperature were also determined for Tedlar, Mylar and Teflon FEP as shown in Figures 6.2-1 and Figure 6.2-2 Yield strength, ultimate strength and elongation were determined using "micro-tensile specimens.

6.2.2 Joint

Tensile lap shear tests were conducted on ultrasonically welded, impulse welded and bonded joints of Tedlar and Mylar. The same test procedures were followed in joint tests as were used in tensile property tests of the parent materials. The test results are summarized in Table 6.2-2.

In all cases the joint failure stress exceeds the design stress with the exception of one ultrasonic weld of Tedlar 8606. Post test examination of the Tedlar, 8606 weld showed poor fusion characteristics.

Test data indicates that superior Tedlar joints were obtained with impulse welding.

Table 6.2-1 Tensile Properties

Material identity	Direction	Yield strength MN/m²	Yield elongation %	Modulus GN/m²	Ultimate strength MN/m²	Ultimate elongation %	Test variables
400SG20TR (DuPont Roll Polish) (Mill Roll No. 7825-Standard)	MD	33.4 (31.9-36.2)	3.5 (3.3-3.8)	0.93 (.84-1.02)	72.3 (68.2-77.9)	223 (174-265)	LR = 12.7 cm/min Gage = 15.24 cm
	TD	29.5 (29.3-30.2)	2.7 (2.2-3.3)	1.11 (.89-1.33)	76.5 (75.8-78.5)	212 (195-258)	
400SG20TR (Dunmore Roll Polish) Dun-Lar No. 8152-1 Pkg w/o mylar (DuPont MR #7827)	MD	34.7 (33.9-36.7)	2.3 (2.0-2.5)	1.54 (1.37-1.84)	68.9① (62.7-73.0)	180① (163-190)	
	TD	34.6 (33.1-35.9)	2.3 (2.0-2.5)	1.49 1.37-1.69	62.7① (58.6-69.6)	250① (237-275)	
400SG20TR (Dunmore Roll Polish) (Dun-Lar #8152-2 Pkg w/mylar (DuPont MR 7827)	MD	33.5 (32.8-34.7)	2.2 (2.0-2.5)	1.51 1.34-1.67	67.5① (64.1-71.0)	180① (170-193)	
	TD	34.0 (32.7-34.5)	2.4 (2.2-2.7)	1.41 (1.36-1.56)	50.3① (44.1--58.6)	204① (170-243)	
400SG20TR (Not Polished) Dun Lar #8152-3 (DuPont MR #7827)	MD	35.6 (34.2-37.5)	2.3 (1.7-3.3)	1.60 (1.12-2.20)	81.3① (78.5-85.4)	180 ① (172-193)	
	TD	34.5 (33.3-35.3)	2.3 (2.0-2.5)	1.51 (1.37-1.67)	75.1 ① (72.3-77.9)	223 ① (210-232)	
400SG(EXP)TR (DuPont Roll Polish) (DuPont MR 7826B-- no epon)	MD	33.5 (31.3-35.1)	2.3 (2.0-2.5)	1.50 (1.36-1.75)	77.9 ①② (77.2-79.9)	191①② (182-198)	
	TD	35.7 (33.7-37.6)	2.6 2.3-3.0	1.37 (1.25-1.47)	78.5 ① (75.1-81.3)	178 ① (177-188)	
400SG(EXP)UT (DuPont Press Polish) (DuPont #8378 = UV screen & no epon)	0°	24.0 ② (22.9-24.7)	1.8 ② (1.7-2.0)	1.31 ② (1.24-1.34)	68.9 ①② (66.8-71.0)	241 ①② (232-246)	LR = 5.1 cm/min 10.2 cm gage
	90°	26.9 ② (24.7-28.7)	1.9 ② 1.7-2.0	1.41 ② (1.36-1.45)	93.0 ② (89.6-98.5)	150 ② (141-165)	
(DuPont Polish) (DuPont MR 8606 no additive)	MD	28.1 (27.5-28.3)	2.6 (2.5-2.7)	1.14 (1.10-1.17)	73.8 (73.1-74.5)	182 (180-185)	LR = 12.7 cm/min Gage = 15.24 cm
	TD	–	–	–	–	–	
200XM648A (as received from DuPont)	0°	86.8 81.3-89.6	2.2 2.1-2.3	3.97 (3.84-4.07)	243 ③ (240-247)	77.7 ② (76.7-78.3)	
	90°	84.7 (82.0-88.2)	2.3 (2.2-2.5)	3.62 (3.50-3.71)	183 (158-190)	114 (101-118)	
200XM648A Dunmore Roll #8152-2 copolished with Tedlar	MD	86.1 (80.6-95.1)	2.4 (1.8-3.3)	3.70 (2.87-4.72)	158 (144-171)	71.9 (53.9-96.7)	
	TD	75.1 (62.7-80.6)	1.7 (1.8-2.0)	4.35 (4.11-4.49)	225 (214-231)	70.8 (59.2-78.0)	
FEP (10 mil) (as received from DuPont)	MD	10.1 (9.4-11.0)	2.8 (2.5-3.0)	0.37 (.31-.40)	32.6 (28.0-3.91)	367 ③ (333-397)	
	TD	9.9 (9.3-10.1)	2.4 (2.2-2.7)	0.42 (.37-.44)	30.4 (25.1-34.0)	404 (362-442)	

① Data may be conservative due to significant number of jaw and near-jaw failures
② Average of 3 specimens
③ Average of 4

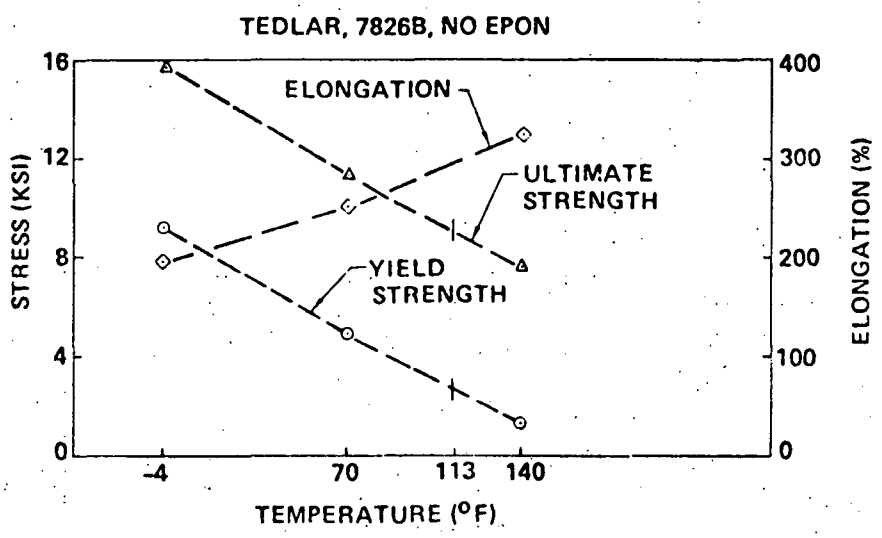

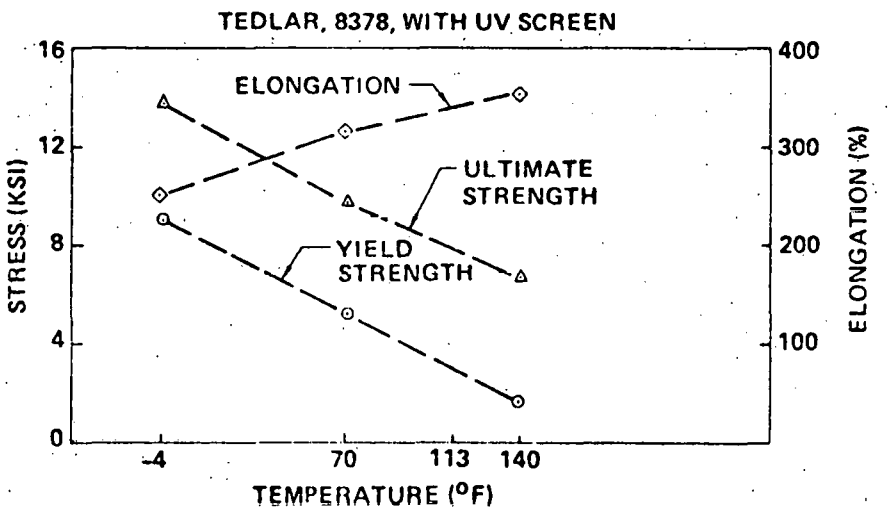

Figure: 6.2-1 Mechanical Properties versus Temperature

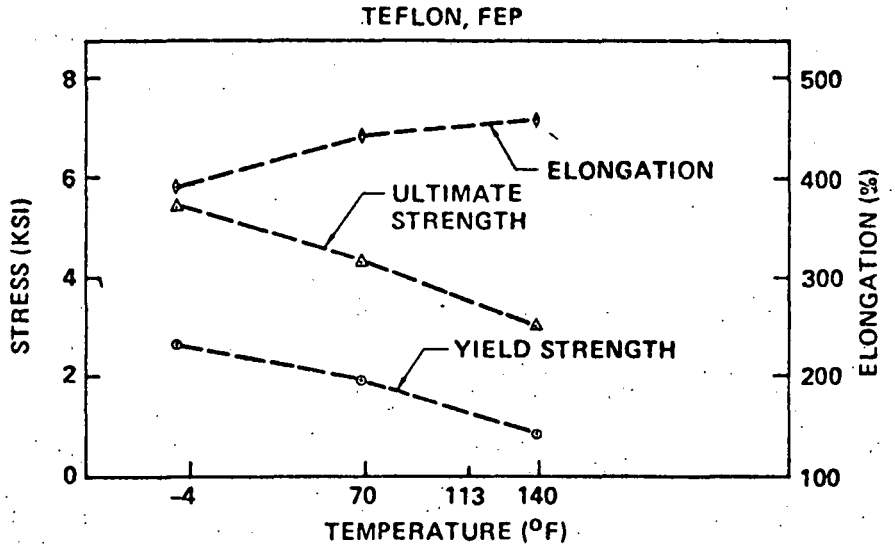

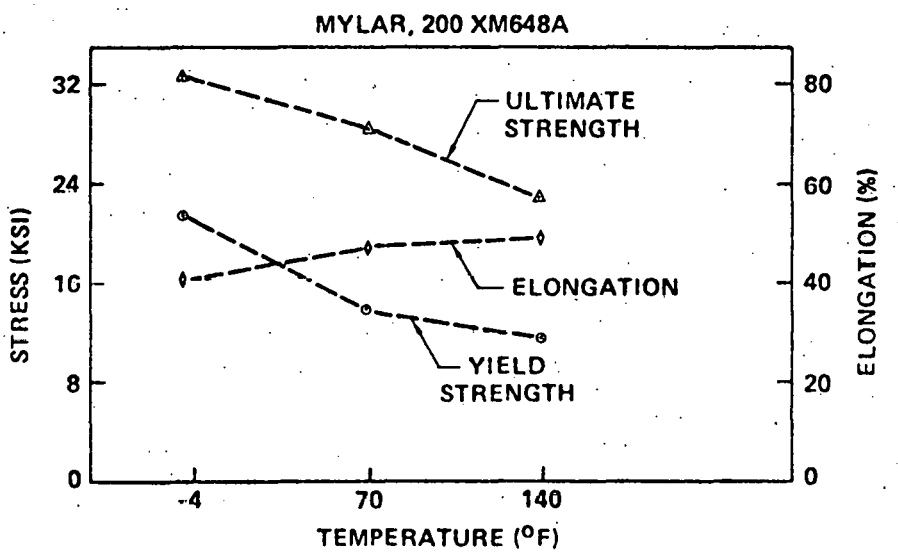

Figure: 6.2-2 Mechanical Properties versus Temperature

TABLE 6.2-2

JOINT TENSILE TEST RESULTS

Material	Type of Joint	Film Stress at Failure MN/m^2	Type of Failure
Tedlar, 4 Mil MR # 7827	Ultransonic 3/16" Anvil	45.3	Tear parallel to weld. Film fully yielded
	Ultrasonic 1/16"Anvil Wide stop	39.3	Tear parallel to and separation of weld. Film fully yielded
	Ultrasonic 1/16" Anvil Small Stop	37.4	Tear parallel to weld. Film not yielded
Tedlar, 4 Mil MR # 8378 with UV Screen	Ultrasonic	36.5	Tear parallel to weld. Film fully yielded
Tedlar, 4 Mil MR # 8606 No Additives	Ultrasonic	17.0 (8.0 to 32.5) Range	Tear parallel to and separation of weld. Film not yielded
	Impulse (Hot Ribbon)	52.5	Tear parallel to weld. Film fully yielded
Tedlar, 8 Mil MR # 8605 No Additives	Impulse (Hot Ribbon)	52.0	Tear parallel to weld. Film fully yielded
Mylar, 2 Mil 200XM648A	Adhesive Tape Dupont 46971/ RC805	141.3	Shear failure of adhesive. Film fully yielded
Mylar, 2 Mil 200XM648A to Rigid Urethane Foam to Aluminum	Adhesive Epoxy Type 38	54.7	Shear failure of adhesive at Mylar to foam bond. Film not yielded Note: Bonded area = 3.2 cm^2 (0.5 IN^2) Shear Stress at Failure = 228 KN/m^2 (33 PSI)
Mylar, 2 Mil 200XM648A to Foam to Aluminum	Adhesive Polyurethane 3M XA354981A	103.4	Shear failure of adhesive at Mylar to foam bond film fully yielded Note: Bonded area = 3.2 cm^2 (0.5 IN^2) Shear Stress at Failure = 440 KN/m^2 (64 PSI)

6.2.3 Creep

Creep studies were performed on Tedlar, Mylar, Teflon FEP and various joints as shown in Tables 6.2-3 and 6.2-4. Tests were conducted at 45°C (113°F) and 60°C (140°F) in accordance to ASTMD2990 using a 2.54 cm wide by 30.48 cm long specimen.

Figure 6.2-3 shows the 2 temperature controlled test boxes, temperature controllers, readouts and microscope used in the overall test setup. Time/creep histories are shown graphically in Figures 6.2-4 and 6.2-5 for Mylar 200XM648A and Tedlar 7826B (Baseline) under baseline design loading and maximum design temperature conditions. Approximately 80% of the observed creep strains occurs during the first 50 hours of exposure. Data presented on the tables and graphs show that neither of the baseline materials nor material joints show significantly long-term creep effects. The creep observed is not considered to have significant impact on dome or reflector optical or mechanical performance.

6.3 ENVIRONMENTAL EXPOSURE

6.3.1 Accelerated Ultraviolet

The purpose of this testing was to obtain data for the comparison of ultraviolet resistance of candidate films. It is not intended that these tests provide quantitative ultraviolet life data, since principles of accelerated testing are not fully understood and beyond the scope of this study.

A Spectrolab X-200 solar simulator with special filtering and a water window (to remove infrared radiation) was utilized to provide ultraviolet radiation at approximately 9.5 "suns" in the wavelength region less than 400 nanometers (based on air mass 2 spectrum). Figures 6.3-1 and 6.3-2 show the overall test setup and specimen monitoring board, respectively. Table 6.3-1 lists the specimen material and the associated tests performed before, during and after ultraviolet exposure. Transmittance and reflectance specimens were exposed and periodically withdrawn during exposure. Microtensile specimens were removed from the mounting board at various intervals, and tested for tensile properties.

TABLE 6.2-3

CREEP TESTS RESULTS OF SEAMS/JOINTS

Material Identity	Stress Level MN/m^2	Test Temp. °C	Exposure Time Hrs.	Creep Strain %
Tedlar to Tedlar, 4 Mil, MR #8378, No EPON, With UV Screen, Ultrasonic Weld Seam	5.00	45	65	1.82
			120	1.90
			400	2.00
			890	2.08
FEP to FEP, 10 Mil, As Received Heat Seal Welded Seam	1.79	45	65	0.36
			120	0.35
			400	0.36
			890	0.38
Mylar to Mylar, 2 Mil, 200XM648A, Mylar/Adhesive Tape Joint	6.89	60	65	0.15
			120	0.16
			400	0.20
			890	0.22
Mylar to Rigid Urethane Foam Type 38 Epoxy Adhesive Joint	6.89	60	65	0.33
			120	0.30
			400	0.40
			890	0.40
Mylar to Rigid Urethane Foam Polyurethane Adhesive Joint	6.89	60	65	0.13
			120	0.16
			400	0.19
			890	0.20

TABLE 6.2-4
CREEP TEST RESULTS

Material Identity	Stress Level MN/m^2	Test Temp. ^oC	Exposure Time Hrs	Creep Strain %
Tedlar, 4 mil MR #7826B No Epon, Less Solids	5.00	45	50 310 890 1660	1.34 1.53 1.60 1.61
Tedlar, 4 mil MR #8378 No Epon, with UV Screen	3.76	45	45 305 885 1660	1.06 1.20 1.34 1.34
	5.00	45	45 310 890 1660	1.62 1.83 1.98 1.99
FEP, 10 mil As Received	1.79	45	50 310 890 1660	0.41 0.44 0.48 0.48
Mylar, 2 mil 200XM 648 A Virgin	6.89	45	45 310 885 1660	-0.02 0.02 0.02 0.02
	3.45	60	40 305 885 1660	0.03 -0.01 -0.02 -0.05
	6.89	60	45 310 890 1660	0.14 0.14 0.18 0.15

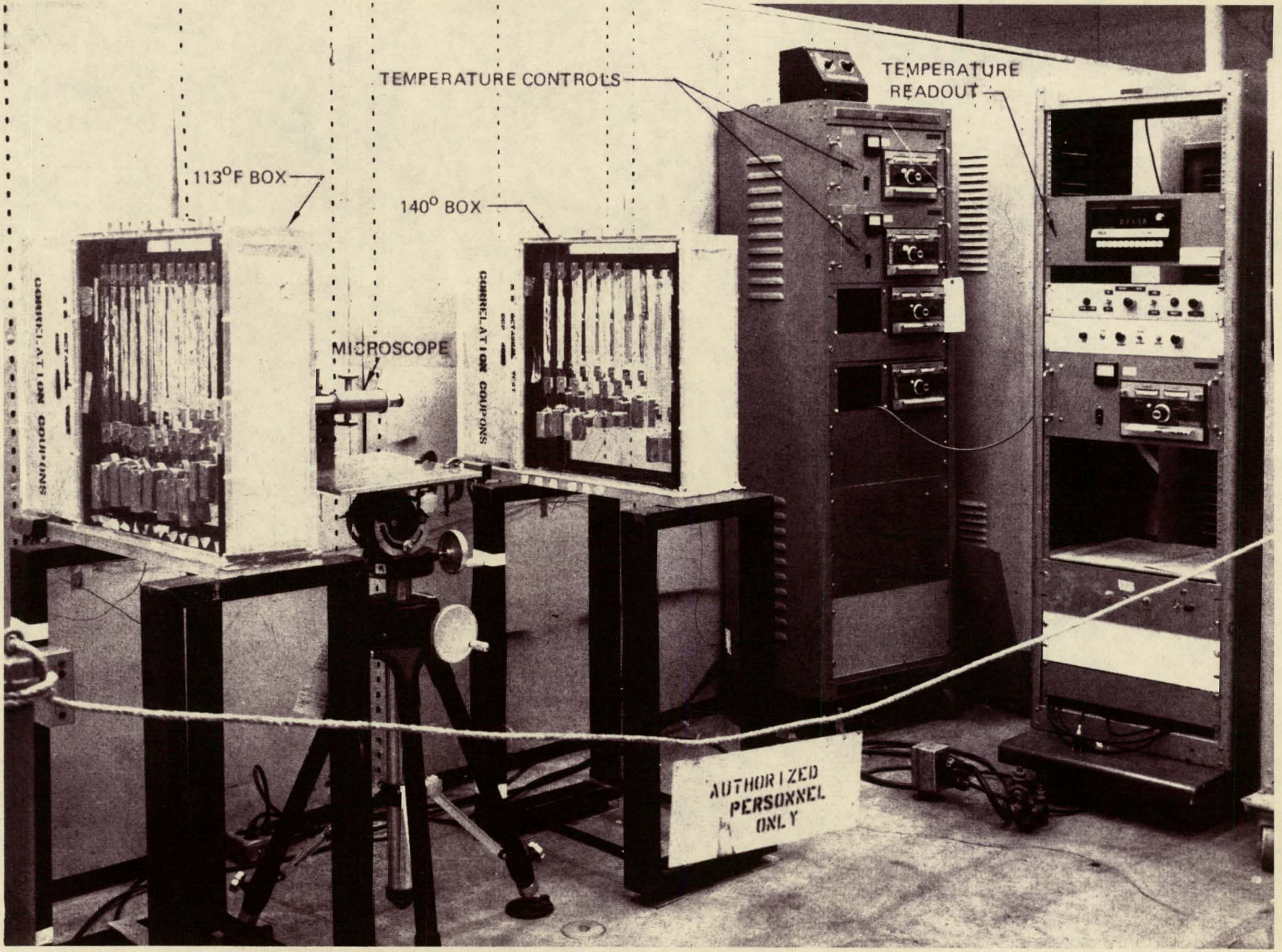

Figure 6.2.3. Overall Test Set-Up

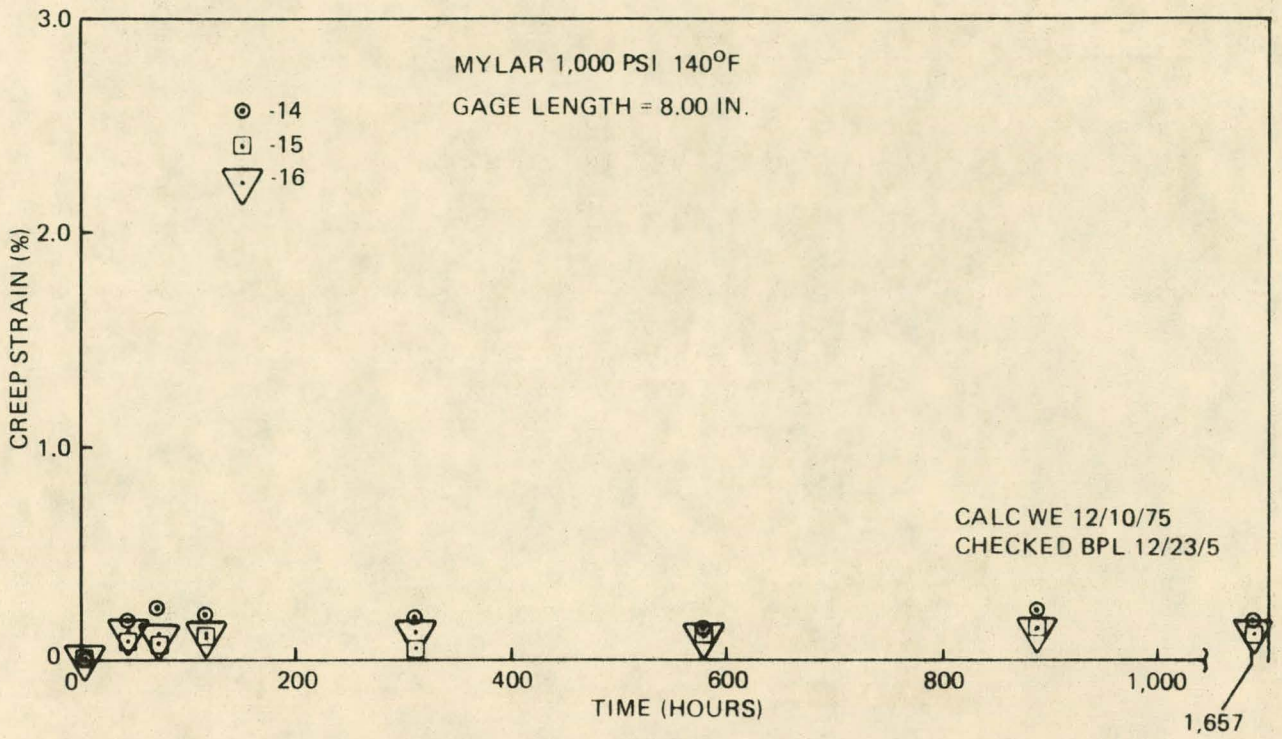

Figure: 6.2-4. Time-Creep History—Mylar

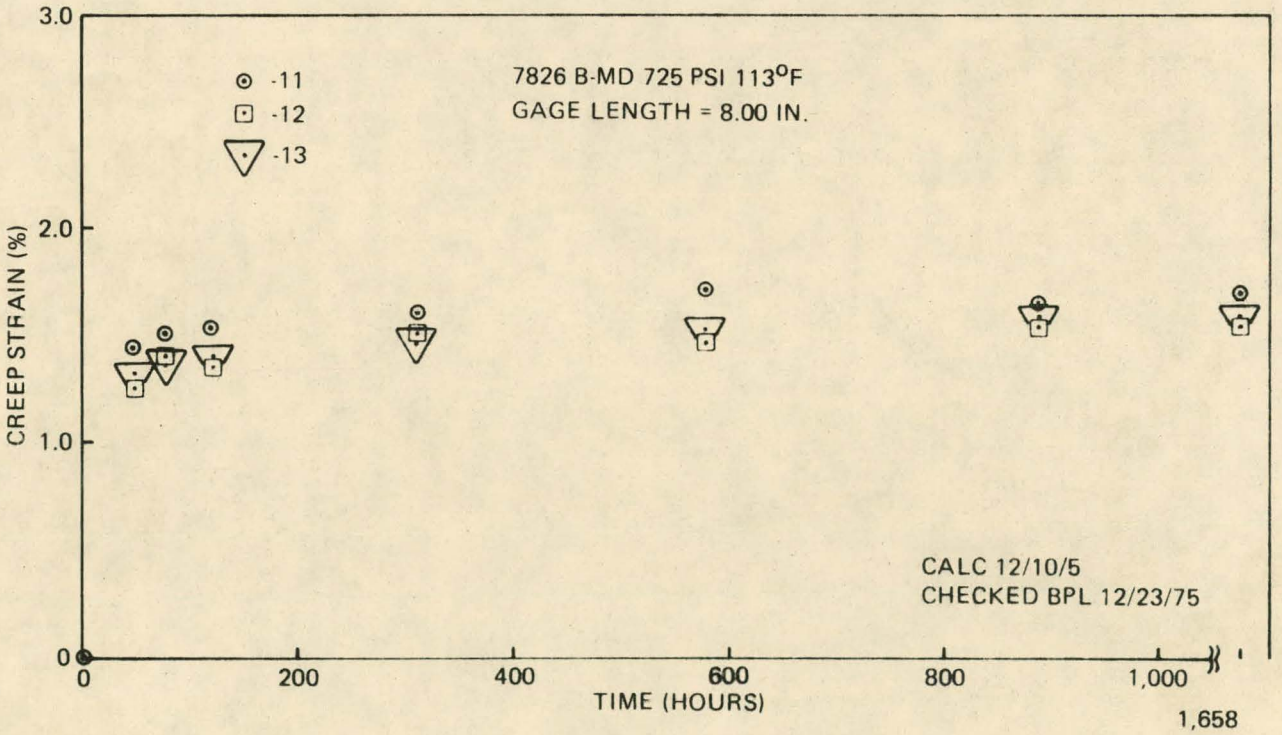

Figure: 6.2-5 . Time-Creep History—Tedlar

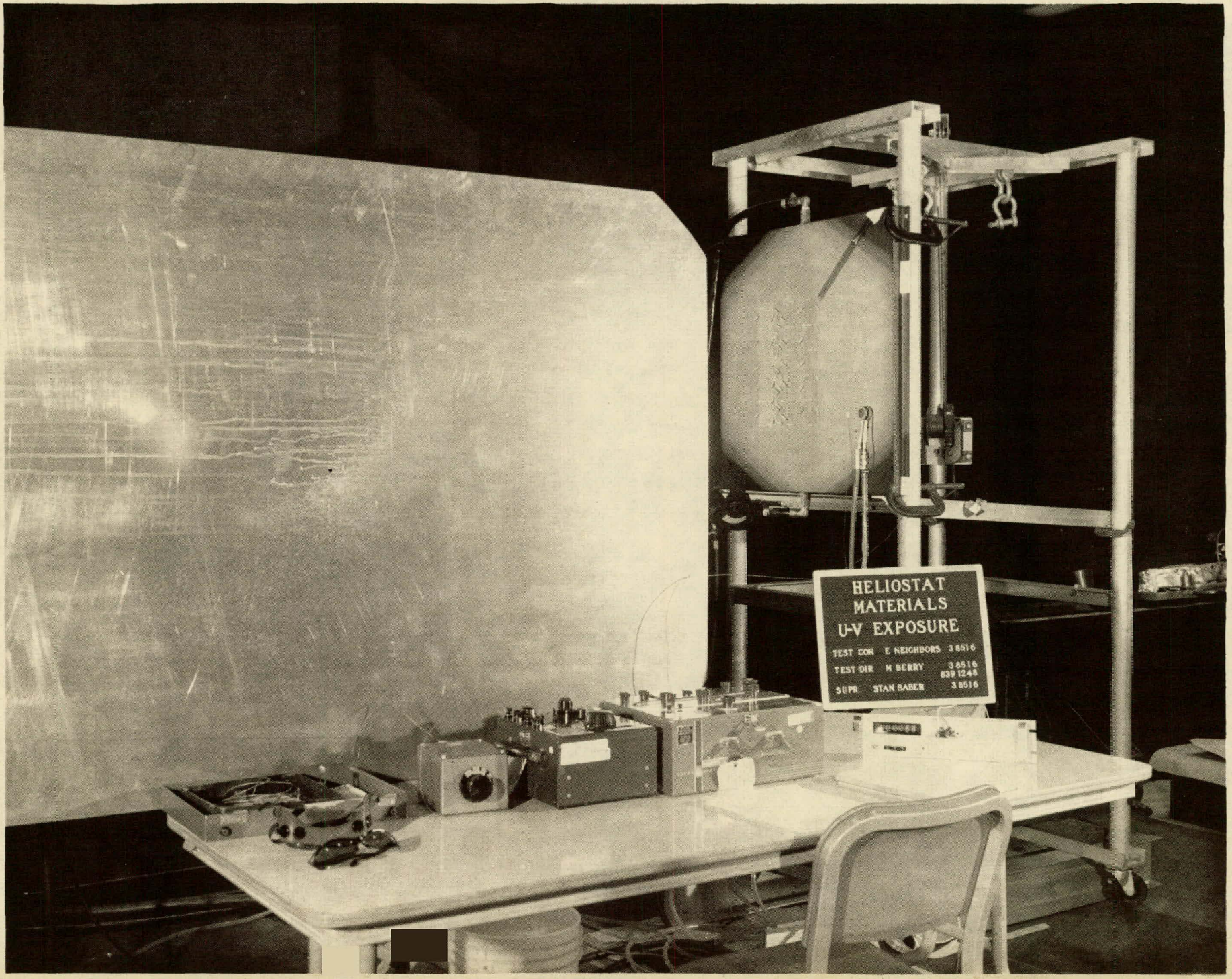

Figure: 6.3-1 Overall Test Setup

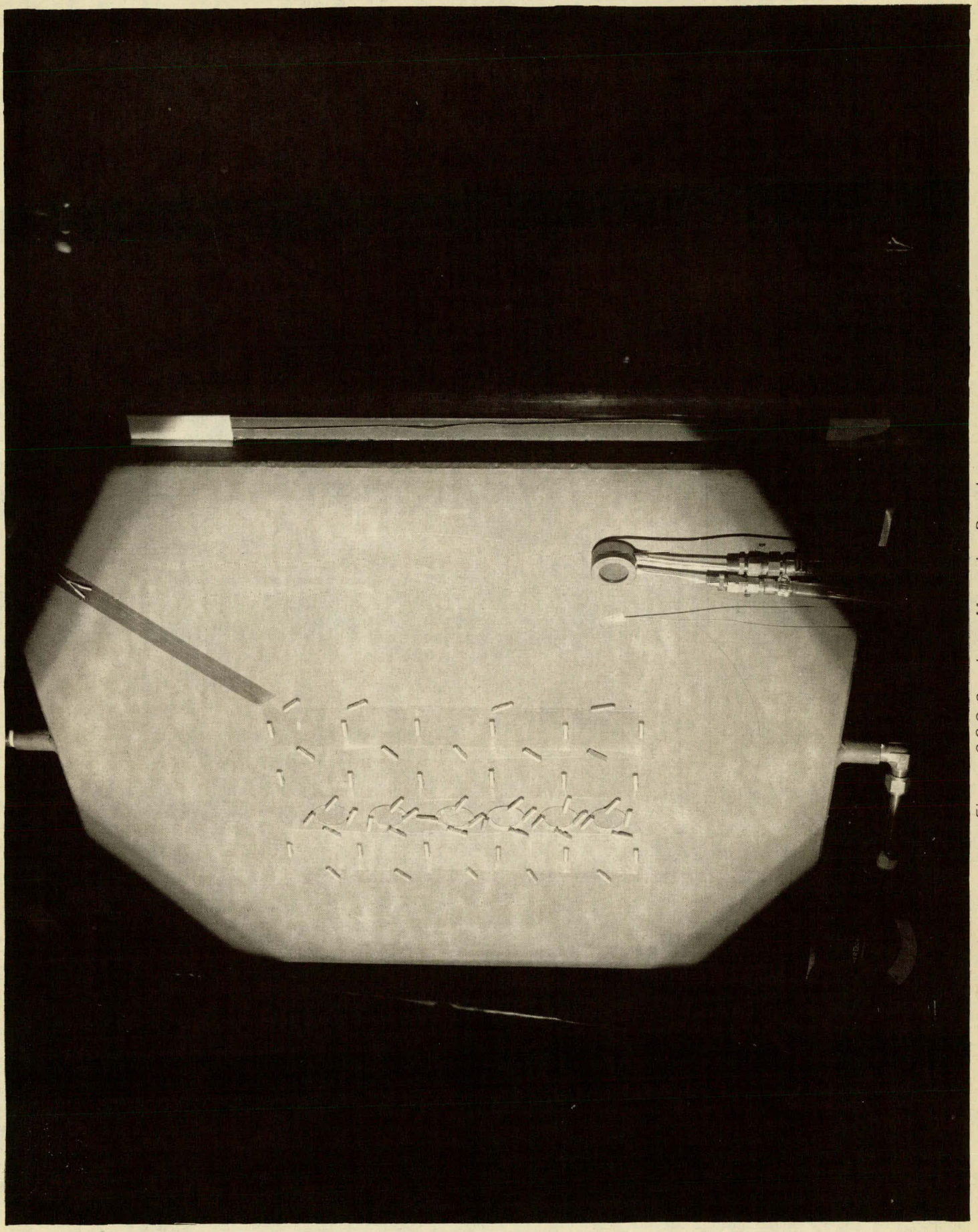

Figure: 6.3-2 Specimen Mounting Board

TABLE 6.3-1

Accelerated UV Screening Specimens

Material Identity	Tests Performed
Tedlar, 4 Mil MR #7826B No Additives	Microtensile, Transmittance Tests (Baseline Dome Material)
Tedlar, 4 Mil MR #7825 Standard with EPON	Microtensile, Transmittance Tests (Commercial Grade Material)
Tedlar, 4 Mil MR #8378 W/UV Screen, No EPON	Microtensile, Transmittance Tests (Ultraviolet Screen Material)
FEP Teflon, 10 Mil As Received	Microtensile, Transmittance Tests (Alternate Baseline Dome Material)
Mylar 2 Mil (200XM648A) Aluminized (1000 Angstroms) (1st Surface Toward Source)	Reflectance Tests (Baseline Reflector Material)
Aluminized Mirror (Nickel Substrate)	Contamination Control Specimen for Reflectance
Sapphire Disc	Contamination Control Specimen for Transmittance

Figures 6.3-3 through 6.3-7 are curves of optical and mechanical properties as a function of exposure hours for Tedlar, Teflon FEP, and Mylar. The exposure in the figures is plotted in terms of real-time solar simulator exposure at normal incidence to the light beam.

Results of tests on the three types of Tedlar indicate that the baseline material (#7826B) showed no degration in 1474 hours. FEP Teflon showed only slight degradation in the test. Standard composition Tedlar (#7825) degraded in transmittance from about 81 to 74.5%.

The aluminized Mylar specimen (200XM648A Mylar - deposited with 1000 Angstroms pure Al) was exposed with aluminum surface toward source for 500 hours. The measured reflectance after exposure was 87.4%. This compares with a pre-test reflectance of 88.9%.

Reflectance and transmittance control specimens were measured for optical properties prior to and following exposures. The purpose of these specimens was to monitor contamination that might be present in the vicinity of the test setup. No significant reflectance or transmittance change was detected.

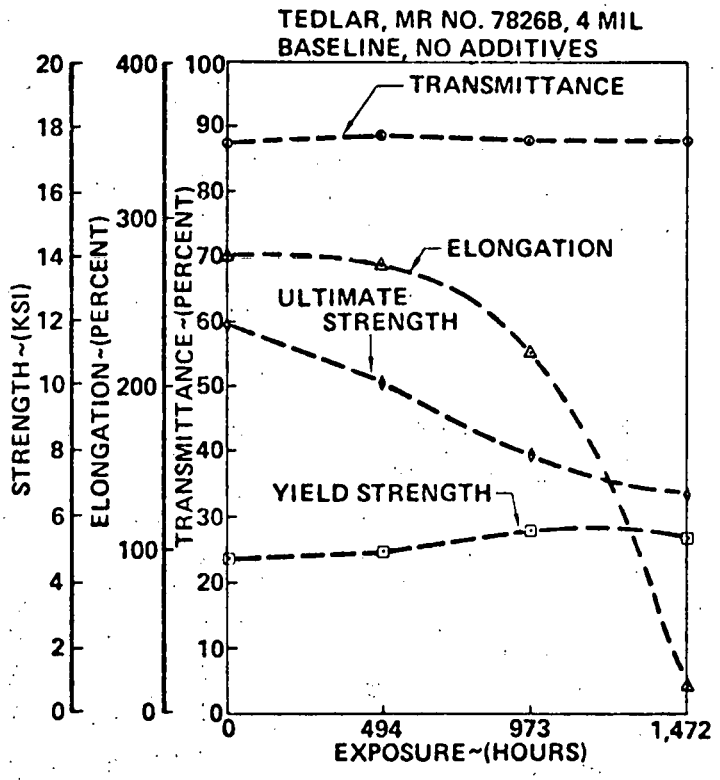

Figure: 6.3-3 Accelerated Ultraviolet Degradation

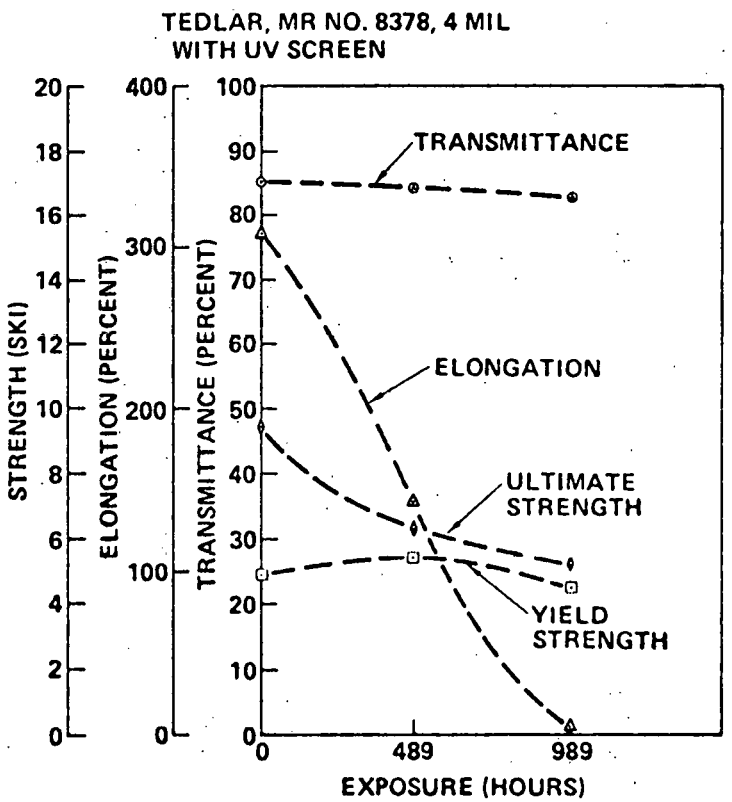

Figure: 6.3-4 Accelerated Ultraviolet Degradation

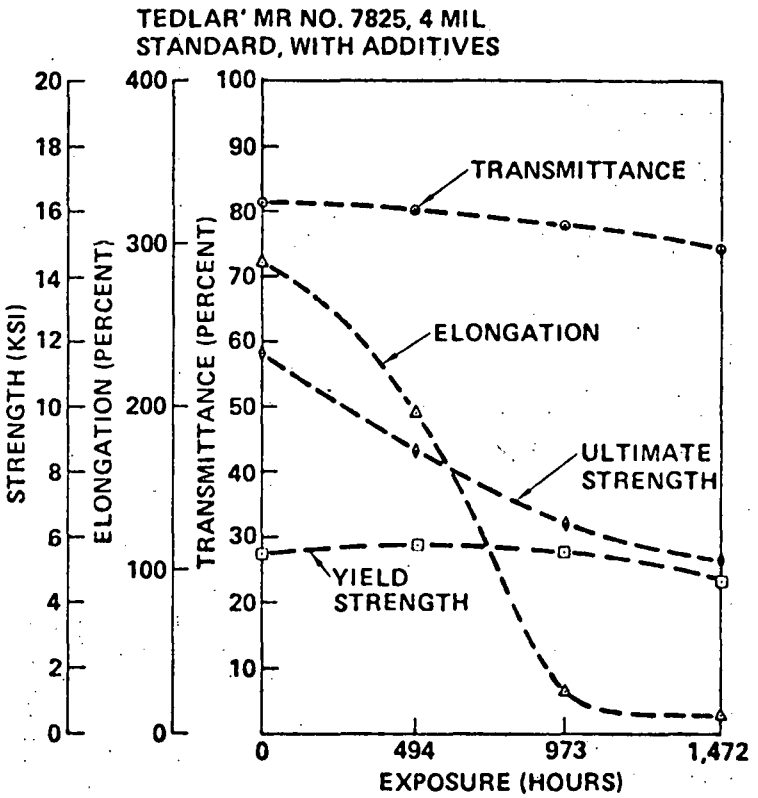

Figure: 6.3-5 Accelerated Ultraviolet Degradation

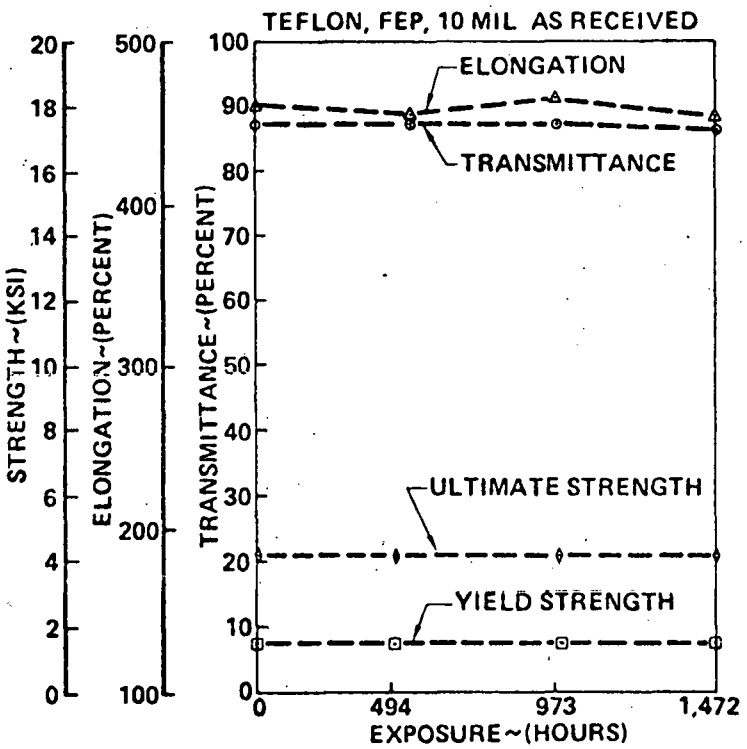

Figure: 6.3-6 Accelerated Ultraviolet Degradation

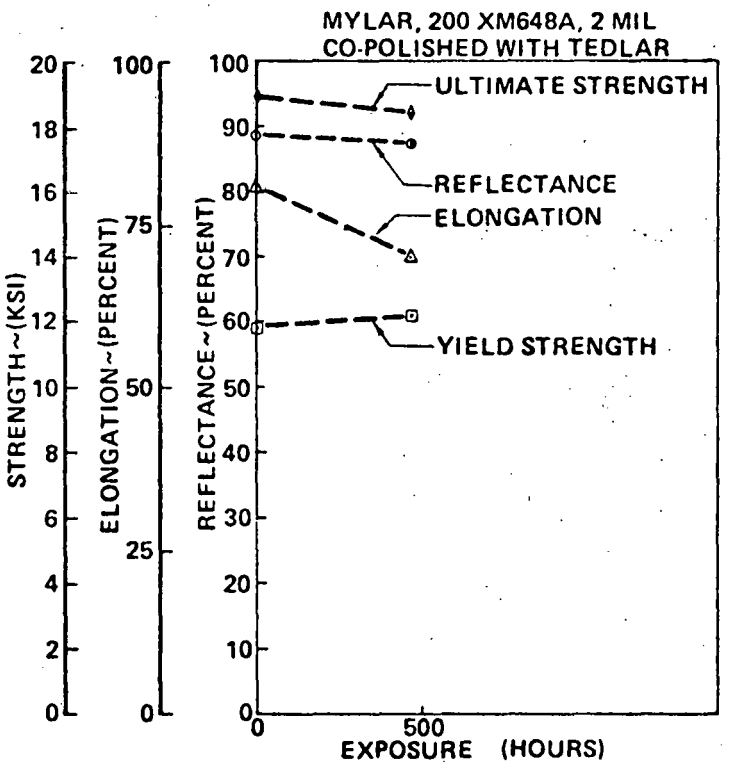

Figure: 6.3-7 Accelerated Ultraviolet Degradation

6.3.2 Desert Exposure

Specimens of candidate materials are being subjected to real time exposure in the desert environments and will be measured for optical and mechanical property degradation. Of particular interest are ultraviolet degradation and sand abrasion. Testing will be performed in two phases:

(1) desert exposure (Albuquerque, N.M. and Inyokern, California)

(2) laboratory measurements (Boeing-Kent Labs)

The plastic film candidates were mounted on text fixtures and shipped to the desert test sites, where the fixtures were erected in dedicated areas. The exposure will continue for approximately 18 months unattended. The only activity required duirng this exposure period will be the extraction of specimens for evaluation at pre-determined intervals (sample extraction at 6, 12 and 18 months).

The test apparatus is shown in Figure 6.3-8. It consists of a 20 ft. tower with 28 cylindrical specimen mounts. The tower is held in its vertical orientation by guy wires. The base plate is held down with tent stakes.

Specimens extracted from the desert exposure test setup will be sent to the Boeing-Kent laboratory for optical and mechanical testing.

6.3.3 Weatherometer and Humidity Tests

One sample each of 4 mil Tedlar (MR #7826A) and aluminized Myler (200XM648A) was placed in the weatherometer chamber, and one sample of each was placed in the humidity chamber. The weatherometer environment was 60°C (140°F), carbon arc solar simulation, and 18 minutes of rain every two hours. The Tedlar and Mylar specimens were exposed to 590 hours of this environment. The humidity chamber environment was 49°C (120°F) and 100% relative humidity. The Tedlar and Mylar specimens were exposed to 984 hours of this environment.

Tedlar remained unchanged in yield strength, ultimate strength and ultimate elongation following these exposures. A drop in transmission of approximately 2% was measured, in both cases, however.

The aluminized Mylar samples showed substantial degradation in reflectance and ultimate elongation as expected following the exposures. Reflectance decreased to 58% following weatherometer exposure and 0% following humidity (aluminum washed off). The ultimate elongation decreased by 22% due to weatherometer exposure and 42% due to humidity exposure. The yield strength increased by 13% and the ultimate strength decreased by approximately 5% for both exposures.

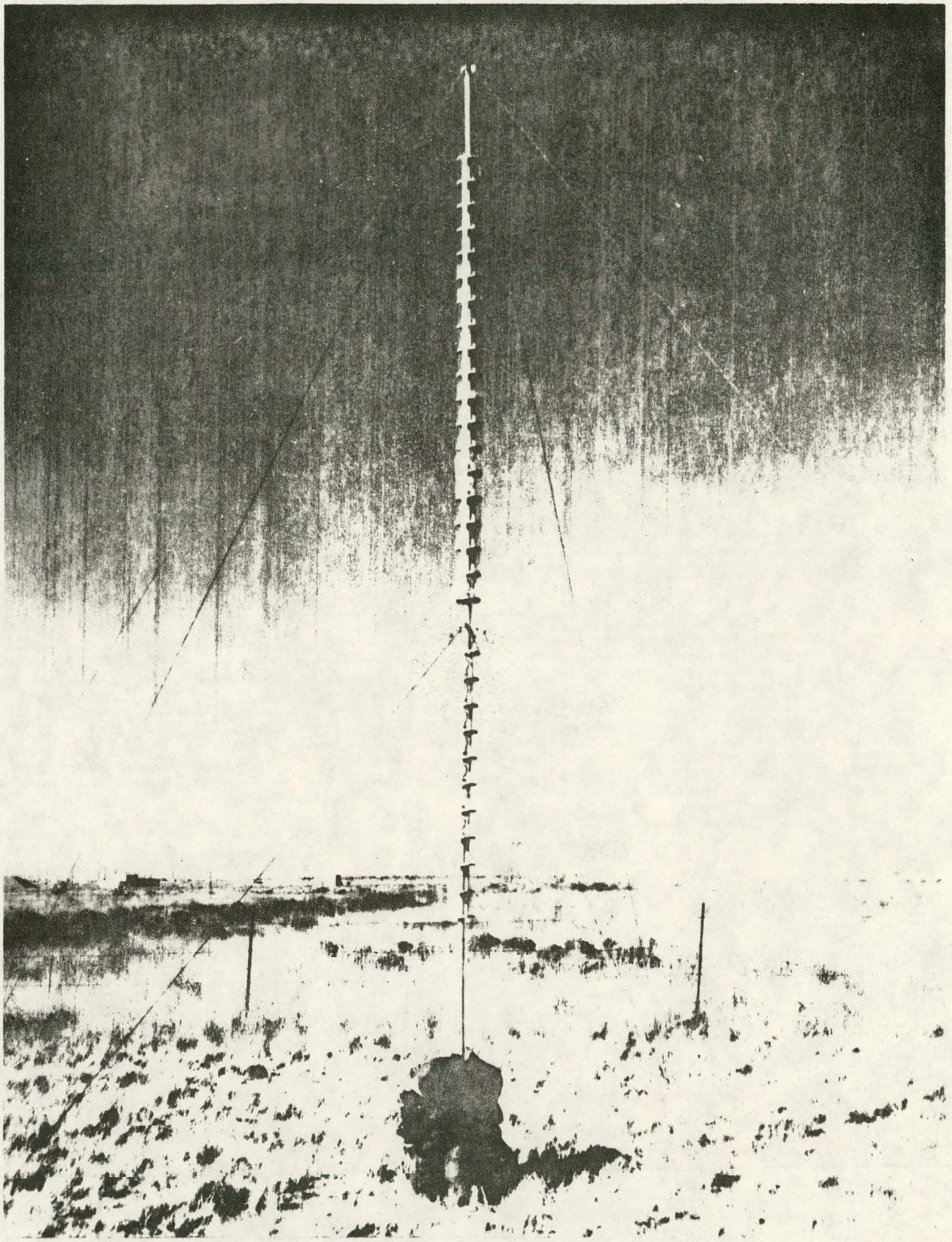

Figure: 6.3-8 : Desert Exposure Test Setup

6.3.4 Corrosive Environments

Tedlar and Mylar specimens were exposed to corrosives representative of those anticipated at plant locations. Included were cleaning solutions and bird droppings.

Aluminized Mylar specimens were exposed to repeated washes (on aluminized side only) with distilled water and with ethyl alcohol with no loss in specular reflectance.

Tedlar specimens were subjected to a 24 hour soak in detergent solution and a 30-day exposure to bird droppings. In both cases the loss in transmission after cleaning was less than 1%.

6.4 CLEANABILITY

The objective of these tasks was to assist in the selection of a cleaning technique for the protective enclosure and reflective assembly surfaces. The intent was to identify an acceptable technique for baseline materials rather than conduct a comprehensive study of cleanability of heliostat materials.

Visual appearance, transmittance and reflectance measurements were taken prior to and following contaminating exposure and cleaning operation.

The results of using various cleaning methods are tabulated in Table 6.4-1.

Data shows that all contaminants associated with the protective enclosure are cleanable with detergent, water and a soft brush, with minimal loss in transmission. If dust is the only contaminant a simple water rinse was shown to be satisfactory.

Cleaning of the reflective assembly with ethyl alcohol or distilled water was found to be satisfactory for dust contamination, which is expected to be the most likely contaminant. For combined dust and moisture (humidity) contamination a distilled water/soft brush technique was used with negligible loss in reflectance.

The most promising techniques, as discussed above, will be used to clean full scale assemblies later in the test program.

Table 6.4-1. Test Results Cleanability of Tedlar and Mylar

Exposures
1) Rain
2) Dust
3) Water/dust
4) Bird droppings
5) Bird droppings allowed to dry for 30 days
6) Detergent solution 23-1/2-hour soak

Cleaning method
A) Detergent/water
B) Detergent/water/soft brush
C) Compressed gas (GN_2)
D) Vacuum cleaner
E) Alcohol (ethyl)
F) Distilled water
G) Water rinse (tap)
H) Distilled water/soft brush

Material	Exposure	Cleaning method	Transmittance/reflectance	
			Before exposure	After cleaning
Tedlar, 4-mil MR No. 8378 with UV screen	1)	N/A	84.6% transmittance	No change
	2)	A)	84.6% transmittance	No change
	2)	B)	84.6% transmittance	No change
	2)	C)	84.6% transmittance	80.6%
	2)	D)	84.6% transmittance	73.0%
	2)	G)	84.6% transmittance	No change
	3)	A)	84.6% transmittance	Unacceptable
	3)	B)	84.6% transmittance	82.6%
	3)	C)	84.6% transmittance	81.0%
	3)	D)	84.6% transmittance	72.0%
	3)	G)	84.6% transmittance	Unacceptable
	4)	A)	84.6% transmittance	Unacceptable
	4)	B)	84.6% transmittance	84.0%
	5)	B)	84.6% transmittance	83.8%
	6)	G)	84.6% transmittance	84.0%
Mylar, 2-mil aluminized 200 XM 648A	1)	E)	90.0% reflectance	No change
	1)	F)	90.0% reflectance	No change
	2)	C)	90.0% reflectance	87.3%
	2)	E)	90.0% reflectance	89.4%
	2)	F)	90.0% reflectance	85.5%
	3)	E)	90.0% reflectance	Unacceptable
	3)	F)	90.0% reflectance	Unacceptable
	3)	H)	90.0% reflectance	88.5%

7.0 REFERENCES

2-1 Preliminary Requirements Specification for Collector Subsystem - Central Receiver Solar Thermal Power System, Boeing Document D277-10002-1, prepared under ERDA Contract E-(04-3)-1111.

3.1-1 Design Manual for Spherical Air Supported Radomes (Revised), "W. W. Bird and M. Kamrass, Cornell Aeronautical Laboratory Report No. UB-909-D-2, Rome Air Development Center Contract No. AF30(602)-976.

3.1-2 American National Standards Institute, Inc., "American National Building Code Requirements for Minimum Design Loads in Buildings and Other Structure," ANSI A58.1-1972. American National Standards Institute, Inc., 1430 Broadway, New York, N. Y. 10018.

3.1-3 Document No. TR-20-(Vol. 6), "Multiprotection Design, "Defense Civil Preparedness Agency, Washington, D. C., December, 1974.

3.1-4 Journal of the Structural Division Proceedings of the ASCE, "New Distributions of Extreme Winds in the United States." H.C.S. Thom, July, 1968.

3.4-1 Boeing Engineering Thermal Analyzer Program (AS 1917, Boeing Document D190-10016-1.

3.4-2 Performance of Low Cost Solar Reflectors for Transferring Sunlight to a Distant Collector, R. C. Zentner, The Boeing Company, paper delivered at Int. Solar Energy Society Mtg., Los Angeles, CA., 8/75.

3.4-3 DuPont Bulletin of Tedlar Optical Properties

3.4-4 DuPont Bulletin of Mylar Optical Properties

3.4-5 Boeing Memo 2-5790-0000-206 R. C. Zentner to J. R. Gintz entitled, "Reflectometer for Measuring Specularity of Aluminized Plastic Films," dated October 3, 1974.

3.4-6 Insolation/Climatology Data Bank Tapes, Compiled by The Aerospace Corporation, NSF Contract AIR-74 (7417-05)-1.

APPENDIX

STEPPER MOTOR SELECTION

1.0 The output torque required of the drive system is:

$$T = J_m(dw_m/dt) + J_L(dw_L/dt) + J_{cw}(dw_{cw}/dt) + J_A(dw_L/dt) + Bw_L + T_F + T_L$$

where:

J_m = motor inertia

w_m = motor angular velocity

J_L = load inertia

w_L = load angular velocity

J_{cw} = counter weight inertia

J_A = air mass density

B = damping factor

T_F = friction torque

T_L = load torque

1.1 The load torque is defined as the effective weight of the baseline reflective assembly, 86 pounds, on a moment arm of approximately 4.0 inches (R_L).

$$T_L = W_L \cdot R_L = 86 \text{ lbs.} \quad . 4 \text{ in.} = 344 \text{ in.} - \text{lbs.}$$

However, a counter weight of the same torque value is applied as an opposing weight of 28.7 lbs. on a moment arm of 12 inches (R_{cw}).

$$T_{cw} = W_{cw} \cdot R_{cw} = 28.7 \text{ lbs. } (12 \text{ in.}) = 344 \text{ in.} - \text{lbs.}$$

Then the effective load torque is $T_L = 0$.

1.2 The friction torque, T_F, results from the friction in the whole drive assembly. As an estimate,

$$T_F = 0.1\ T_L = 0.1\ (344 \text{ in.} - \text{lbs.}) = 34.4 \text{ in.} - \text{lbs.}$$

1.3 The load angular velocity, w_L, for one motor step is the average velocity, which

1.3 (continued)

is the step divided by the time for one step. Note that the actual velocity during slewing will be the same, as slewing is a sequence of single steps.

The load step increment is:

$1.8^{o}/80 = 0.0225^{o}/\text{step}$

The time for each step is:

$t_s = 0.180$ seconds/step

Therefore,

$$w_L = \frac{0.0225^{o}}{0.180 \text{ sec.}} \times \frac{\pi \text{ rad}}{180^{o}} = 0.0022 \text{ rad/sec.}$$

1.4 The resistance torque due to the damping factor and angular velocity was calculated in reference 1 as 0.6 in -lb. The following approximation method calculation of the damping factor B is presented.

The damping factor, B, results from the action of the reflective assembly rotating about an axis in an air medium.

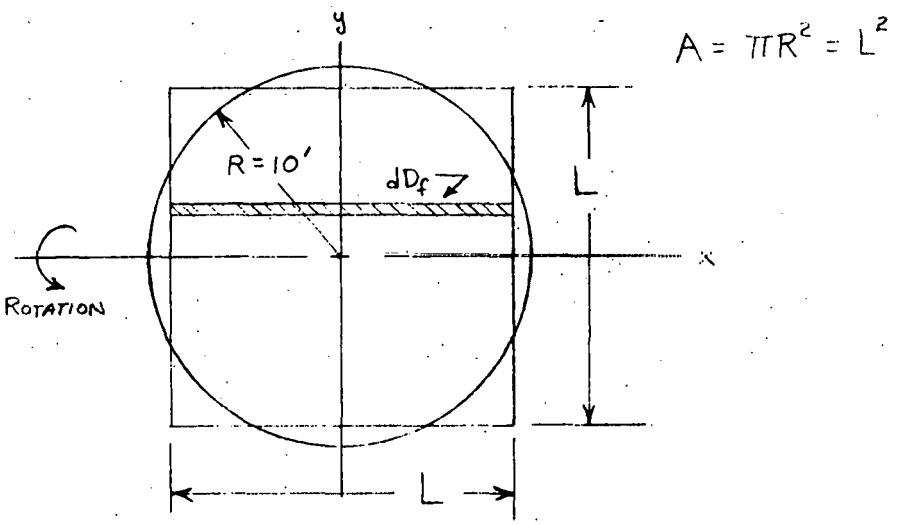

As an approximation, the square membrane is substituted in the calculations.

The torque resulting from air damping is defined as:

$$T = Bw_L = \int y \cdot dD_f$$

where D_f is the damping force.

Then

$$B = \frac{1}{w_L}\int y \ dD_f$$

The aerodynamic equation for drag force is

$$D_f = D_o \ \frac{p}{2} \ v^2 A,$$

where:

D_o = drag coefficient

p = mass density of air

v = translational velocity

A = area of the membrane

Since

$$v = w_L y$$

and

$$A = 2Ly \quad (\tfrac{L}{2} \geq y \geq 0)$$

$$dD_f = D_o \ pw_L \ ^2y^2 \ \frac{1}{2} \ dA; \ \frac{dA}{dy} = 2L$$

then

$$dD_f/dy = D_o \ pw_L \ ^2Ly^2$$

and

$$dD_f = D_o pw_L \ ^2LY^2dy$$

Then

$$B = \frac{1}{w_L} \int_o^{L/2} y \cdot D_o p w_L \, {}^2 L y^2 dy$$

or:

$$B = D_o p w_L L \int_o^{L/2} y^3 dy = \frac{1}{64} D_o p w_L \, L^5$$

Since:

$$L = \pi^{1/2} R$$

$$B = \frac{\pi^{5/2}}{64} D_o \, p w_L \, R^5$$

For a flat plate

$D_o = 1.9$

$p = 0.00249$ slug/ft. ^{3}

$w_L = 0.0022$ rad./sec.

$R = 10$ ft.

then:

$$B = 0.27(1.9) \ (0.00249 \text{ slug/ft.}^3) \ (0.0022 \text{ rad./sec.}) \ (10 \text{ ft.})^5 \left(\frac{\text{lb./ft./sec.}^2}{\text{slug}}\right)$$

$B = .3$ ft. -lbs. -sec.

$B = 3.38$ in. -lbs. -sec.

and:

$Bw_L = (3.38 \text{ in. - lbs. - sec.}) (0.0022 \text{ rad./sec.})$

$Bw_L = 0.01$ in. -lb.

1.5 The angular acceleration, dw/dt, of the load weight is estimated graphically as follows: For each step,

$w_o = 0$

$w_f = 0$

w_L = average velocity

t_s = 0.180 sec.

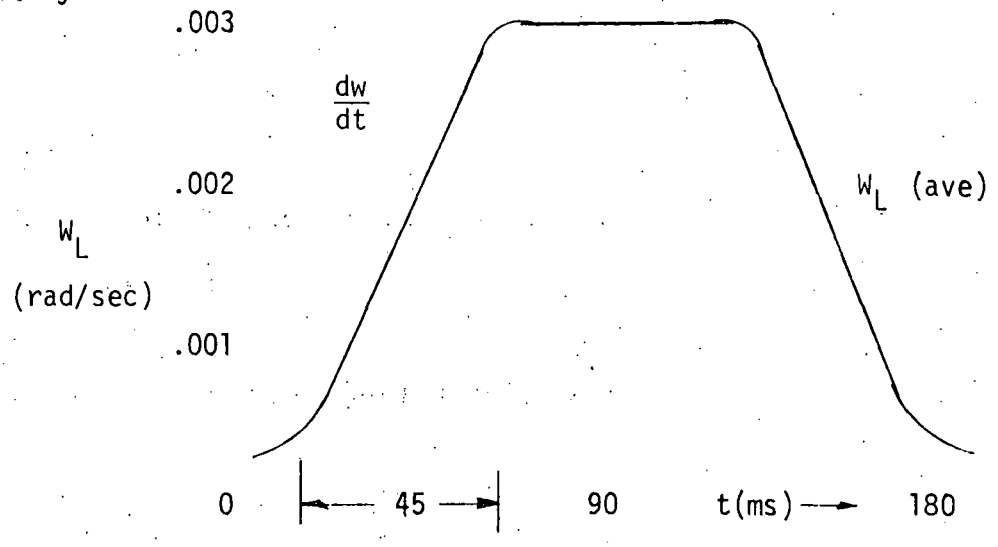

Graphic Estimation of Angular Load Velocity during a Step

From the graphic representation,

$$\frac{dw_L}{dt} = \frac{0.003 \text{ rad./sec.}}{0.045 \text{ sec.}} = .074 \text{ rad./sec.}^2$$

The angular acceleration of the motor rotor, dw_m/dt, can be estimated as:

$$\frac{dw_m}{dt} = 80 \frac{dw_L}{dt} = 6 \text{ rad./sec.}^2$$

where 80 is the gear reduction factor between motor and load.

1.6 The resistance torque due to the acceleration and inertia of the air mass, is:

$J_A (dw_L/dt) = (373.6 \text{ in -lbs -sec}^2) (.074 \text{ rad./sec.}^2) = 27.7 \text{ in -lbs.}$

1.7 The inertia of the counter weight is calculated as:

Therefore, total output torque is:

T_o = (0 + 81.7 + .8 + 27.7 + 0 + 34.4) in. -lbs.

T_o = 145 in -lbs.

Since all torques but rotor inertia are reduced by the gear reduction (80:1) the effective motor torque is calculated as:

T_m = 145/80 = 1.82 in -lb

T_m = 1.82 in. -lb (16 0z/lb) = 29 in. -oz.

The stepper motor specification are then:

(1) nominal running torque: 35 in -0z.

(2) detent torque: 2 oz -in (minimum)

(3) stepper motor size: 23

(4) operating temperature: -20^{o} to + 60^{o} C

(5) slew speed: 6 step/second

The drive actuation specifications are then:

(1) gear reduction: 80/1

(2) output torque: 200 in. - lbs.

1.7 (continued)

$$J_{cw} = W_{cw} \cdot R_{cw}^2$$

$$= (28.7 \text{ lbs.}) \cdot (12 \text{ in.})^2 = 4132 \text{ in}^2 \text{ -lbs.}$$

1.8 The resistance torque due to the acceleration and inertia of the load, from reference 1, is:

$$J_L (dw_L/dt) = (1104 \text{ in. -lbs -sec}^2) (.074 \text{ rad./sec.}^2) = 81.7 \text{ in -lbs.}$$

1.9 The inertia of the motor rotor is estimated from various vendor catalogs as:

$$J_m = .1 \text{ in}^2 \text{ - lbs.}$$

2.0 From Section 1.0

$$T_o = J_m \frac{dWm}{dt} + J_L \frac{dw_L}{dt} + J_{cw} \frac{dw_{cw}}{dt} + J_A \frac{dW_L}{dt} + BW_L = T_F = T_L$$

$$J_m \frac{dWm}{dt} = (2.1 \text{ in}^2 \text{ -lbs}) (6 \text{ rad/sec}^2) / (386.06 \text{ in/sec}^2)$$

$$= \text{negligible}$$

$$J_L \frac{dW_L}{dt} = 81.7 \text{ in -lbs.}$$

$$J_{cw} \frac{DW_L}{dt} = (4132 \text{ in}^2 \text{ -lbs}) (.074 \text{ rad/sec})^2 (386.06 \text{ in/sec})^2$$

$$= .8 \text{ in -lbs}$$

$$J_A \frac{dW_L}{dt} = 27.7 \text{ in -lbs}$$

$$BW_L = \text{negligible}$$

$$T_F = 34.4 \text{ in -lbs}$$

$$T_L = 0.$$

DISTRIBUTION LIST:

8 copies to:

Mr. George Kaplan
Division of Solar Energy
USERDA
Washington, D. C. 20545

3 copies to:

Mr. Vito Magliano, Director
Contract Services Division
USERDA
1333 Broadway
Oakland, California 94612

3 copies to:

Mr. A. C. Skinrood
Division 8184
Sandia Laboratories
Livermore, California 94550

2 copies to:

Mr. Howard Webb
Energy and Transportation Division
The Aerospace Corporation
P. O. Box 92957
Los Angeles, California 90009